Distribution Agreement

In presenting this thesis or dissertation as a partial fulfillment of the requirements for an advanced degree from Emory University, I hereby grant to Emory University and its agents the non-exclusive license to archive, make accessible, and display my thesis or dissertation in whole or in part in all forms of media, now or hereafter known, including display on the world wide web. I understand that I may select some access restrictions as part of the online submission of this thesis or dissertation. I retain all ownership rights to the copyright of the thesis or dissertation. I also retain the right to use in future works (such as articles or books) all or part of this thesis or dissertation.

Signature:

_____ _____

Ha Eun Kong Date

Identification of genetic modifiers of
Fragile X-Associated Tremor/Ataxia Syndrome

By

Ha Eun Kong
Doctor of Philosophy

Genetics and Molecular Biology

Peng Jin, Ph.D.
Advisor

Thomas S. Wingo, MD.
Co-Advisor

Stephen T. Warren, Ph.D., FACMG
Committee Member

Michael J. Gambello MD., PhD.
Committee Member

Stephanie Sherman, Ph.D.
Committee Member

David Cutler, Ph.D.
Committee Member

Accepted:

Lisa A. Tedesco, Ph.D.
Dean of the James T. Laney School of Graduate Studies

Date

Identification of genetic modifiers of Fragile X-Associated Tremor/Ataxia Syndrome

By

Ha Eun Kong
A.B. Princeton University, 2013

Advisor: Peng Jin, Ph.D.

An abstract of
A dissertation submitted to the Faculty of the
James T. Laney School of Graduate Studies of Emory University
in partial fulfillment of the requirements for the degree of
Doctor of Philosophy in
Graduate Division of Biological and Biomedical Science
Genetics and Molecular Biology
2019

Abstract

Identification of genetic modifiers of
Fragile X-Associated Tremor/Ataxia Syndrome

By Ha Eun Kong

Fragile X-Associated Tremor/Ataxia Syndrome (FXTAS) is a debilitating late-onset neurodegenerative disorder that occurs in premutation carriers of the expanded CGG repeat in *FMR1*. FXTAS results in a spectrum of neurological manifestations, such as gait ataxia, intention tremor, and parkinsonism. Though all premutation carriers are at risk, FXTAS is incompletely penetrant, such that only over a third of male premutation carriers develop the phenotype in their lifetime. This dissertation aims to expand our understanding of the mechanism behind the incomplete penetrance and thereby gain insight into potential biomarkers for diagnosis/prognosis as well as potential therapeutic targets for FXTAS.

In Chapter 1 and 2, we use mouse metabolomics and a *Drosophila* genetic screen to investigate the genetic modifiers of FXTAS and identify 12 genetic modifiers of FXTAS neurotoxicity, highlighting sphingolipid metabolism as a key altered pathway in FXTAS. In Chapter 3, we combine WGS of 110 human *FMR1* premutation carriers and *Drosophila* genetics to identify 19 genetic modifiers of FXTAS CGG-associated neurodegeneration. Furthermore, in Chapter 4, we demonstrate in *Drosophila* and Neuro2A cells that *PSMB5* is a genetic modifier of FXTAS that ameliorates CGG-associated neurotoxicity upon knockdown and identify $PSMB5^{rs11543947\text{-}A}$ as a potential prognostic biomarker.

Identification of genetic modifiers of Fragile X-Associated Tremor/Ataxia Syndrome

By

Ha Eun Kong
A.B., Princeton University, 2013

Advisor: Peng Jin, Ph.D.

A dissertation submitted to the Faculty of the
James T. Laney School of Graduate Studies of Emory University
in partial fulfillment of the requirements for the degree of
Doctor of Philosophy in
Graduate Division of Biological and Biomedical Science
Genetics and Molecular Biology
2019

Acknowledgements

It takes a village to raise a child, and it has truly taken a lot of Emory to foster my growth and development as an independent and critical thinker. I thank God for leading me to the wonderful people at Emory (MD/PhD program, Dept of Human Genetics, GMB).

I'd like to give my thanks to my advisor Dr. Peng Jin, who not only gave me the opportunity to work on very stimulating projects, but also provided me with guidance and resources to carry the projects forward at my pace. He taught me to be efficient, resourceful and collaborative, and did not ever stop to support me in my learning. I'd also like to thank my co-mentor Dr. Wingo, who spent hours with me to teach me how to code from the basics, and who has always been someone I can turn to for advice and support. I'm indebted to the formidable members of my Dissertation committee, Dr. Stephen Warren, Dr. Stephanie Sherman, Dr. Michael Gambello, Dr. David Cutler for all their wisdom, insight and encouragement throughout my training. It has been an honor to have them in my committee meetings, and it has been a blessing to receive their scientific insight as well as their concern and care for my holistic development and personal wellbeing.

This page is not enough to hold all of my gratitude and warm feelings towards the Jin lab. Just to name a few, I am thankful for : Dr. Feiran Zhang (my bench-buddy), Dr. Yujing Li and Dr. Yunhee Kang (the great teachers), Junghwa Lim (wonderful fly expert), Zhiqin Wang and Mengli Wang (such helpful and kind friends) as well as Hyerim Kim (lovely friend and "sun-bae").

I'd like to thank all my collaborators inside and outside Emory for their contributions and help throughout this journey, and I thank my medical school advisors Dr. Maura George and Dr. Emily Herndon and their small groups for their support and friendship. Last but not least, I'd like to thank my loving family and treasured friends for their continued love and support, especially my parents, brother, Joo Young Kim, Julie Hwang and Irene Lo who have been praying for me.

Table of Contents

List of Figures 3
List of Tables 6
INTRODUCTION 1
CHAPTER 1 : Untargeted Metabolic profiling of a murine model of Fragile X-Associated Tremor/Ataxia Syndrome 19
ABSTRACT 20
KEYWORDS 20
INTRODUCTION 21
METHODS 23
RESULTS 25
DISCUSSION 33
ACKNOWLEDGEMENTS 35
SUPPLEMENTAL MATERIALS 36
Chapter 2: Sphingolipid pathway modulates the neuronal toxicity associated with Fragile X-Associated Tremor/Ataxia Syndrome 45
ABSTRACT 46
KEYWORDS 47
INTRODUCTION 47
METHODS 48
RESULTS 52
DISCUSSION 58
ACKNOWLEDGEMENTS 63
SUPPLEMENTAL MATERIALS 64
CHAPTER 3: Identification of genetic modifiers of FXTAS by combining whole genome sequencing with fly genetics 71
ABSTRACT 72
KEYWORDS 72
INTRODUCTION 73
METHODS 74
RESULTS 77
DISCUSSION 81

ACKNOWLEDGEMENTS 83
SUPPLEMENTAL MATERIALS 83
CHAPTER 4: Targeting PSMB5 may ameliorate neuronal toxicity in Fragile X-Associated Tremor/Ataxia Syndrome 91
ABSTRACT 92
KEYWORDS 92
INTRODUCTION 93
METHODS 94
RESULTS 99
DISCUSSION 109
ACKNOWLEDGEMENTS 113
SUPPLEMENTAL MATERIALS 113
CHAPTER 5: CONCLUSIONS AND FUTURE DIRECTIONS 119
CONCLUSIONS 120
FUTURE DIRECTIONS 121
REFERENCES 127

List of Figures

Figure 1: Illustration of the main mechanisms of FXTAS pathogenesis. 9

Figure 2: Potential therapeutic strategies for FXTAS 15

Figure 3: Metabolic profiling demonstrates significant metabolic perturbations in the presence of $r(CGG)_{90}$ repeats 25

Figure 4: Representation of the superpathways of metabolism affected in the 200 significantly altered metabolites ($p<0.05$). 26

Figure 5: Representation of the percentage of superpathways of metabolism altered in the 200 significantly altered metabolites ($p<0.05$) out of the total number of metabolites assessed in each superpathway. 26

Figure 6: Altered metabolites by pairwise comparison. 27

Figure 7: Schematic depicting key components of the Purine metabolism pathway and their perturbations in FXTAS vs. WT comparisons. 28

Figure 8: A heatmap showing the metabolite alterations in purine metabolism for young WT, aged WT, young FXTAS, and aged FXTAS mice. 29

Figure 9: IMP Dehydrogenase *(Impdh1)* catalyzes the conversion of IMP to XMP in the rate-limiting step of guanine nucleotide biosynthesis. 30

Figure 10: Schematic depicting key components of the Sphingolipid pathway and their perturbations in FXTAS vs. WT comparisons. 31

Figure 11: A heatmap showing the metabolite alterations in sphingolipid metabolism for young WT, aged WT, young FXTAS, and aged FXTAS mice. 32

Figure 12: Ceramide Synthase *(Cers5 (Schlank))* catalyzes the conversion of Sphingosine to Ceramide. Sphingosine Kinase *(Sphk1 (Sk2))* catalyzes the conversion of Sphingosine into Sphingosine-1-phosphate. 32

Figure 13: Knockdown of *Ras* enhances r(CGG)$_{90}$ mediated neurodegeneration in FXTAS *Drosophila* 54

Figure 14: Knockdown of *Schlank and Sk2* enhance r(CGG)$_{90}$ mediated neurodegeneration in FXTAS *Drosophila* 55

Figure 15: A heatmap depicting the 41 most significantly altered lipids ($p<0.05$) in FXTAS vs. control human postmortem cerebellar tissue. 56

Figure 16: Box plot showing levels of Sphingomyelin (36:2) in FXTAS vs. control postmortem cerebellar tissue. 57

Figure 17: Knockdown of Sphingolipid genes enhances r(CGG)$_{90}$ mediated neurodegeneration in FXTAS *Drosophila* 58

Figure 18: Schematic depicting the analysis workflow from WGS analysis to *Drosophila* screen. 77

Figure 19: *Drosophila* screen identifies 19 genetic modifiers of CGG-associated neurotoxicity. 79

Figure 20: Schematic displaying the location of *PSMB5$^{rs11543947\text{-}A}$ in PSMB5.* 99

Figure 21: PSMB5$^{rs11543947\text{-}A}$ is an eQTL resulting in decreased expression of *PSMB5* mRNA.. 100

Figure 22: Knockdown of *prosbeta5* in gmr-GAL4, UAS-(CGG)$_{90}$ EGFP flies suppresses of CGG-associated neurotoxicity. 101

Figure 23: siRNA knockdown of *Psmb5* results in suppression of CGG associated neurotoxicity in Neuro2A cells 102

Figure 24: Screen of *Drosophila* orthologues of proteasome subunits demonstrates enhancement of four genes, such as *Prosalpha3 (PSMA4), Prosalpha6T (PSMA1), Prosalpha7 (PSMA3), Rpn3 (PSMD3)* upon RNAi knockdown..... 103

Figure 25: Pharmacologic inhibition of Psmb5 with 0.25 nM Ixazomib Citrate results in suppression of CGG associated neurotoxicity in Neuro2A cells..... 104

Figure 26: *PSMB5* Knockdown significantly diminishes RAN translation of *FMR1* 5'UTR CGG repeats. 106

Figure 27: Schematic illustrates a proposed model depicting a potential mechanism of CGG-associated toxicity in FXTAS. 107

Figure 28: Immunoprecipitation of FLAG-DGCR8 shows less *PSMB5* mRNA binds to DGCR8 in the presence of CGG repeats. 108

List of Tables

Table 1 : Eight candidate genes that exhibit modulation of r(CGG)$_{90}$ toxicity in *Drosophila* 53

Table 2: List of 19 human genes and corresponding *Drosophila* orthologues that demonstrated genetic modulation of CGG-associated neurodegeneration in the FXTAS *Drosophila* screen. .. 78

Table 3: Translating Ribosome Affinity Purification Sequencing shows differences in mRNA bound to ribosomes in FXTAS vs. WT. 80

Table 4: PSMB5$^{rs11543947\text{-}A}$ is enriched in delayed onset premutation carriers compared to premutation carriers with early onset of ataxia and tremor. 100

INTRODUCTION

This chapter was originally published in *Frontiers in Cellular Neuroscience*:
Front Cell Neurosci. 2017 May 5;11:128. doi: 10.3389/fncel.2017.00128.

Fragile X-associated tremor/ataxia syndrome (FXTAS) is a neurodegenerative disorder caused by a CGG triplet repeat expansion within the 5' UTR of FMR1. Normally, individuals possess between 5 to 54 CGG repeats, and full mutation CGG repeats greater than 200 lead to the neurodevelopmental disease fragile X syndrome (FXS), which results from the excessive methylation of *FMR1* and loss of FMRP protein (Kremer et al., 1991; Verkerk et al., 1991; Hagerman et al., 2002; Colak et al., 2014). Individuals with 55-200 CGG repeats are referred to as premutation carriers (Cronister et al., 2008).

Over a third of males with an expanded CGG repeat premutation develop FXTAS later in adulthood (Jacquemont et al., 2004), whereas only about 6-15% of female premutation carriers develop FXTAS, most likely due to the protective effect of random X-inactivation (Coffey et al., 2008; Hagerman et al., 2004; Zülhke et al., 2004). Clinically, FXTAS presents with intention tremor, gait ataxia, and other features including parkinsonism, cognitive defects, brain atrophy, and white matter abnormalities on MRI (Jacquemont et al., 2003; Hagerman et al., 2015). Neuropathologically, FXTAS is distinguished by the characteristic ubiquitin-positive intranuclear inclusions in the brain and spinal cord as well as peripheral tissues (Greco et al., 2002; Greco et al., 2006; Gokden et al., 2009; Hunsaker et al., 2011).

Animal models have played a critical role in revealing the mechanisms of FXTAS pathogenesis. FXTAS mouse and *Drosophila melanogaster* models effectively mimic the molecular and cellular alterations and clinical symptoms of FXTAS. Several knock-in and transgenic mouse models are available for studying various aspects of FXTAS pathology

(Bontekoe et al., 2001; Entezam et al., 2007; Hashem et al., 2009; Peier et al., 2002). Aside from obviously elevated *FMR1* mRNA levels, reduced FMRP expression, and intranuclear inclusion formation, mouse models of FXTAS also exhibit abnormal dendritic spine morphology, impaired motor coordination, and cognitive deficits, recapitulating many features of FXTAS patients (Bontekoe et al., 2001; Willemsen et al., 2003; Entezam et al., 2007; Hunsaker et al., 2009; Hukema et al., 2015). In flies, the FXTAS transgenic *Drosophila* model expressing 90 CGG repeats displays locomotor deficits and retinal degeneration (Jin et al., 2003). Animal models allow researchers to investigate pathological mechanisms of FXTAS, identify potential modifiers, and pursue treatment development.

The two widely accepted mechanisms for the pathogenesis of FXTAS are RNA toxicity and RAN protein toxicity (via Repeat Associated Non-AUG or RAN translation). Several lines of evidence support the RNA toxicity mechanism. First, older adults with the full mutation (>200 repeats), who do not express *FMR1* mRNA and lack FMRP, do not develop FXTAS (Feng et al., 1995). Second, in FXTAS, there is significant upregulation (2-8 fold) of the expanded CGG-repeat *FMR1* mRNA, resulting in formation of nuclear RNA aggregates. These aggregates sequester rCGG-binding proteins, preventing them from performing their normal biological functions, such as mRNA transcription and splicing, as well as dendritic mRNA transport (Tassone et al., 2000; Kenneson et al., 2001; Pretto et al., 2014). The level of FMR1 protein in cells from premutation carriers, however, remains relatively unaltered (Tassone et al., 2000; Kenneson et al., 2001). Third, *FMR1* RNA is present in the intranuclear inclusions of postmortem FXTAS brain tissue (Tassone et al., 2004), and animal and cell models expressing rCGG repeats develop similar inclusions (Jin et al., 2003; Willemsen et al., 2003; Arocena et al., 2005). But RNA toxicity alone is not sufficient to account for the large ubiquitin-positive intranuclear inclusions in the brains of FXTAS patients,

a neuropathological hallmark of the disease. In fact, in addition to the RNA-binding proteins, these inclusions contain proteins that do not bind to CGG-repeat mRNA and are reminiscent of the neuronal intranuclear inclusions found in protein-mediated neurodegenerative disorders and polyglutamine diseases (Greco et al., 2006; Iwahashi et al., 2006; Williams and Paulson, 2008). In light of this, a protein-driven mechanism of FXTAS pathogenesis was uncovered, in which the premutation CGG repeat expansion was found to induce RAN translation within the 5' UTR of *FMR1* mRNA via an AUG-independent mechanism (Todd et al., 2013). The resulting polyglycine-containing protein, FMRpolyG, is present in the brains of FXTAS patients and was found to be toxic to human cell lines as well as *Drosophila* neurons, leading to retinal degeneration in FXTAS *Drosophila* (Todd et al., 2013).

To date, CGG repeat-mediated RNA toxicity and RAN protein toxicity stand as the two most important mechanisms in FXTAS pathophysiology, leading to the sequestration of specific proteins and the generation of the toxic protein product FMRpolyG, respectively. Besides these two main mechanisms, others have been uncovered, such as antisense *FMR1* RNA (Ladd et al., 2007), epigenetic modulation, mitochondrial dysfunctions (Hukema et al., 2014), and R-loop-induced DNA damage response (Loomis et al., 2014). Here I summarize the current understanding of the underlying mechanisms of FXTAS and discuss potential therapeutic strategies.

RNA-mediated FXTAS pathogenesis via RBP sequestration

A defining molecular signature of FXTAS is the elevation of premutation *FMR1* mRNA levels with no detectable or only a modest reduction in FMRP protein levels (Tassone et al., 2000; Kenneson et al., 2001; Pretto et al., 2014). Along with the presence of *FMR1* mRNA in ubiquitin-

positive intranuclear inclusions of FXTAS patient brains, these observations point to a toxic RNA gain-of-function mechanism for FXTAS pathogenesis, which could lead to sequestration of various rCGG repeat-binding proteins (Tassone et al., 2004).

Using mass spectrometric analysis combined with immunohistochemical analysis, more than 20 proteins have been identified in inclusions in the frontal cortex of FXTAS patients, including RNA-binding proteins hnRNP A2/B1 and MBNL1, and some neurofilament proteins, such as lamin A/C and α-internexin, which are involved in various neurological disorders (Iwahashi et al., 2006). Pur α and hnRNP A2/B1 are found to bind directly to rCGG repeats in inclusions. In fact, in a *Drosophila* model expressing premutation CGG repeat expansions, overexpression of Pur α and hnRNP A2/B1 leads to suppression of neurodegeneration phenotypes (Sofola et al., 2007; Jin et al., 2007). Sequestration of other proteins, such as CUGBP1, Sam68, Rm62, and DGCR8, leads to altered mRNA splicing and transport, as well as dysregulated microRNAs (Sofola et al., 2007; Sellier et al., 2010; Qurashi et al., 2011; Sellier et al., 2013; Tan et al., 2012a). These findings support a toxic RNA gain-of-function mechanism, which is mediated by the expanded CGG repeats in FMR1.

Heterogeneous nuclear ribonucleoprotein (hnRNP A2/B1) is an RNA-binding protein noted for its presence in intranuclear inclusions of FXTAS patients. hnRNP A2/B1 has been shown to bind directly to rCGG repeats and, interestingly, overexpression of hnRNP A2/B1 and its two homologs in *Drosophila* results in suppression of the neurodegenerative eye phenotype caused by the rCGG repeat (Sofola et al., 2007). hnRNP A2/B1 is also known to mediate the indirect interaction between CGG repeats and CUGBP1, an RNA-Binding Protein (RBP) noted for its binding of CUG repeats and involvement in myotonic dystrophy type 1 (DM1) (Timchenko et al.,

1996; Timchenko et al., 2001; Timchenko et al., 2004). Overexpression of CUGBP1 also suppresses the FXTAS phenotype in *Drosophila* (Sofola et al., 2007). Moreover, Muslimov et al. found that premutation CGG-repeat RNA binds competitively to hnRNP A2/B1 and leads to the alteration of neuronal RNA dendritic transport, which can be partially reversed by overexpression of hnRNP A2 (Muslimov et al., 2011). Furthermore, our group has shown that in a *Drosophila* model, rCGG repeats trigger the activation of certain retrotransposons, such as gypsy. We also demonstrated that hnRNP A2/B1 may regulate the activation of gypsy by recruiting heterochromatin protein 1(HP1) for transposon silencing. As a result, in FXTAS, the expanded rCGG repeats may sequester hnRNP A2/B1 and diminish the recruitment of HP1 to genomic regions containing retrotransposons, further contributing to retrotransposon activation (Tan et al., 2012b). Significantly, we also found that hnRNP A2/B1 regulates expression of miR-277, a miRNA that, when overexpressed, results in enhancement of rCGG repeat-mediated neurodegeneration (Tan et al., 2012a).

Also present in intranuclear inclusions of FXTAS patients, Pur α is an RNA- and specific single-stranded DNA-binding protein that plays an essential role in DNA replication, neuronal mRNA transport, and translation. Pur α knockout mice display developmental delay along with severe tremor and spontaneous seizures at two weeks after birth, and the expression and distribution of axonal and dendritic proteins are also altered (Khalili et al., 2003; Hokkanen et al., 2012). Similar to hnRNP A2/B1, Pur α has been implicated in FXTAS pathogenesis due to the fact that overexpression of Pur α in a *Drosophila* model results in dose-dependent suppression of rCGG-mediated neurodegeneration.

Probing the Pur α interactome has also led to the identification of Rm62 as a possible mediator of FXTAS pathogenesis. Rm62 was identified via a proteomic approach as a potential regulator of rCGG-mediated neurodegeneration (Qurashi et al., 2011). Rm62 is the *Drosophila* ortholog of p68 RNA helicase, a transcriptional regulator that is also involved in pre-mRNA splicing, RNA interference, and nucleocytoplasmic shuttling (Bond et al., 2001; Ishizuka et al., 2002; Lin et al., 2005; Liu et al., 2002; Wilson et al., 2004). In FXTAS *Drosophila*, rCGG repeats diminish post-transcriptional expression of Rm62, and overexpression of Rm62 can suppress the neuronal toxicity caused by the premutation rCGG repeats (Qurashi et al., 2011). The decrease in Rm62 expression in turn leads to the nuclear accumulation of mRNAs involved in stress and immune responses, as well as the accumulation of Hsp70 mRNA, a target of Rm62 (Qurashi et al., 2011), which has actually been found in inclusions from both human FXTAS brains and animal models of FXTAS (Jin et al., 2003).

The alternative splicing regulator Src-Associated substrate during mitosis of 68-kDa (Sam68) is another RBP shown to be sequestered by rCGG repeats. One study revealed that Sam68 colocalizes with the giant dynamic aggregates that form from mRNAs containing expanded CGG repeats in both premutation CGG-expressing cells and FXTAS patient brain sections (Sellier et al., 2010). The sequestration of Sam68 results in the loss of its ability to perform splicing regulation and causes pre-mRNA alternative splicing misregulation in CGG-transfected cells and FXTAS patients (Sellier et al., 2010). Sam68 localization is regulated by tyrosine phosphorylation, and the phosphatase inhibitor tautomycin was shown to prevent aggregation of both Sam68 and CGG RNA (Sellier et al., 2010). Taken together, the sequestration of Sam68 must play a role in FXTAS pathogenesis via a splicing alteration mechanism.

TAR DNA-binding protein (TDP-43) is an amyotrophic lateral sclerosis (ALS)-associated RBP, a marker of neurodegeneration commonly found in inclusions in ALS (Baloh 2012). In the cerebellar Purkinje neurons of mice expressing 90 CGG repeats, the mRNA for *Tardbp*, which encodes TDP-43, showed a reduced association with ribosomes (Galloway et al., 2014). In the same study, the authors went on to find that in the *Drosophila* model of FXTAS, wild-type TDP-43 expression leads to suppression of neurodegeneration, while knockdown of the endogenous *Tardbp* fly ortholog, *Tbph*, enhanced the eye phenotype. Another study also independently reported that TDP-43 suppresses CGG repeat-induced toxicity in a Drosophila model of FXTAS (He et al., 2014). Interestingly, this suppression was shown to depend on hnRNP A2/B1, such that deletion of the C-terminal domain of TDP-43 and thereby the prevention of interactions with hnRNP A2/B1 led to abrogation of the TDP-43-dependent rescue of CGG repeat toxicity (He et al., 2014).

The DiGeorge syndrome critical region 8 (DGCR8) is yet another protein reported to bind to premutation rCGG repeats and cause partial sequestration of DGCR8 and its partner, DROSHA, within the premutation RNA aggregates (Sellier et al., 2013). DGCR8 and DROSHA play a critical role in microRNA biogenesis. In the first step of microRNA biogenesis, RNA polymerase II transcribes miRNAs as primary miRNA (pri-miRNA) transcripts. DROSHA, a type III RNase, is anchored to the pri-miRNA by DGCR8, and processes pri-miRNA into precursor miRNA (pre-miRNA) (Lee et al., 2003; Denli et al., 2004; Landthaler et al., 2004; Gregory et al., 2004; Han et al., 2004). Sellier et al. found that the sequestration of DGCR8 and DROSHA precludes them from their normal functions, leading to reduced processing of pri-miRNAs in cells expressing expanded CGG repeats and also in the brains of FXTAS patients. Consequently, levels of mature miRNAs are reduced (Sellier et al., 2013). The authors also found evidence that sequestration of SAM68 in

the CGG aggregates is mediated through DROSHA or DGCR8, but restoration of SAM68 function is not sufficient to restore all normal neuronal cell functions. In contrast, expression of DGCR8 alone in cultured premutation mouse cortical neurons could rescue their dendritic morphological abnormalities and diminished neuronal viability. This work suggested a model for the mechanism of FXTAS pathogenesis in which sequestration of the DROSHA-DGCR8 microprocessor by expanded rCGG repeats may lead to reduced mature miRNA expression, resulting in neuronal cell dysfunction and degeneration.

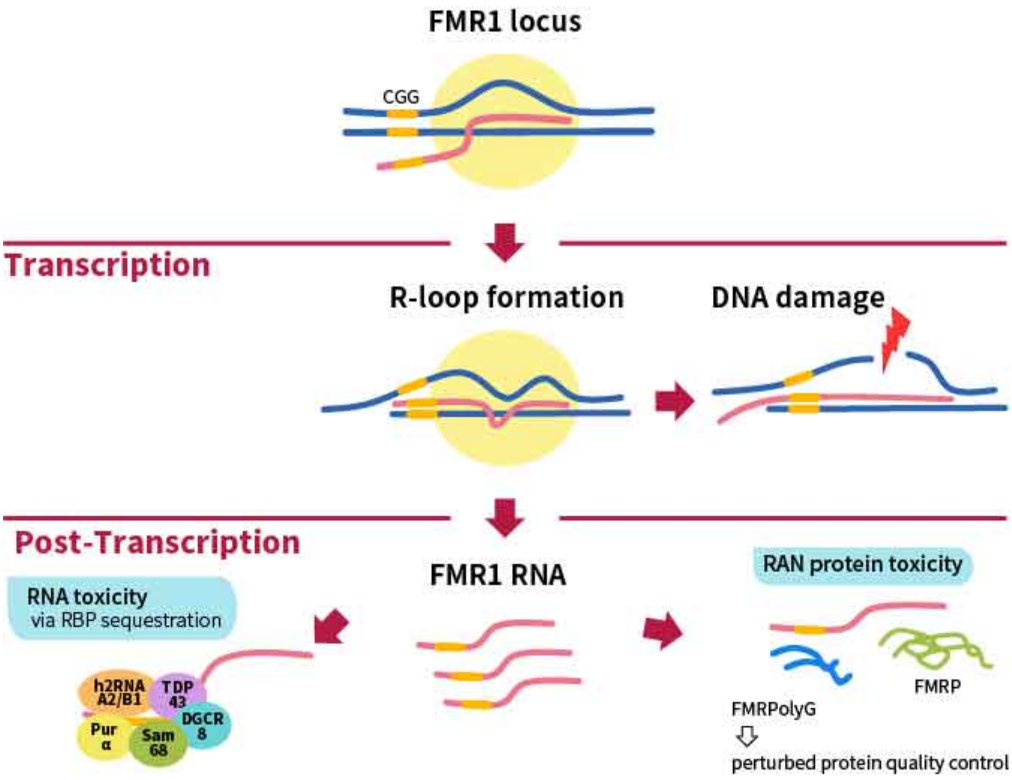

Figure 1: Illustration of the main mechanisms of FXTAS pathogenesis.
During transcription of the *FMR1* locus, the formation of RNA:DNA hybrid R-loops through GC interaction of the expanded CGG repeats (depicted by yellow bar) can activate the DNA damage response and result in DNA breaks and the accumulation of γH2AX. The two main mechanisms linked to FXTAS pathology are post-transcriptional. In the RNA toxicity mechanism, RNA-binding proteins are sequestered by the expanded CGG repeats, such as h2RNA A2/B1, Pur α, Sam68, TDP43, and DGCR8; these are illustrated together for figurative purposes but do not necessarily form a complex simultaneously. In the RAN protein toxicity mechanism, the expanded CGG repeat induces AUG-independent RAN translation of FMRpolyG, which is found to form inclusions in patient brains as well as animal models of FXTAS. Other mechanisms not shown in this figure include the antisense transcript *ASFMR1*, mitochondrial dysfunction, and 5hmC-mediated epigenetic modulation in FXTAS (Kong et al, 2017).

In summary, I have presented a broad overview of the RNA-binding proteins (RBPs) that are sequestered via the RNA toxicity mechanism, as well as our current limited understanding of the downstream effects of sequestration (Figure 1). The challenge remains to bring the pieces of the puzzle together to figure out how the sequestration of the RBPs interplay to cause FXTAS pathology (Hagerman 2012).

RAN translation in FXTAS pathogenesis

In FXTAS pathogenesis, RAN protein toxicity plays a synergistic role with the RNA toxicity mechanism and offers a potential explanation for the presence of non-RBPs in the distinctive ubiquitin-positive intranuclear inclusions found in the brains of FXTAS patients. First discovered in CAG expansion constructs, RAN translation initiates in an AUG-independent manner and is known to occur in several repeat expansion disorders, among them Spinocerebellar Ataxia type 8 (SCA8), Myotonic Dystrophy type 1 (DM1) Frontotemporal Dementia (FTD), and Amyotrophic Lateral Sclerosis (ALS), as well as FXTAS (Zu et al., 2011, Ash et al., 2013, Mori et al., 2013, Zu et al., 2013). RAN translation initiation requires an m^7G cap, the EIF4A helicase, and 40S ribosomal scanning and is strongly influenced by repeat length (Kearse et al., 2016). In CGG-induced RAN translation of *FMR1* mRNA, initiation of translation is similar to canonical translation but only 30-40% as efficient. The expanded premutation CGG repeat expansion induces AUG-independent RAN translation of FMRpolyG, which accumulates in the ubiquitin-positive intranuclear inclusions in transfected cells, FXTAS Drosophila, mouse models, and patient brains (Todd et al., 2013). Out of three possible reading frames in the 5' UTR of *FMR1*, RAN translation occurs in both the glycine (+1 frame) and alanine (+2 frame) reading frames, producing the FMRpolyglycine and FMRpolyalanine proteins, respectively, with no polyarginine product (+0

frame) detected as yet (Todd et al., 2013). However, only the polyglycine-containing protein, FMRpolyG, is detected in both cultured cells and animal models of FXTAS, and most importantly, in inclusions in FXTAS patient brains (Todd et al., 2013). Moreover, the expression of FMRpolyG is known to be toxic to *Drosophila* neurons, leading to retinal degeneration that can be enhanced by increasing FMRpolyG product and suppressed by eliminating RAN translation (Todd et al., 2013).

To determine the mechanism by which FMRpolyG production may contribute to FXTAS pathogenesis, Oh et al. (2015) examined ubiquitin-proteasome system (UPS) impairment in *Drosophila* and cell models of CGG repeat-induced toxicity. UPS impairment in FXTAS *Drosophila* led to enhanced neurodegeneration, whereas overexpression of HSP70 suppressed this toxicity. Furthermore, in cell models, the expression of FMRpolyG increased induction of UPS impairment, whereas prevention of RAN translation resulted in diminished UPS impairment (Oh et al., 2015). These findings indicate that RAN translation-induced FMRpolyG production may drive FXTAS pathogenesis by perturbing the protein quality control pathway through UPS failure (Oh et al., 2015).

Recently, researchers found that RAN translation also occurs from antisense *FMR1* transcript containing CCG repeats from three different potential reading frames generating polyproline, polyarginine, and polyalanine proteins. More importantly, these novel proteins are found to colocalize with ubiquitinated intranuclear inclusions in FXTAS patient neurons. These new findings provide additional support for RAN protein toxicity in FXTAS pathophysiology (Krans et al., 2016).

Other mechanisms of FXTAS pathogenesis

R-loop-mediated DNA damage

In addition to post-transcriptional changes, there is evidence to suggest that the increase in FXTAS *FMR1* RNA transcript results in molecular dysfunction at the transcriptional level. Loomis et al. have found that, upon transcription of the endogenous *FMR1* locus, the nascent G-rich RNA transcribed from the GC-rich region of *FMR1* 5' UTR binds to the C-rich DNA template and forms a stable RNA:DNA hybrid, or R-loops (Reddy et al., 2011; Loomis et al., 2014). Notably, R-loop formation can be increased by enhanced transcription (Loomis et al., 2014). Excessive R-loop formation activates the DNA damage response and leads to DNA breaks, resulting in accumulation of γH2AX, a histone variant associated with DNA damage repair that is also present in the inclusions of FXTAS patient neurons (Hoem et al., 2011; Iwahashi et al., 2006). These results clearly show that FXTAS pathology from the RNA toxicity mechanism may also occur co-transcriptionally via increased R-loop formation upon increased *FMR1* transcription, leading to subsequent DNA damage.

Antisense transcript: ASFMR1

A lasting conundrum in the pathogenesis of FXTAS is that only a fraction of male premutation carriers develop FXTAS (Jacquemont et al., 2004), and there is considerable variability in the phenotype of FXTAS patients. Such observations raise the likelihood that *FMR1* is not the sole gene responsible for FXTAS pathogenesis. In the search for alternate gene involvement, Ladd et al. identified an antisense transcript spanning the *FMR1* CGG repeat region in the antisense direction, which they dubbed the antisense transcript at the *FMR1* locus, *ASFMR1*

(Ladd et al., 2007). Congruous to *FMR1, ASFMR1* is upregulated in premutation carriers but silenced in the full-mutation range. Following transcription, *ASFMR1* is spliced, and then transported to the cytoplasm. *ASFMR1* transcription is driven by two alternative promoters: the *FMR1* bidirectional promoter and the promoter in the second intron of *FMR1*. The latter is considered to be the major promoter in cells with premutation alleles and drives the transcription of the transcript, which spans the CGG repeat of the *FMR1* gene in the CCG orientation and exhibits premutation-specific alternative splicing (Ladd et al., 2007). These findings suggest that *ASFRM1* is also implicated in the pathogenesis of FXTAS.

Mitochondrial dysfunction

There is also evidence to indicate that *FMR1* premutation-associated disorders, such as FXTAS and fragile X-associated primary ovarian insufficiency (FXPOI), involve mitochondrial dysfunction. Using doxycycline (dox)-inducible transgenic mouse models expressing 90 CGGs in the RNA, Hukema et al. have found that dox-induced 90 CGG RNA-expressing mice not only experience loss of weight, death within five days, steatosis, and apoptosis in the liver, but that they also show altered expression of GPX1 and cytochrome C, markers of mitochondrial dysfunction (Hukema et al., 2014). Mitochondrial dysfunction is also seen in FXTAS human patients and mouse cultured cells. Along with decreased oxidative phosphorylation capacity, there is a defect in the import of mitochondrial proteins in premutation carriers (Napoli et al., 2011). Hippocampal neuronal cultures from premutation CGG knock-in mice exhibit mitochondrial abnormalities in the number, metabolic function, and mobility of mitochondria (Kaplan et al., 2012). Mitochondrial abnormalities are also seen in granulosa cells and oocytes in a FXPOI mouse model, including reduced mitochondrial content, abnormal mitochondrial structure, and decreased expression of the

mitochondrial genes *Mfn2* and *Opa1* (Conca Dioguardi et al., 2016). Hence, these findings point to mitochondrial dysfunction as another possible component of FXTAS pathology.

5-hydroxymethylcytosine (5hmC)-mediated epigenetic modulation

Though initially regarded as only an intermediate of active DNA demethylation products (Pfaffeneder, T. et al., 2011), 5-hydroxymethylcytosine (5hmC) has gained attention more recently as an epigenetic modification with a significant role in processes like neurodevelopment and differentiation (Branco et al. 2011). 5hmC is converted from 5mC via catalysis by Ten-eleven translocation 1 (TET1), a 2-oxoglutarate (2OG)- and Fe (II)-dependent enzyme (Tahiliani et al., 2009). Our group has examined the global levels of 5hmC in the cerebella of rCGG mice compared to wild-type age-matched littermate controls (Yao et al., 2014.) Significantly, 5hmC was reduced genome-wide in the cerebella of the rCGG mice, while several repetitive elements as well as cerebellum-specific enhancers exhibited increases in 5hmC levels. The differential 5-hydroxymethylated regions (DhMRs) were highly correlated with genes and transcription factors that play key roles in neuronal development. While these data support 5hmC-mediated epigenetic modulation as a player in FXTAS pathogenesis, further studies, such as characterizing the level of 5hmC at the *FMR1* locus, are warranted to reveal more about the role of the 5hmC mark in the pathogenic mechanism of FXTAS (Al-Mahdawi et al., 2014).

Therapeutic developments

As there are still no effective treatment options for FXTAS, current therapeutic strategies are limited mainly to treatments aimed at ameliorating specific symptoms of FXTAS patients.

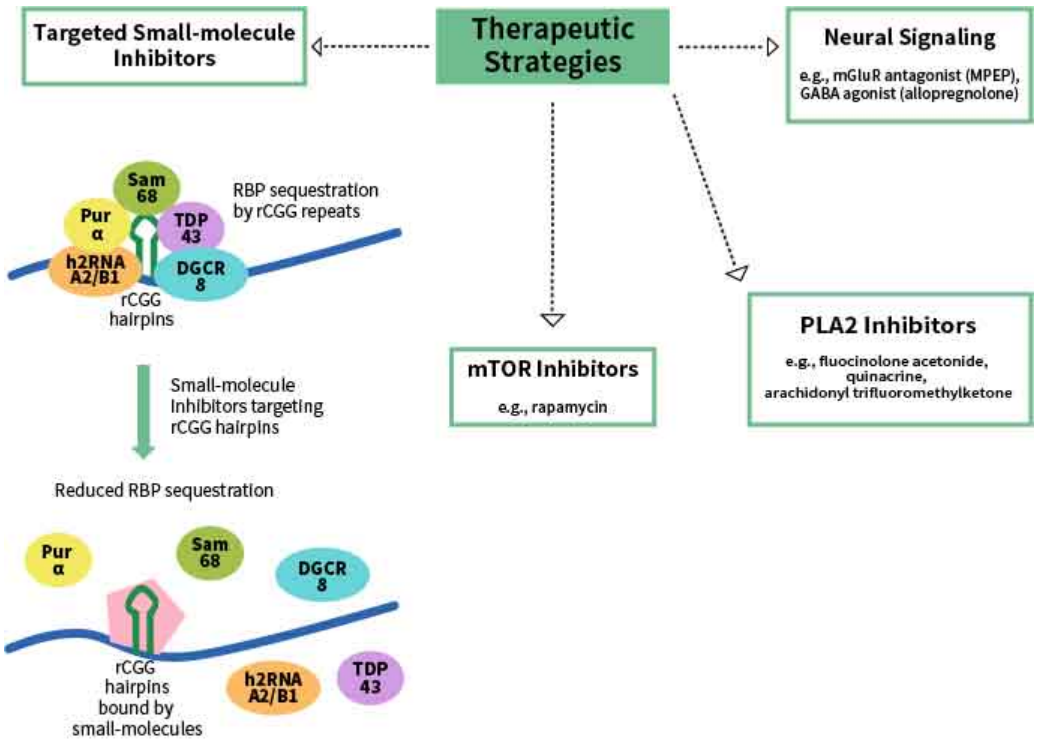

Figure 2: Potential therapeutic strategies for FXTAS

To date, there are no treatments available for FXTAS. Therapeutic strategies explored include targeting the RBP sequestration mechanism of FXTAS pathogenesis, such as via the use of small-molecule inhibitors that bind to CGG hairpins with high affinity, thereby reducing the sequestration of the RBPs (Disney et al., 2012). Other potential targets include the mTOR inhibitor rapamycin, phospholipase A2 (PLA2) inhibitors, an mGluR antagonist (MPEP), and a GABA agonist (allopregnanolone) (Kong et al, 2017).

Selective serotonin and norepinephrine reuptake inhibitors have been effective for anxiety and depression (Hagerman et al., 2015). Psychosis and tremor can be improved by atypical antipsychotics, such as propranolol and primidone (Muzar et al., 2014; Zesiewicz et al., 2005). Although the NMDA receptor antagonist memantine, an FDA-approved compound for the treatment of Alzheimer's disease, did not show any significant improvement on tremors, balance problems, or executive function deficits in FXTAS patients compared to placebo (Seritan et al., 2014), verbal memory was improved when assessed by the event-related potential (ERP) paradigm in a subgroup of patients in a recent clinical trial (Yang et al., 2016a). At the same time, however, the end goal is not mere symptomatic treatment, but rather effective treatments that target the

pathogenic mechanism(s) of disease. Here we discuss some ongoing efforts to identify potential compounds and therapeutic targets in FXTAS both *in vitro* and *in vivo* (Figure 2).

MPEP and allopregnanolone, an mGluR antagonist and a GABA agonist, respectively, are potential therapeutics that may mitigate some of the RNA toxicity effects. Cortical astrocytes from mice expressing premutation CGG repeats display decreased expression of Glu transporters (GLT-1 and GLAST) and Glu uptake, and enhanced spontaneous asynchronous Ca^{2+} oscillations (Cao et al., 2013). An mGluR5 antagonist, 2-methyl-6-(phenylethynyl) pyridine hydrochloride (MPEP), suppresses the intracellular Ca^{2+} increase induced by Glu (Cao et al., 2012; Cao et al., 2013). Although MPEP is neurotoxic to humans and cannot be used for therapy, these results shed light on Glu transport and Ca^{2+} signaling as potential targets for treatment. The natural neurosteroid allopregnanolone is a GABA signaling agonist, and it was found to ameliorate the clustered burst firing in hippocampal neurons from mice with *FMR1* premutation alleles (Reddy et al., 2012; Cao et al., 2012). Allopregnanolone exhibits effective rescue in Alzheimer's disease mouse models and human cells, such as restoring learning and memory, in addition to improving neuronal proliferation and survival (Wang et al., 2010; Chen et al., 2011; Singh et al., 2012). Allopregnanolone is already in use in Alzheimer's disease and traumatic brain injury clinical trials, making it a very likely treatment choice for FXTAS (Lozano et al., 2015).

In a chemical screen of efficient small molecules to suppress locomotion deficits and neurodegeneration of FXTAS *Drosophila*, several phospholipase A2 (PLA2) inhibitors were found to have significant effects, namely fluocinolone acetonide, quinacrine, and arachidonyl trifluoromethyl ketone. These findings suggest a role for altered PLA2 activity in FXTAS and present a potential therapeutic target (Qurashi et al., 2012). Another potential target is the

mammalian target of rapamycin (mTOR). Although the mTOR inhibitor rapamycin was shown to suppress neurotoxicity via autophagy activation in various neurodegenerative disease animal models, it can also enhance the neurodegeneration phenotypes in FXTAS *Drosophila*, such as aggravation of retinal degeneration and locomotion defects, as well as a shorter lifespan of flies (Lin et al., 2013). In contrast, genetic activation of mTOR signaling significantly suppresses the neurodegeneration phenotype (Lin et al., 2013).

Although a number of therapeutic strategies are being explored that specifically target some of the underlying pathogenic mechanisms of FXTAS discussed above, as of now targeted therapeutic development is far from clinical trials. Small molecules are being developed with a high affinity for rCGG hairpins that inhibit target proteins from binding to rCGG hairpins *in vitro*, thereby reducing the sequestration of RBPs by rCGG (Disney et al., 2012). Some compounds, such as 9-hydroxy-5,11-dimethyl-2-(2-(piperidin-1-yl)ethyl)-6H-pyrido[4,3-b]carbazol-2-ium, improve pre-mRNA splicing deficits and reduce the number and size of CGG protein aggregates in FXTAS cells (Disney et al., 2012; Tran et al., 2014). Moreover, most recently, Yang et al. reported the generation of designer, modularly assembled small molecules that bind rCGG expanded repeats and potently improve FXTAS-associated defects in cells (Yang et al., 2016b).

Finally, in addition to small molecules, the histone acetyltransferase inhibitors garcinol and anacardic acid have also been pursued as potential therapeutics for FXTAS. In an effort to understand why there is *FMR1* mRNA buildup in FXTAS pathology, Todd et al. examined histone acetylation at the human *FMR1* locus (Todd et al., 2010) and found, interestingly, that histone acetylation was increased at the *FMR1* locus in premutation carriers compared to control or FXS-derived cell lines, which correlated with increased *FMR1* mRNA levels in premutation cell lines.

This study went on to show that in premutation carrier cell lines, the histone acetyltransferase (HAT) inhibitors garcinol and anacardic acid can repress *FMR1* mRNA expression down to the level of control and can also extend the lifespan of *Drosophila* expressing the CGG repeat expansion (Todd et al., 2010). Based on these results, a novel mechanism was posited for the increased premutation *FMR1* mRNA in FXTAS pathology. According to the proposed model, the expanded CGG repeats in FXTAS induces chromatin remodeling in cis, which leads to increased expression of *FMR1* mRNA. This study provides the basis for a new potential therapeutic strategy for FXTAS by using HDACs to control the increased expression of *FMR1* mRNA-containing expanded CGG repeats. Although it would be a challenge to bring these compounds to the bedside in the immediate future, development of these compounds enriches our understanding of therapeutic targets and extends the frontier of therapeutic development.

CHAPTER 1: Untargeted Metabolic profiling of a murine model of Fragile X-Associated Tremor/Ataxia Syndrome

This chapter was originally published in *Human Molecular Genetics*:
Hum Mol Genet. 2019 Mar 15;28(6):980-991. doi: 10.1093/hmg/ddy410.

ABSTRACT

Fragile X-Associated Tremor/Ataxia Syndrome (FXTAS) is an adult-onset neurodegenerative disorder that affects premutation carriers (55–200 CGG repeats) of the *Fragile X Mental Retardation 1* (*FMR1*) gene. Much remains unknown regarding the metabolic alterations associated with FXTAS, especially in the brain, and the most affected region, the cerebellum. Investigating the metabolic changes in FXTAS will aid in the identification of biomarkers as well as in understanding the pathogenesis of disease. To identify the metabolic alterations associated with FXTAS, we took advantage of our FXTAS mouse model that expresses 90 CGG repeats in cerebellar Purkinje neurons and exhibits the key phenotypic features of FXTAS. We performed untargeted global metabolic profiling of age-matched control and FXTAS mice cerebella at 16-20 weeks and 55 weeks. Out of 506 metabolites measured in cerebellum, we identified 186 metabolites that demonstrate significant perturbations due to the $(CGG)_{90}$ repeat ($p<0.05$), and we found that these metabolic perturbations increase dramatically with age. A broad range of classes of metabolites were affected in FXTAS, including energy, lipids, carbohydrates and nucleotides. In particular, we found that Sphingolipid and Purine metabolic pathways were significantly perturbed in FXTAS.

KEYWORDS

Metabolomics, FXTAS, Sphingolipid, Purine

INTRODUCTION

Fragile X-associated tremor/ataxia syndrome (FXTAS) is a late-onset neurodegenerative disorder characterized by intention tremor, cerebellar ataxia, brain atrophy and parkinsonism (Hagerman and Hagerman, 2015; Jacquemont et al., 2003). Neuropathologically, FXTAS is defined by ubiquitin-positive intranuclear inclusions in neurons and astrocytes of the brain, as well as Purkinje neurons of the cerebellum (Ariza et al., 2016; Greco et al., 2006). The cerebellum is significantly affected in this disease, as demonstrated by Purkinje cell loss and axonal degeneration (Greco et al., 2002). FXTAS is distinct from other causes of tremor and ataxia in that it is found in carriers of the premutation, individuals with 55-200 expanded CGG repeats in the 5'UTR of *FMR1*. Typically, individuals carry 5-54 CGG repeats, and individuals who harbor greater than 200 CGG repeats in *FMR1* develop fragile X syndrome (FXS) due to methylation-mediated silencing of *FMR1* transcription and translation (Colak et al., 2014; Hagerman and Hagerman, 2002; Kremer et al., 1991; Verkerk et al., 1991). Premutation carriers are found quite frequently in the population, with an estimated prevalence of 1:259 women and 1:813 men (Dombrowski et al., 2002; Rousseau et al., 1995). Interestingly, only a proportion of premutation carriers develop FXTAS; approximately 40% of males and 16% of females develop FXTAS in late adulthood (Hagerman and Hagerman, 2015; Jacquemont et al., 2004). The incomplete penetrance of FXTAS has puzzled researchers and clinicians for over a decade and identifying the molecular basis of FXTAS pathogenesis will allow us to identify biomarkers to predict who will develop disease and will significantly advance efforts to develop treatment.

Since the identification of FXTAS in 2001 (Hagerman et al., 2001), various animal models have been developed to study the molecular and genetic basis of FXTAS. In addition to knock-in

mouse models that are available (Bontekoe, 2001; Entezam et al., 2007), we generated a murine model of FXTAS that expresses r(CGG)$_{90}$ in the context of *FMR1* in Purkinje neurons (Hashem et al., 2009).

Investigations into the molecular basis of the pathogenesis of FXTAS have only recently focused on metabolic changes associated with FXTAS. Metabolism encompasses all the essential aspects of life; chemical reactions catalyzed by enzymes are responsible for providing the power, energy and building blocks to sustain the growth and maintenance of living cells. Through metabolomics, we are able to sensitively measure and analyze the levels of metabolites and obtain a snapshot of the physiological state of the organism (Roessner and Bowne, 2009). Other studies have used metabolomics to gauge the global responses to external factors such as stress, to profile the global metabolic characteristics in a disease state (Van Assche et al., 2015; Burté et al., 2017; Johansen et al., 2009), generate hypotheses to uncover mechanisms of disease pathogenesis (Patti et al., 2012), or identify biomarkers of disease (Havelund et al., 2017; Mielke and Lyketsos, 2010; Peng et al., 2015).

Studying the metabolomics of FXTAS is of interest because metabolic alterations have been identified in other neurodegenerative CNS disorders such as Alzheimer's, Huntington's and Parkinson's Diseases (Burté et al., 2017; Johansen et al., 2009; Mastrokolias et al., 2016; Trushina et al., 2013). In addition to using human patient samples, metabolomics studies on animal disease models have proven to be advantageous for the study of neurodegenerative diseases. Model organisms present a more simplified and accessible system to study the metabolic changes in disease, especially in tissues such as the brain, for which an ample quantity of human samples is

challenging to acquire. Model systems also avoid the problem of genetic heterogeneity in human samples.

A recent study by Giulivi et al. evaluated the plasma metabolic profiles of human premutation carriers and controls, and reported that FXTAS premutation carriers exhibited mitochondrial dysfunction, markers of neurodegeneration and pro-inflammatory damage (Giulivi et al., 2016a). However, as of yet, there has been no published study investigating the metabolic changes associated with FXTAS in the cerebellum, the most affected tissue in FXTAS. Here, we take advantage of the FXTAS murine model to expand our understanding of metabolic alterations in FXTAS by comparing the metabolites in the cerebellum of FXTAS mice expressing $r(CGG)_{90}$ in Purkinje cells with wildtype mice. In particular, we demonstrate that significant metabolic changes occur in sphingolipid and purine metabolism in the cerebella of FXTAS mice.

METHODS

Animals

FXTAS mice expressing human *FMR1* $r(CGG)_{90}$ repeat in Purkinje neurons (published previously; (Hashem et al., 2009)) and wildtype control littermates were housed, maintained, and euthanized according to Institutional Animal Care and Use Committee guidelines at Emory University and Baylor College of Medicine.

Sample preparation for Metabolomics

For each of the 4 groups (young WT (16-20 wk.), aged WT (55 wk.), young FXTAS (16-20 wk.), and aged FXTAS (55 wk.)), cerebellum tissue was collected from 9 mice and kept at -80°C. A total of 36 mice cerebellum tissues were sent for untargeted biochemical profiling at Metabolon, Inc. (Morrisville, NC). After the samples were homogenized and subjected to

methanol extraction, they were split into aliquots for analysis by ultrahigh performance liquid chromatography/mass spectrometry (UHPLC/MS) in the positive (two methods: Pos Early and Pos Late) and negative (two methods: Neg and Polar) mode methods (Bridgewater BR et al., 2014).

Metabolomics Compounds identification and quantification

Raw data was extracted, peak-identified and QC processed using Metabolon's hardware and software as previously described (DeHaven et al., 2010). Compounds were identified by comparison to library entries of purified standards, based on the retention time/index (RI), mass to charge ratio (m/z) and chromatographic data (including MS/MS spectral data). Library matches for each compound were checked for each sample and corrected if necessary. Peaks were quantified using area-under-the-curve. The biochemical data were normalized to mass:volume extraction ratio, missing values were imputed with minimum observed values for each compound and the results were median-scaled.

Statistical Analysis of Metabolites

Two-way ANOVA models were tested. Post hoc pairwise comparisons were used to identify significantly altered biochemicals differentiating the experimental groups ($p < 0.05$). The analysis was conducted using log transformed data in ArrayStudio, version 7.2 (OmicsSoft Corporation, Research Triangle Park, NC).

RESULTS

Figure 3: Metabolic profiling demonstrates significant metabolic perturbations in the presence of r(CGG)$_{90}$ repeats
A heatmap of the top 93 most significantly altered metabolites ($p<0.005$) distinguishes the FXTAS and WT mouse cerebellum samples. For the complete heatmap of 200 significantly altered metabolites ($p<0.05$), see Supplementary Figure 1. Heatmap was generated using average linkage hierarchical clustering in Heatmapper (Babicki et al., 2016). *Red* indicates high and *green* indicates low intensity of the metabolite relative to the median (*black*). Names of the corresponding metabolites are coded in color to represent the appropriate superpathway: Lipid (blue), Amino acid (red), Nucleotide (yellow), Carbohydrate (orange), Energy (purple), Cofactors and Vitamins (navy), Peptide (gray), and Xenobiotics (black).

Metabolic profiling demonstrates significant metabolic perturbations in the presence of r(CGG)$_{90}$, especially during aging

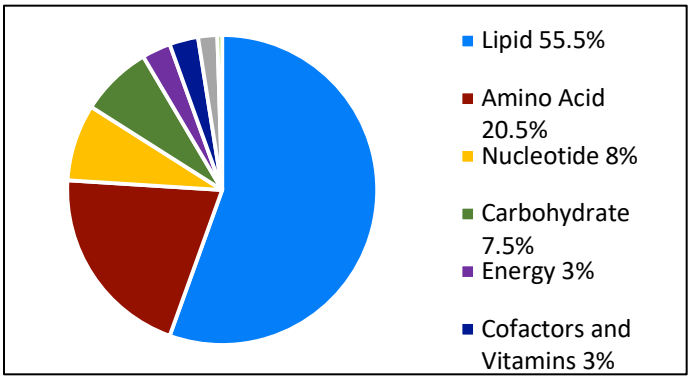

Figure 4: Representation of the superpathways of metabolism affected in the 200 significantly altered metabolites (p<0.05).

In order to identify the metabolic alterations that are associated with CGG toxicity and progression of FXTAS, we performed untargeted global metabolic profiling of wildtype and FXTAS mice at 16-20 weeks and 55 weeks. The FXTAS mice express a human FMR1 r(CGG)$_{90}$ repeat in Purkinje neurons and wildtype littermates were used as controls (Hashem et al., 2009). Out of 506 metabolites identified, 200 showed significant alterations ($p<0.05$) in the post hoc pairwise comparisons of an ANOVA model when comparing aged WT vs. young WT, aged FXTAS vs. young FXTAS, young FXTAS vs. young WT and aged FXTAS vs. aged WT (Supplementary Figure S1, Table S1). The 93 most significantly altered metabolites ($p<0.005$) are shown in Figure 3. Greater than half of the 200 altered metabolites were lipids, followed by amino

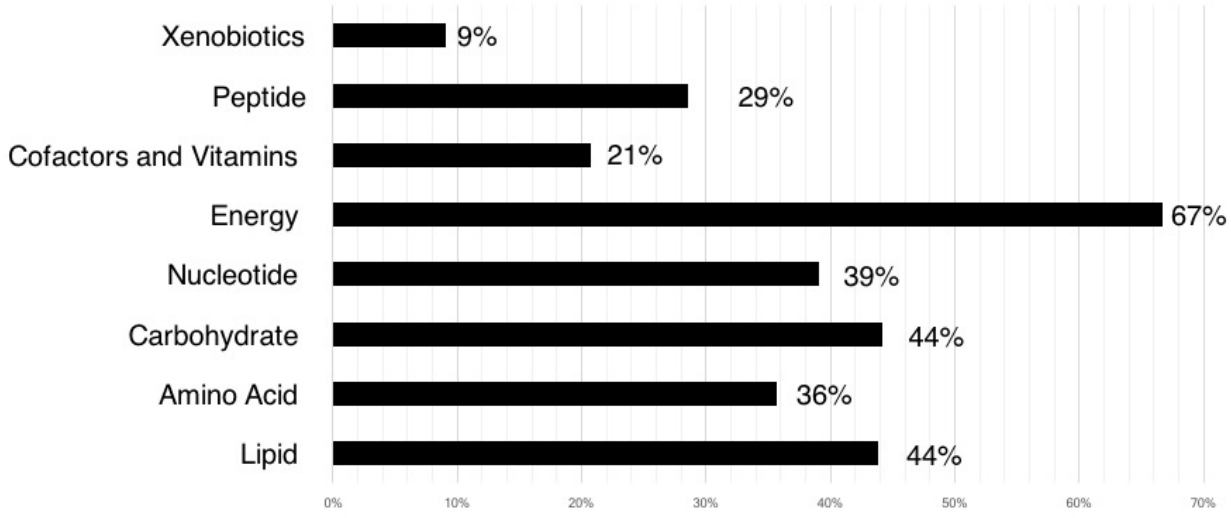

Figure 5: Representation of the percentage of superpathways of metabolism altered in the 200 significantly altered metabolites (p<0.05) out of the total number of metabolites assessed in each superpathway.

The corresponding fractions are as follows: Xenobiotics (1/11), Peptide (4/14), Cofactors and Vitamins (6/29), Energy (6/9), Nucleotide (16/41), Carbohydrate (15/34), Amino Acid (41/115), Lipid (111/253).

acids, nucleotides and carbohydrates (Figure 4). We also identified the proportion of each superpathway that is significantly altered in the ANOVA contrasts ($p<0.05$) out of the total metabolites assessed per pathway (Figure 5). Intriguingly, examining all the proportion of metabolites altered, energy was the most affected superpathway, with 6 out of 9 energy-related metabolites in the cerebellum being altered, followed by carbohydrates (15 out of 34), and lipids (111 out of 253) (Figure 5).

We used an UpSet plot (Figure 6) to summarize the significantly altered metabolites that

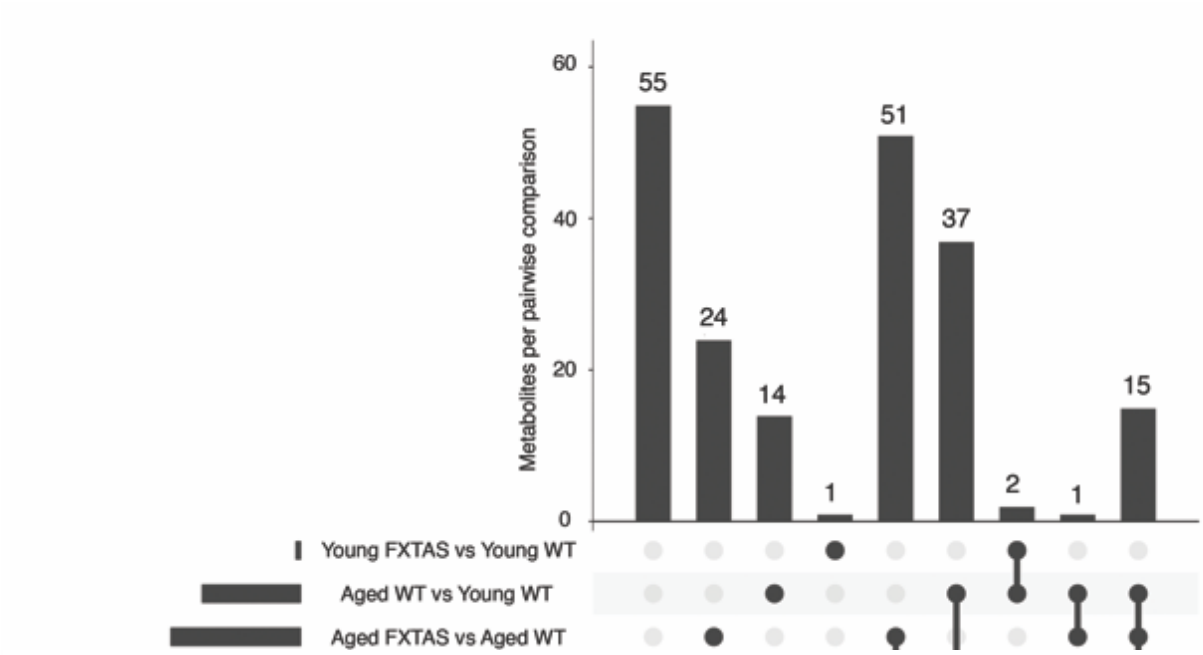

Figure 6: **Altered metabolites by pairwise comparison.**

An UpSet plot was generated in R to visualize the metabolites altered in each comparison (Conway et al., 2017).The horizontal bars indicate the total number of metabolites per pairwise comparison. The vertical bars indicate the number of metabolites in each combination of pairwise comparisons.

are unique to each comparison as well as the altered metabolites that are seen in multiple comparison groups. Importantly, only 1 metabolite was altered uniquely in young FXTAS vs. young WT mice, demonstrating that early in the disease, there are minimal metabolic alterations due to the presence of the $r(CGG)_{90}$ (Figure 6, Supplementary Figure S2C). In contrast, upon aging,

metabolic perturbations substantially increase in the progression of FXTAS: the aged FXTAS vs. young FXTAS comparison demonstrates the highest number of altered metabolites unique to one group, followed by the aged FXTAS vs. aged WT comparison (Figure 6, Supplementary Figure S2B). Furthermore, 14 out of the 200 altered metabolites were uniquely perturbed in normal aging (aged WT vs. young WT comparison) and were excluded from further analyses (Figure 6). The highest number of metabolites that are shared between comparisons are seen in both the aged FXTAS vs. aged WT and the aged FXTAS vs young FXTAS comparisons, revealing that 51 metabolites are altered due to the presence of the r(CGG)$_{90}$ toxicity and the progression of FXTAS. Further details about the metabolites altered in each comparison and the superpathways impacted can be found in Supplementary Figures S2-4.

Purine metabolism is perturbed in FXTAS

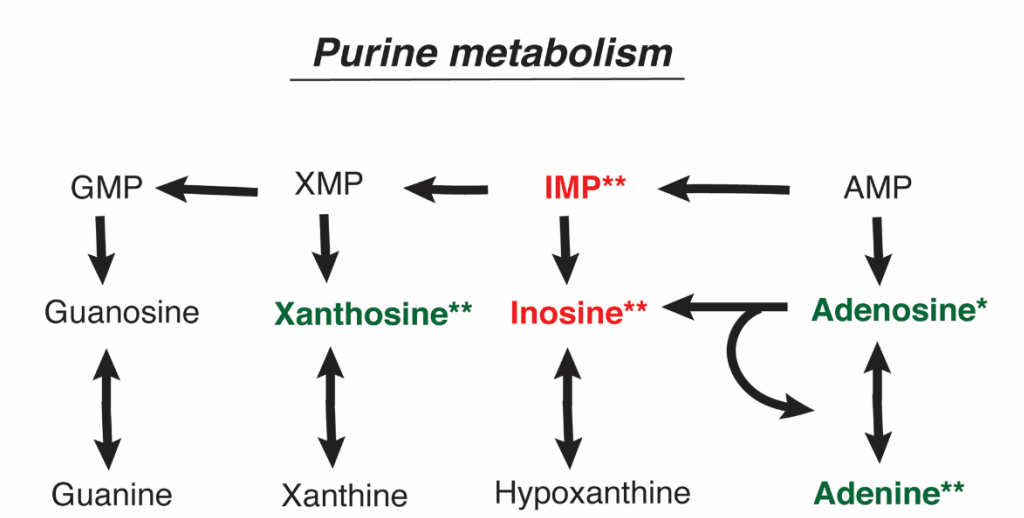

Figure 7: Schematic depicting key components of the Purine metabolism pathway and their perturbations in FXTAS vs. WT comparisons.
Red and green denote increased and decreased fold changes in the pairwise comparisons, respectively. One asterisk (*) indicates changes in the aged FXTAS vs. young FXTAS comparison, whereas two asterisks (**) indicate changes in the aged FXTAS vs. aged WT comparison.

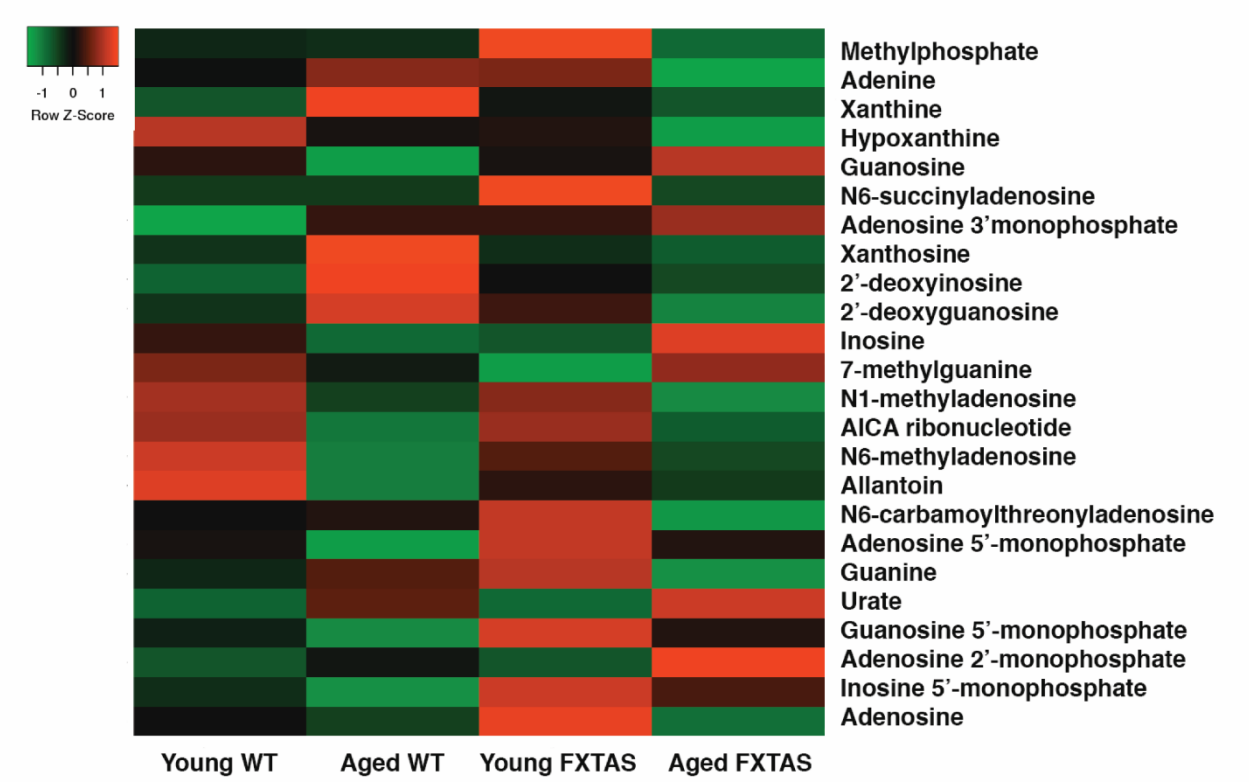

Figure 8: A heatmap showing the metabolite alterations in purine metabolism for young WT, aged WT, young FXTAS, and aged FXTAS mice.
Heatmap was generated using the average metabolite intensity of each group, using average linkage hierarchical clustering in Heatmapper (Babicki et al., 2016). *Red* indicates high and *green* indicates low intensity of the metabolite relative to the median (*black*).

To highlight some of the metabolic pathways that were significantly altered in FXTAS, purine metabolism was significantly perturbed in the presence of CGG (aged FXTAS vs. aged WT, Figure 7-8) as well as in the progression of FXTAS (aged FXTAS vs. young FXTAS, Figure 7-8) .The results of metabolic profiling indicated a significant increase in the levels of IMP in the aged FXTAS mice compared to aged wildtype ($p = 0.0055$, $q = 0.0591$, Figure 9), as well as a significant decline in the levels of Xanthosine in the same comparison, which is generated from XMP ($p = 0.0276$, $q = 0.1327$, Figure 9). The increase in IMP coinciding with the decrease in levels of Xanthosine in the aged FXTAS vs. aged WT comparison led us to hypothesize that IMP Dehydrogenase (Impdh) function may be significantly altered in FXTAS.

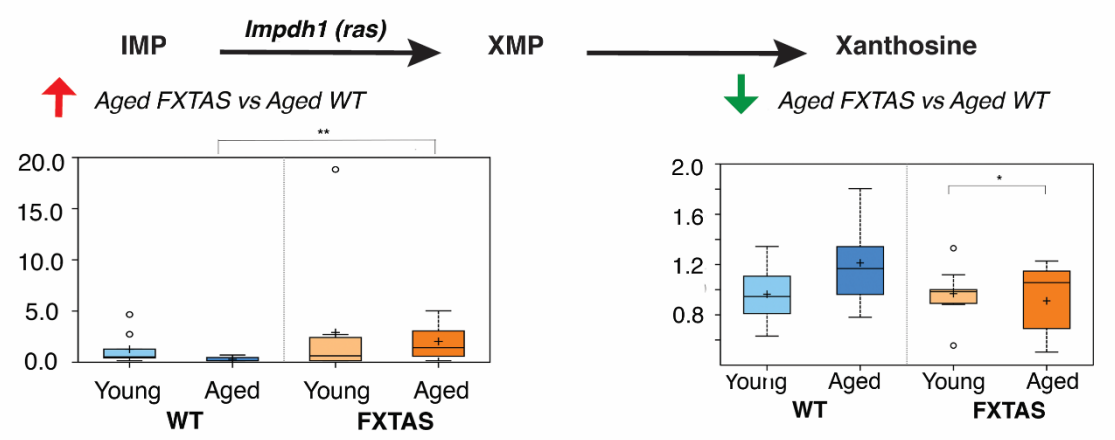

Figure 9: IMP Dehydrogenase (Impdh1) catalyzes the conversion of IMP to XMP in the rate-limiting step of guanine nucleotide biosynthesis.
Box plots displaying significant differences between aged FXTAS vs. aged WT mice in IMP ($p = 0.0055$, $q = 0.0591$) and Xanthosine ($p = 0.0276$, $q = 0.1327$). X-axis indicates the genotype.

Sphingolipid metabolism is perturbed in FXTAS: knockdown of *Schlank (Cers5)* and *Sk2 (Sphk1)* result in enhancement of premutation CGG repeat-mediated neurodegeneration

The untargeted global metabolic profiling revealed that a significant number of metabolites were altered in the lipid pathway in FXTAS comparisons (Figure 3). Among the lipids, the sphingolipid pathway was significantly perturbed in the onset and progression of CGG toxicity in the cerebellum (Figure 10-11). Although sphingolipids were not altered early on in the disease (young FXTAS vs. young WT, Supplementary Figure S2C), upon progression of FXTAS, aged FXTAS mice cerebella demonstrated significant perturbations in sphingolipids compared to aged WT as well as young FXTAS mice (Figure 10).

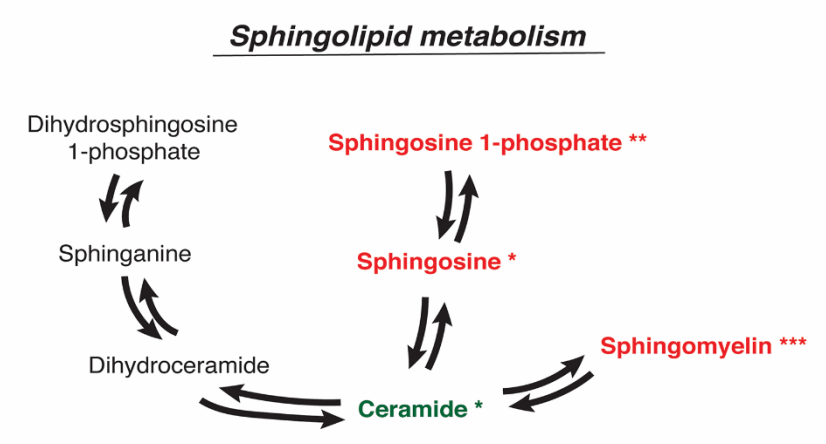

Figure 10: Schematic depicting key components of the Sphingolipid pathway and their perturbations in FXTAS vs. WT comparisons.
Red and *green* denote increased and decreased fold changes in the pairwise comparisons, respectively. One asterisk (*) indicates changes in the aged FXTAS vs. young FXTAS comparison, whereas two asterisks (**) indicate changes in the aged FXTAS vs. aged WT comparison. Three asterisks (***) indicate changes in both comparisons.

Ceramide synthase is the enzyme responsible for converting sphingosine to ceramide, known as the chemical backbone of all sphingolipids (Figure 12, (Park et al., 2014)). Upon taking a closer look at the altered metabolites and the enzymes involved, we found that the level of Sphingosine, the substrate of Ceramide Synthase (Cers5), was significantly elevated in the progression of FXTAS (aged FXTAS vs young FXTAS, $p = 0.0151$, $q = 0.0263$, Figure 12). In contrast, the level of Ceramide, the product of the acylation reaction catalyzed by CerS, was significantly decreased in the aged FXTAS mice compared to the younger counterparts ($p = 0.0313$, $q= 0.0441$, Figure 12). As shown in Figure 12, the elevation in the levels of the substrate Sphingosine, coinciding with a reduction in the product Ceramide in the aged FXTAS vs. young FXTAS cerebella motivated us to posit that CerS function may be perturbed in the progression of FXTAS owing to a genetic interaction between *Cers* and the expanded CGG repeat in FXTAS (Figure 12).

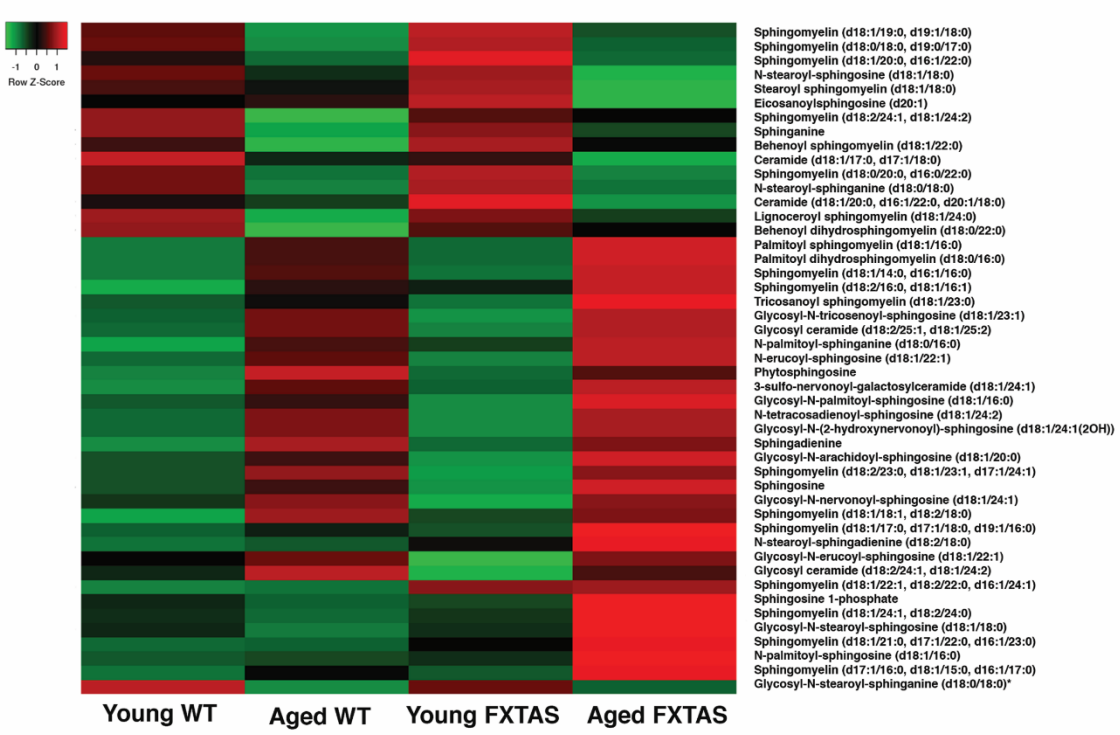

Figure 12: A heatmap showing the metabolite alterations in sphingolipid metabolism for young WT, aged WT, young FXTAS, and aged FXTAS mice.
Heatmap was generated using the average metabolite intensity of each group, using average linkage hierarchical clustering in Heatmapper (Babicki et al., 2016). *Red* indicates high and *green* indicates low intensity of the metabolite relative to the median (*black*).

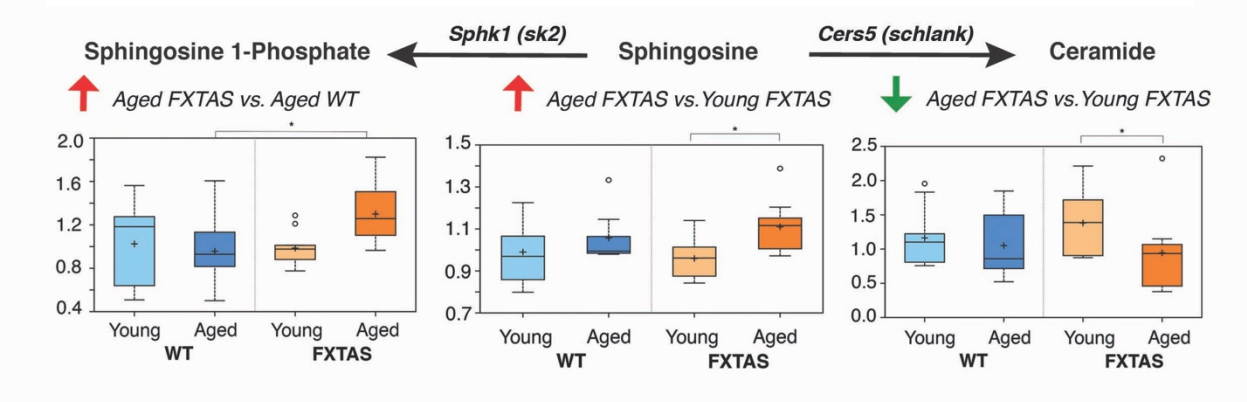

Figure 11: Ceramide Synthase (Cers5 (Schlank)) catalyzes the conversion of Sphingosine to Ceramide. Sphingosine Kinase (Sphk1 (Sk2)) catalyzes the conversion of Sphingosine into Sphingosine-1-phosphate.
Box plots displaying the scaled intensity values (y-axis) for Sphingosine-1-phosphate, Sphingosine and Ceramide (d18:1/20:0, d16:1/22:0, d20:1/18:0). For Sphingosine-1-phosphate, significant alterations were seen in aged FXTAS vs. aged WT mice ($p = 0.0232$, $q = 0.119$). Significant differences are seen between aged FXTAS vs. young FXTAS mice with $p = 0.0151$, $q = 0.0263$ for Sphingosine, and $p = 0.0313$, $q= 0.0441$ for Ceramide. X-axis indicates the genotype.

Furthermore, the mouse metabolomics data shed light on an additional enzyme in the sphingolipid pathway. Sphingosine Kinase catalyzes the phosphorylation of Sphingosine into

Sphingosine 1-phosphate (Figure 12). In the comparison of aged FXTAS vs. aged WT mice, the level of Sphingosine was not significantly elevated but instead Sphingosine 1-phosphate was significantly elevated ($p = 0.0232$, $q = 0.119$, Figure 12), which led us to hypothesize that Sphingosine Kinase may play a role in the toxicity of $r(CGG)_{90}$ in FXTAS.

DISCUSSION

Metabolic profiling of mice cerebella revealed significant metabolic perturbations in the aging of FXTAS mice carrying $r(CGG)_{90}$ in Purkinje cells, especially in pathways of Lipid, Amino Acid and Nucleotide metabolism. This finding correlates with the late-onset phenotype of FXTAS in human premutation carriers, suggesting that metabolic perturbations in the cerebellum may be associated with the neurodegenerative phenotype in human premutation carriers.

Sphingolipids have been implicated in multiple neurodegenerative disorders such as Alzheimer's, Parkinson's and Huntington's Diseases (Cutler et al., 2004; Mielke and Lyketsos, 2010; Piccinini et al., 2010; Wang et al., 2008). Our study has identified the sphingolipid metabolic pathway and in particular, the levels of Ceramide, Sphingosine and Sphingosine-1-phosphate as being significantly perturbed in the progression of CGG toxicity in the mouse cerebellum (Figure 3). Furthermore, we have identified two enzymes that may play a potential role in FXTAS, such as Ceramide Synthase *(CerS)* and Sphingosine Kinase *(Sk2)*. Ceramide Synthase (CerS) plays a central role in sphingolipid metabolism by synthesizing the backbone of all sphingolipids—Ceramide—from Sphingosine. Sphingosine kinases are responsible for phosphorylating Sphingosine to yield Sphingosine 1-phosphate (S1P).

Moreover, our study has also found that purine metabolism is significantly perturbed in the presence of CGG repeats in aged FXTAS vs. young FXTAS mice cerebella. Disruptions in purine metabolism were also reported in the metabolic profiling of plasma from human FXTAS premutation carriers (Giulivi et al., 2016a). Imbalances in purine synthesis can have significant biological consequences by influencing a myriad of processes such as replication, transcription, as well as DNA repair. Based on the metabolite alterations, we identified Impdh, an enzyme that catalyzes the rate-limiting "gateway" reaction for nucleotide synthesis, as a potential player in FXTAS pathology.

Finally, to date, no molecular biomarker of FXTAS has been identified, which has delayed the diagnosis, treatment and prognosis of FXTAS patients. The 186 metabolites that were identified in this study to be significantly altered in the cerebella of FXTAS mice present a novel and useful resource in the search for biomarkers for FXTAS.

In summary, we present a unique report of high-throughput unbiased metabolic profiling on a mouse model of FXTAS to better understand the metabolic alterations involved in FXTAS pathology. Our findings have shed new light on the metabolic perturbations that are associated with FXTAS and have shown that these perturbations aggravate over the course of aging. Furthermore, our study has highlighted the purine and sphingolipid pathways as being significantly altered in FXTAS. Our report of the 186 significantly altered metabolites in the cerebellum present a useful resource to generate hypotheses on potential players in FXTAS pathogenesis, such as *Impdh* and *Cers*.

ACKNOWLEDGEMENTS

This work was supported by the National Institutes of Health [NS051630 to D.L.N, P.J., U54 HD083082 to D.L.N., 2T32GM007526 support for Y.G. and NS091859 to E.G.A, P.J.].

SUPPLEMENTAL MATERIALS

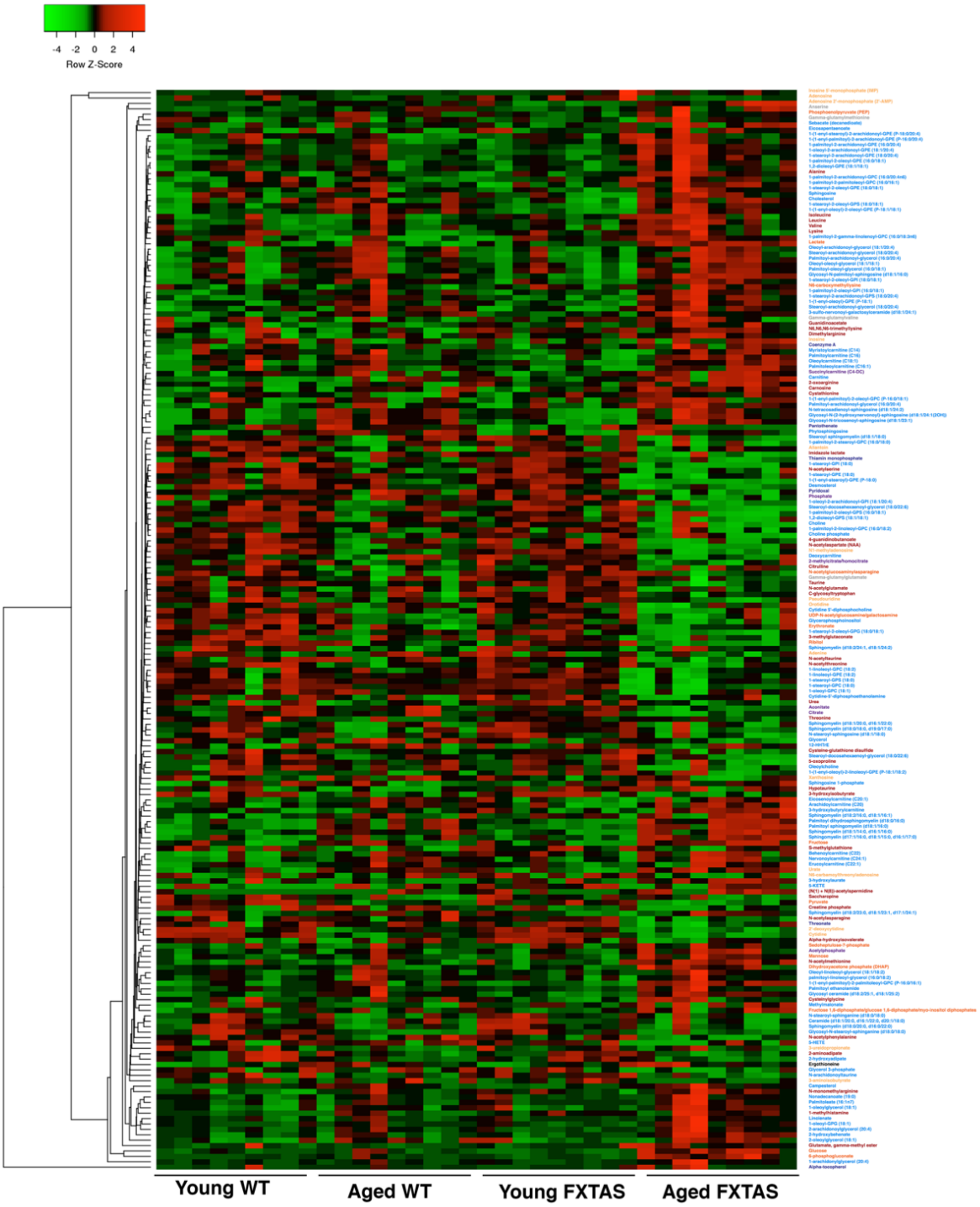

Figure S1. Metabolic profiling demonstrates significant metabolic perturbations in the presence of r(CGG)$_{90}$ repeats. A heat map of the 200 significantly altered metabolites ($p<0.05$) distinguishes the FXTAS and WT mouse cerebellum samples. Heatmap was generated using average linkage hierarchical clustering in Heatmapper (Babicki et al., 2016). Red indicates high and green indicates low intensity of the metabolite relative to the median (black). Names of the corresponding metabolites are coded in color to represent the appropriate superpathway: Lipid (blue), Amino acid (red), Nucleotide (yellow), Carbohydrate (orange), Peptide (gray), Cofactors and Vitamins (navy), Energy (purple) and Xenobiotics (black).

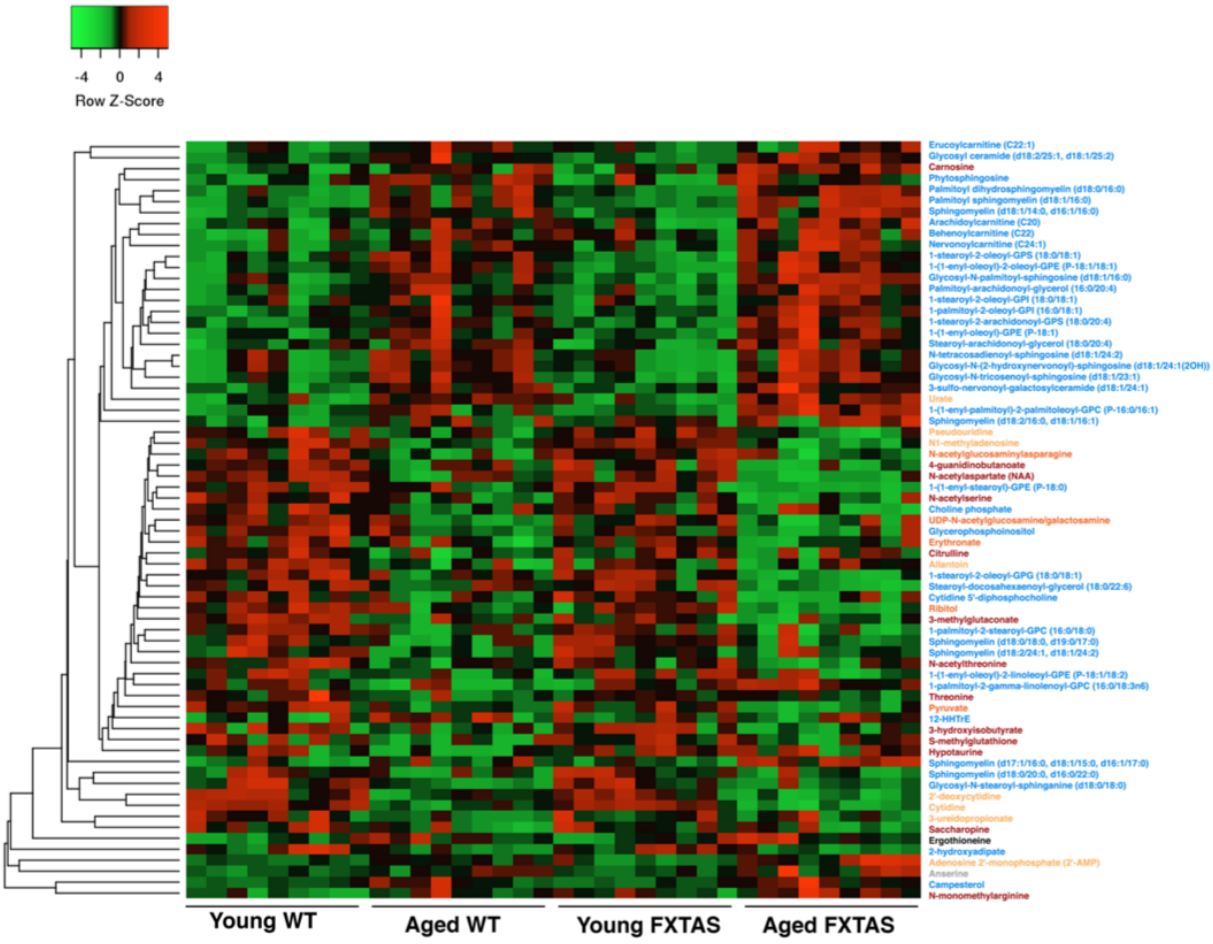

Figure S2A. Altered metabolites in aged WT vs. young WT comparison ($p<0.05$). Heatmap was generated using average linkage hierarchical clustering in Heatmapper (Babicki et al., 2016). Red indicates high and green indicates low intensity of the metabolite relative to the median (black). Names of the corresponding metabolites are coded in color to represent the appropriate superpathway: Lipid (blue), Amino acid (red), Nucleotide (yellow), Carbohydrate (orange), Peptide (gray), Cofactors and Vitamins (navy), Energy (purple) and Xenobiotics (black).

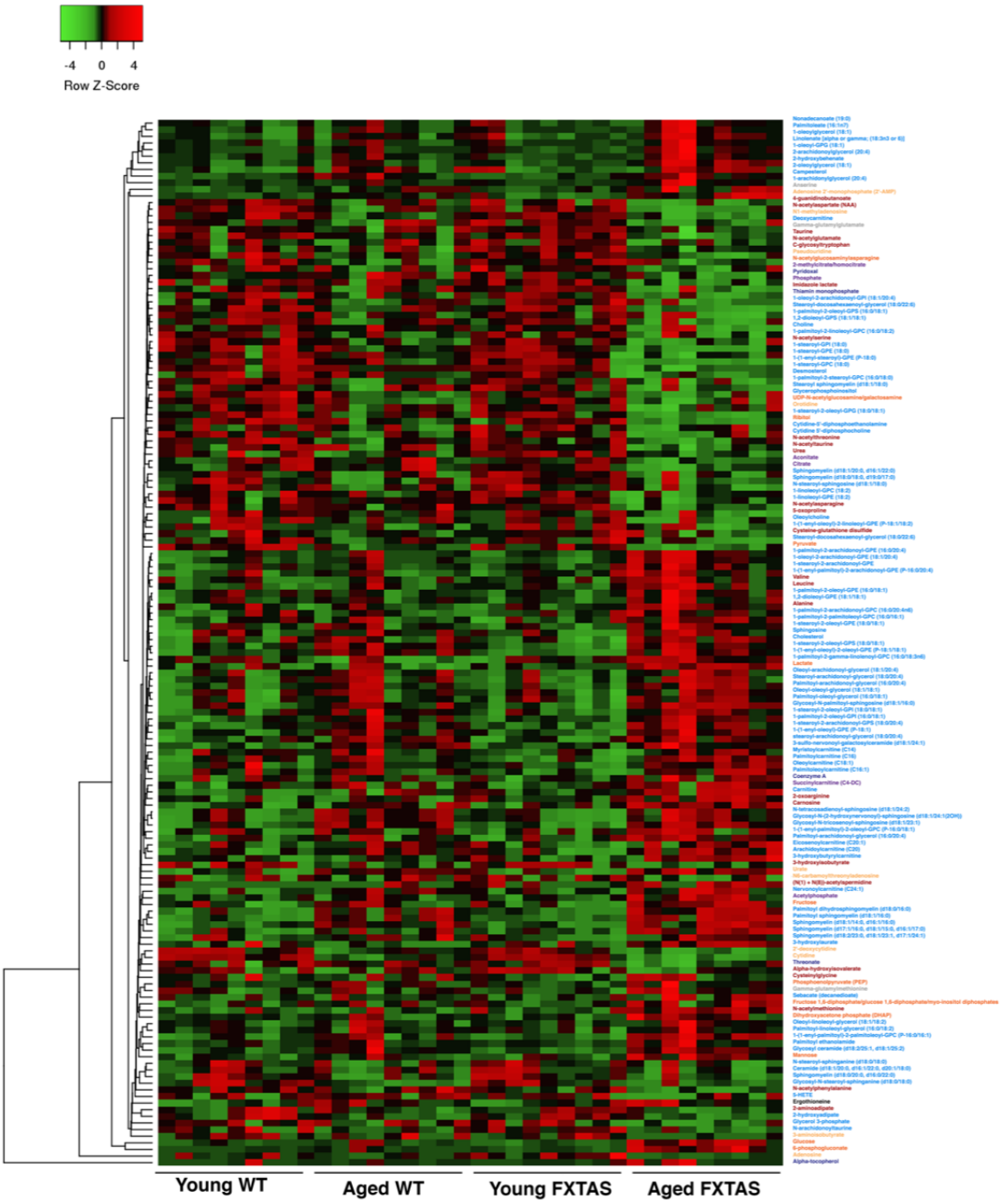
-4
0
4
Row Z-Score
Young WT
Aged WT
Young FXTAS
Aged FXTAS

Figure S2B. Altered metabolites in aged FXTAS vs. young FXTAS comparison ($p<0.05$). Heatmap was generated using average linkage hierarchical clustering in Heatmapper (Babicki et al., 2016). Red indicates high and green indicates low intensity of the metabolite relative to the median (black). Names of the corresponding metabolites are coded in color to represent the appropriate superpathway: Lipid (blue), Amino acid (red), Nucleotide (yellow), Carbohydrate (orange), Peptide (gray), Cofactors and Vitamins (navy), Energy (purple) and Xenobiotics (black).

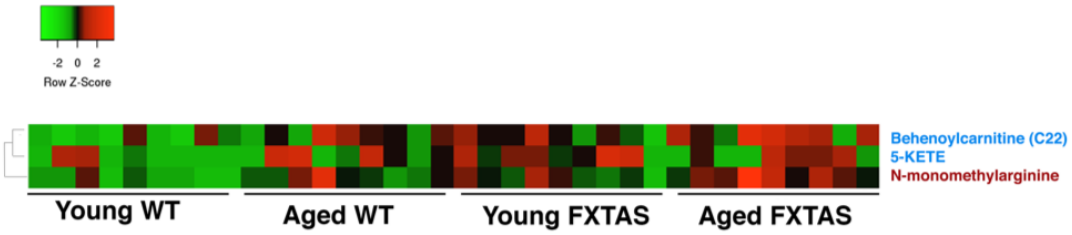

Figure S2C. Altered metabolites in young FXTAS vs. young WT comparison ($p<0.05$). Heatmap was generated using average linkage hierarchical clustering in Heatmapper (Babicki et al., 2016). Red indicates high and green indicates low intensity of the metabolite relative to the median (black). Names of the corresponding metabolites are coded in color to represent the appropriate superpathway: Lipid (blue), Amino acid (red), Nucleotide (yellow), Carbohydrate (orange), Peptide (gray), Cofactors and Vitamins (navy), Energy (purple) and Xenobiotics (black).

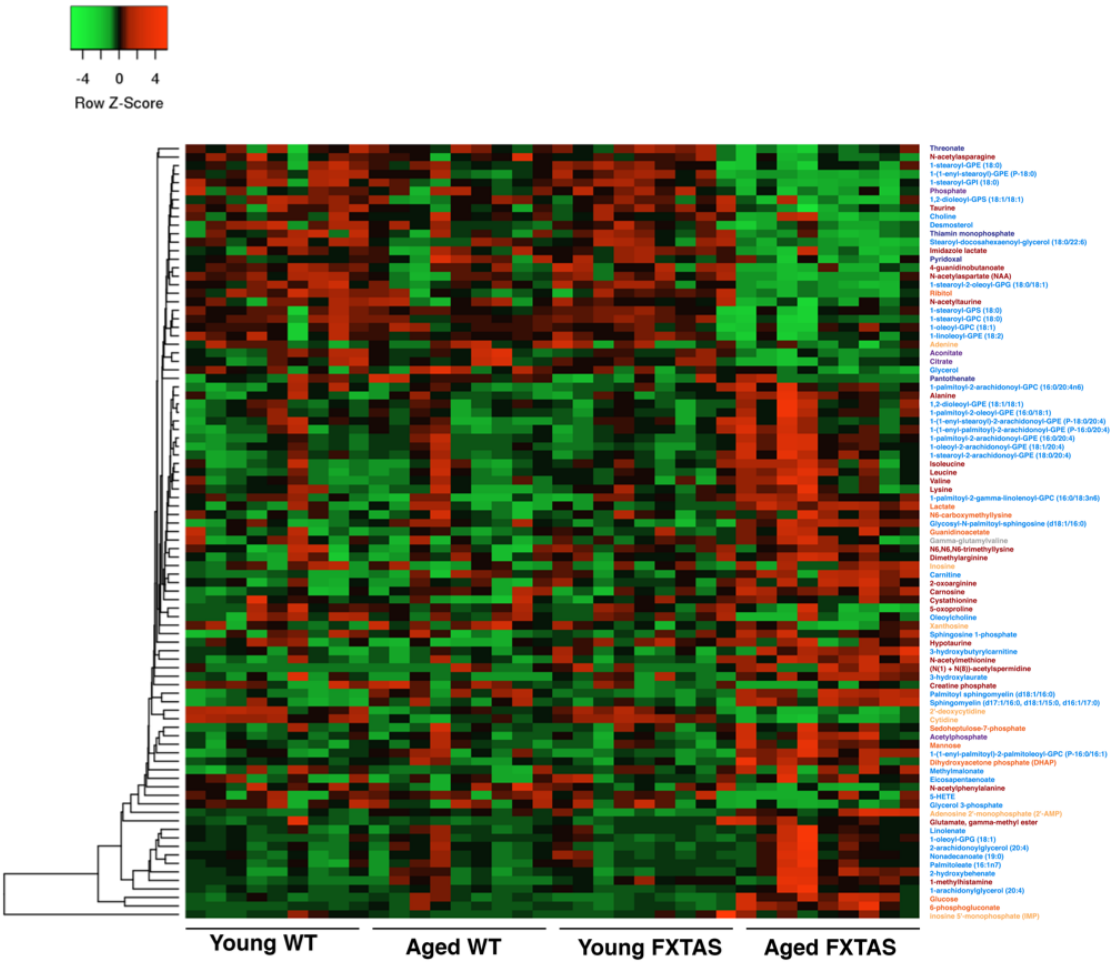

Figure S2D. Altered metabolites in aged FXTAS vs. aged WT comparison ($p<0.05$). Heatmap was generated using average linkage hierarchical clustering in Heatmapper (Babicki et al., 2016). Red indicates high and green indicates low intensity of the metabolite relative to the median (black). Names of the corresponding metabolites are coded in color to represent the appropriate superpathway: Lipid (blue), Amino acid (red), Nucleotide (yellow), Carbohydrate (orange), Peptide (gray), Cofactors and Vitamins (navy), Energy (purple) and Xenobiotics (black).

A

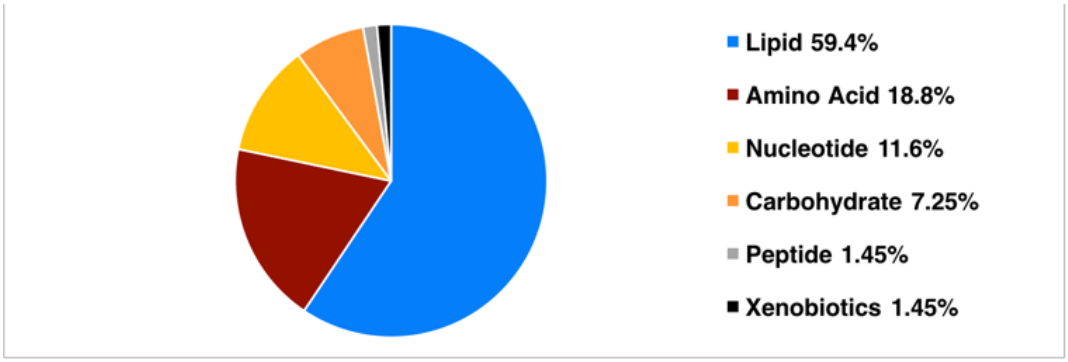
Lipid 59.4%
Amino Acid 18.8%
Nucleotide 11.6%
Carbohydrate 7.25%
Peptide 1.45%
Xenobiotics 1.45%

B

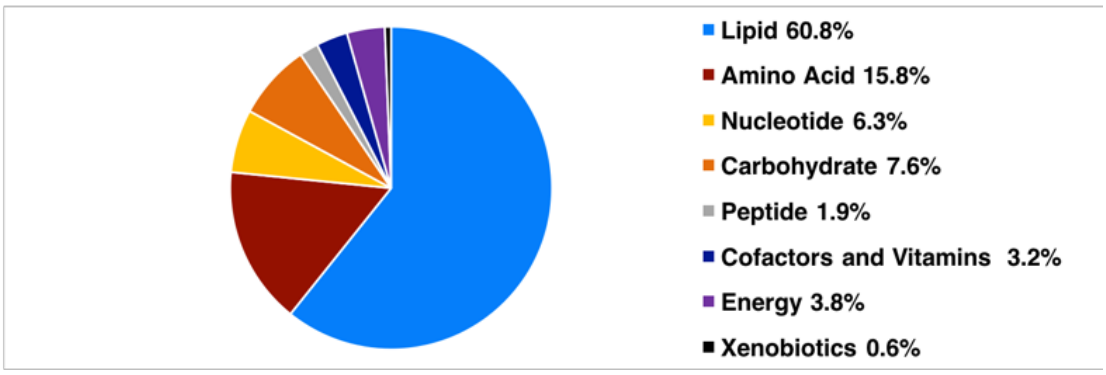
Lipid 60.8%
Amino Acid 15.8%
Nucleotide 6.3%
Carbohydrate 7.6%
Peptide 1.9%
Cofactors and Vitamins 3.2%
Energy 3.8%
Xenobiotics 0.6%

C

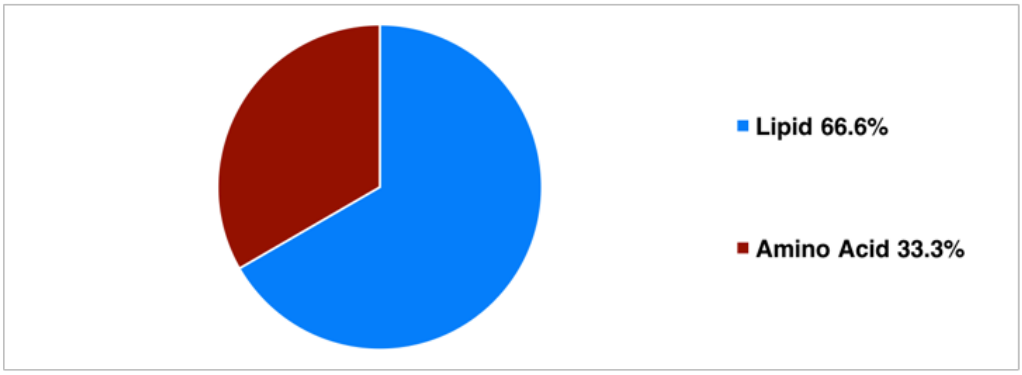
Lipid 66.6%
Amino Acid 33.3%

D

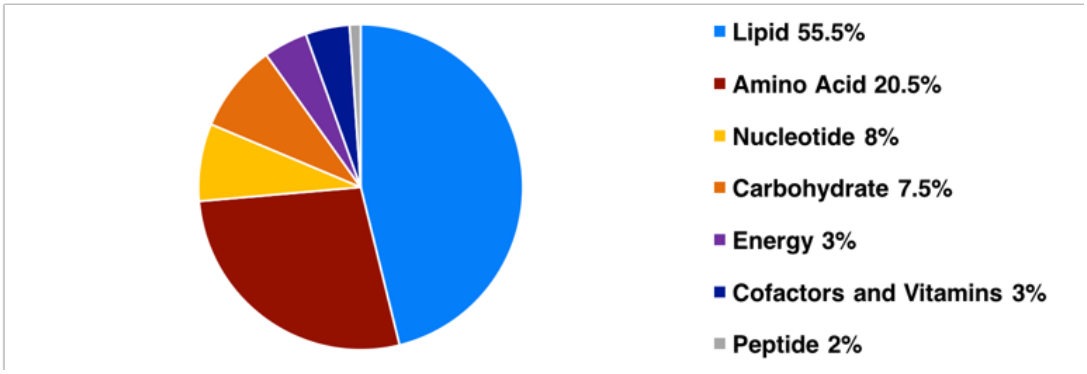
Lipid 55.5%
Amino Acid 20.5%
Nucleotide 8%
Carbohydrate 7.5%
Energy 3%
Cofactors and Vitamins 3%
Peptide 2%

Figure S3

A. Superpathways of metabolism affected in the aged WT vs. young WT comparison ($p<0.05$). Superpathways include Lipid, Amino Acid, Nucleotide, Carbohydrate, Peptide, and Xenobiotics.

B. Superpathways of metabolism affected in the aged FXTAS vs. young FXTAS comparison ($p<0.05$). Superpathways include Lipid, Amino Acid, Nucleotide, Carbohydrate, Peptide, Cofactors and Vitamins, Energy and Xenobiotics.

C. Superpathways of metabolism affected in the young FXTAS vs. young WT comparison ($p<0.05$). Superpathways include Lipid and Amino Acid.

D. Superpathways of metabolism affected in the aged FXTAS vs. aged WT comparison ($p<0.05$). Superpathways include Lipid, Amino Acid, Nucleotide, Carbohydrate, Energy, Cofactors and Vitamins, and Peptide

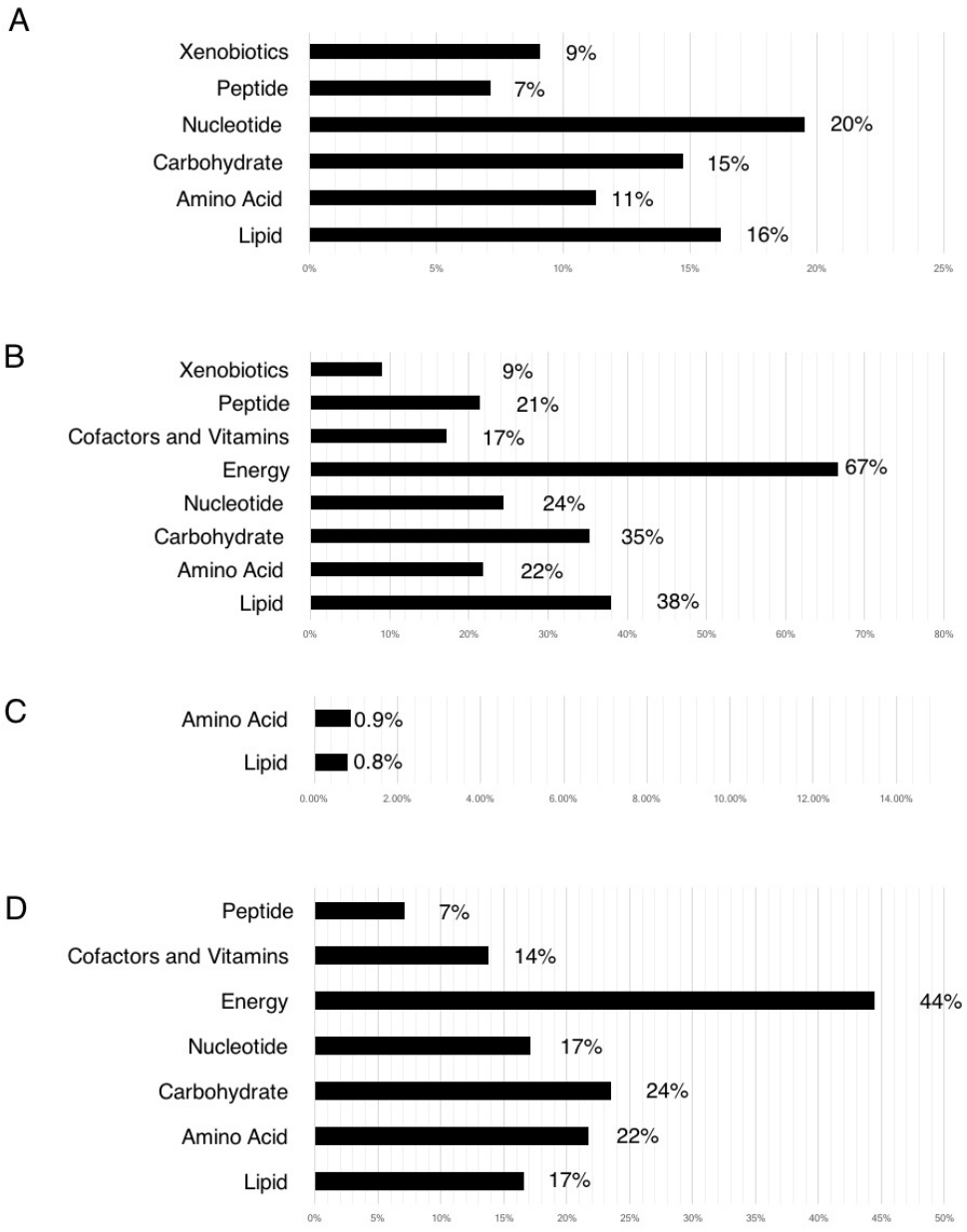

Figure S4. Representation of the percentage of superpathways of metabolism altered ($p<0.05$) out of the total number of metabolites assessed in each superpathway for each comparison.

A. aged WT vs. young WT

B. aged FXTAS vs. young FXTAS

C. young FXTAS vs. young WT

D. aged FXTAS vs. aged WT

Chapter 2: Sphingolipid pathway modulates the neuronal toxicity associated with Fragile X-Associated Tremor/Ataxia Syndrome

Parts of this chapter were originally published in *Human Molecular Genetics*:
Hum Mol Genet. 2019 Mar 15;28(6):980-991. doi: 10.1093/hmg/ddy410.

ABSTRACT

In Chapter 1, to identify key metabolic changes in FXTAS pathogenesis, we performed unbiased global metabolic profiling of mice that express r(CGG)$_{90}$ under a Purkinje-neuron-specific promoter. In the study outlined in Chapter 2, we set out to use the metabolic profiling data to identify genetic modifiers of FXTAS by performing a genetic screen using a *Drosophila* model of FXTAS. Out of 28 genes that we tested in the fly, 8 genes showed significant enhanced neuronal toxicity associated with CGG repeats, including *Ras (Impdh1), Schlank (Cers5), and Sk2 (Sphk1)* demonstrating that as hypothesized in Chapter 1, these enzymes modulate CGG-associated neurotoxicity in FXTAS.

Moreover, we set out to further validate the lipid changes by performing high mass resolution lipid profiling on postmortem human cerebellar tissues from aged premutation carriers and controls. Significantly, we found that sphingolipids accounted for approximately 25% of the most significantly altered lipids ($p<0.05$, one-way ANOVA, post-hoc Fisher's LSD test) in FXTAS compared to control. Taking a step further, we performed a comprehensive *Drosophila* genetic screen of the metabolic genes in the Sphingolipid pathway. Out of 18 genes screened, we found that knockdown of 4 genes result in significant enhancement of the CGG-associated neuronal toxicity in the FXTAS fly eye, such *as Gba1a (GBA1), Glct-1 (UGCG), Cerk (CERK), and Sply (SGPL1).* Together with Chapter 1, this work uses three model systems –human, mouse and fly to demonstrate compelling evidence that implicates sphingolipid metabolism perturbation in FXTAS pathology.

KEYWORDS
FXTAS, Sphingolipid, genetic modifier, *Drosophila* genetic screen, lipidomics

INTRODUCTION

The widely-used fruit fly, *Drosophila melanogaster,* is a powerful tool for studying neurodevelopmental disorders, and has been studied for more than a century. Approximately 75% of human disease-causing genes are estimated to be conserved in *D. melanogaster.* Its rapid life cycle, high fecundity and low-cost maintenance, along with the highly conserved biology has made the fruit fly a very attractive model to study human disease and has contributed to many breakthrough discoveries in biology.

The GAL4-UAS system, first developed by Brand and Perrimon (Brand and Perrimon, 1993) is the most popular tool used in *Drosophila* and has been widely used to perform reverse genetic screens by testing and validating candidate genes for functional effect. Many GAL4 driver lines are available, in which the yeast transcription factor GAL4 is expressed under a cell or tissue-specific promoter such as GMR (Glass Multimer Reporter) for the eye. When these flies are crossed with flies that have GAL4 response elements (UAS) upstream of the desired transgenic element, the resulting progeny express the transgene in the desired tissues or cells. The Bloomington Drosophila Stock Center and the Vienna Drosophila Research Center, among others, house a large collection of UAS-RNAi knockdown strains that are available to researchers worldwide (Dietzl et al., 2007).

Our group has previously described a *Drosophila* disease model of FXTAS that expresses the premutation CGG repeat in the context of the human *FMR1* 5'UTR. Using this *Drosophila*

model, we have demonstrated that the premutation CGG repeats are sufficient to cause FXTAS pathology (Jin et al., 2003). Expression of r(CGG)$_{90}$ under the eye-specific driver in *Drosophila,* gmr-GAL4, results in a rough eye phenotype characterized by cell death, loss of pigmentation and ommatidial disruption (Jin et al., 2003).

In this chapter, we demonstrate a distinctive approach to functionally validate the high-throughput metabolomics via a genetic screen using the *Drosophila* model of FXTAS. More specifically, we demonstrate that *Schlank (Cers5), Sk2 (Sphk1)* and *Ras (Impdh1)*, which encode enzymes in the sphingolipid and purine metabolism, respectively, are genetic modifiers of CGG toxicity in *Drosophila*.

Furthermore, we validate the findings in sphingolipids by performing high resolution lipidomics on human postmortem cerebellar tissue from premutation carriers and controls and demonstrate that sphingolipids account for approximately 25% of most significantly altered lipids in FXTAS compared to control. We also perform a comprehensive genetic screen in *Drosophila* for metabolic enzymes involved in the sphingolipid pathway and identify 4 genes that significantly enhance CGG-associated neuronal toxicity in the FXTAS fly, such as *Gba1a (GBA1), Glct-1 (UGCG), Cerk (CERK), and Sply (SGPL1).*

METHODS

Manual Curation selection criteria

Enzyme gene candidates were selected based on the following criteria: 1) the metabolite is present in the KEGG database, 2) there is a known gene encoding the enzyme involved in its synthesis/degradation, 3) there are less than five enzymes involved in the synthesis/degradation of

biochemical, 4) the reaction catalyzed by the enzyme is not denoted to be reversible in KEGG, and importantly, 5) in order to test the gene candidates using a *Drosophila* genetic screen, gene candidates were limited to those that have fly orthologues and RNAi lines available.

Drosophila genetics

Transgenic flies expressing r(CGG)$_{90}$ were previously described. The gmr-GAL4 and UAS-TRiP lines were obtained from Bloomington Stock Centre (Bloomington, IN, USA). All crosses were grown on standard medium at 25 °C. After performing the crosses, progeny was collected and aged to 7 days. The screen was performed by eye phenotype, which was visualized using light microscopy and confirmed with scanning electron microscopy.

RNA isolation and quantitative RT-PCR

Actin-GAL4 flies were crossed with the corresponding RNAi lines. Larvae were collected, homogenized in Trizol (Invitrogen) with pellet pestles (Fisher) and total RNA was extracted using the manufacturer's protocol. cDNA was synthesized with SuperScript III reverse transcriptase (Invitrogen) using random hexamer primers. Real-Time PCR was performed with primers in Table S3.

Scanning Electron Microscopy

Whole flies were dehydrated in increasing concentrations of ethanol (25%, 50%, 75%, 100%), then incubated for 1 hr with hexamethyldisilazane (Electron Microscopy Sciences). After removing the hexamethyldisilazane, the flies were dried overnight in a fume hood and subsequently analyzed using Topcon DS-130F and DS-150F Field Emission Scanning Electron Microscope.

Lipid extraction

Postmortem cerebellar tissue from 5 aged FMR1 premutation carriers with FXTAS were obtained as a generous gift from Dr. Martinez-Cerdeno, MIND Institute, UCDavis. Postmortem cerebellar tissue from 5 aged controls were obtained as a generous gift from the NIH NeuroBioBank at Harvard University. Tissue samples were kept at -80°C.

The frozen tissues were weighed and immediately homogenized with 200 µl of methanol. The four tissue samples were homogenized in 400 µL of methanol and 200 µL from each were used for further extraction. Further, the homogenates were mixed with 200 µL of methanol and spiked with 15 µL of deuterated internal standard (IS) (SPASH LIPIDOMIX, Avanti Polar Lipids, Inc. Alabaster, Alabama). The homogenate-internal standard mix were vortexed for 20 min at 300 rpm and then centrifuged at 10,000 rpm for 5 min. Clean methanolic extract were collected and transferred to a clean glass vial. 800 µL of methyl tert-butyl ether (MTBE): methanol (3:1 v/v) was added to the previous homogenate and extracted the clean MTBE-methanol extract after previously mentioned condition of vortex and centrifugation. The homogenate was further re-extracted using 500 µL of 3:1 v/v MTBE: methanol under similar condition of vortexing and centrifugation. All the clean extracts are pooled and dried under gentle stream of nitrogen. The dried extracts were stored at -80 °C until data acquisition.

LC-MS analysis

The dried extract was solvated in 500 µL 1:1 v/v isopropanol: methanol mixture and vortexed intermittently for 1 min. 50 µL from each sample was pooled to prepare the quality control (QC) sample. The pre- and post-injection of QC sample was done before the start and after the completion of sample analysis. 1 µl of extract was injected into liquid chromatography-mass spectrometry (LC-MS) for data acquisition. The same volume of QC injection was performed after

every three samples. The lipids were separated using Waters ACQUITY UPLC BEH C18 column (2.1X 50 mm, 1.7 μm particle size) fitted on Vanquish (ThermoFisher Scientific) LC system that is coupled to Q Exactive High Field mass spectrometer (ThermoFisher Scientific). The chromatographic method for sample analysis involved elution with 40:60 water:acetonitrile, 10mM ammonium formate, 0.1% formic acid (mobile phase A) and 90:10 iso-propanol:acetonitrile, 10mM ammonium formate, 0.1% formic acid (mobile phase B) using the following gradient program: 0-1.0 min 40-45% B; 1.0-1.1 min 45-50% B; 1.1-5.0 min 50-55% B; 5.0-5.1 min 55-70% B; 5.1-8.0 min 70-99% B; 8.0-8.1 min 99-40% B; 8.1-9.5 min 40% B. The flow rate was constant at 0.40 mL min-1 for 9.5 min. The column temperature was set to 50 °C, the autosampler tray was set to 4 °C, and the injection volume was 5 μL. The hybrid quadrupole-Orbitrap mass spectrometer was operated in positive and negative mode with a resolution of 240,000 FWHM over a range of 150- 2000 m/z. Ionization was achieved with a HESI probe operating with a capillary temperature of 275 ^{0}C and spray voltage of 3 kV in positive mode and 2.8 kV in negative mode. Sheath gas was 52 arbitrary units, cone gas 14 arbitrary units, and auxiliary gas 4 arbitrary units (heated to 425 ^{0}C). The S-Lens RF level was set at 40V. Select samples were used to collect UPLC-MS/MS experiments utilizing a data-dependent strategy, where following a full MS scan with 120,000 resolution, the top 5 peaks were selected with 0.4 m/z isolation window for ion fragmentation by a with stepped NCE of 10, 30, and 50 eV (HCD). Additional DDAs were run with NCE at 15, 20, 25, 30, 35 eV (HCD).

Data preprocessing and statistical analysis

Data preprocessing was performed using MzMine 2.26 and beta version of LipidMatch (Koelmel et al. 2017). The mass intensity and tolerance were set 1.0E4 and 5 ppm for building chromatogram. The chromatogram deconvolution was performed using Local Minimum Search algorithm with the following parameters set: chromatographic threshold: 20%, search minimum

in retention time (RT) range: 0.10 min, minimum absolute height: 1.0E4, minimum ratio of peak top/edge: 1.5. The mass tolerance and RT tolerance was set at 5 ppm and 0.9 min respectively. The lipids were identified from positive and negative mode ionizations data and merged to obtain a single file containing information on m/z, retention time, and intensities for each samples and the lipids identified, using LipidMatch (beta version) (Koelmel et al., 2017). The raw data was further subjected to statistical analysis using Metaboanalyst 4.0 (Chong et al., 2018).

RESULTS

With the results of the high-throughput unbiased global metabolic profiling of FXTAS mice in hand, we were interested in taking advantage of our FXTAS *Drosophila* model to examine whether these metabolic perturbations in the FXTAS mice cerebella can be attributed to a genetic interaction between the metabolic genes and the r(CGG)$_{90}$. Hence, we set out to identify metabolic enzyme gene candidates that may be associated with the biochemical alterations observed in our comparisons.

From the mouse metabolomics results, after excluding the 14 metabolites that were uniquely altered in normal aging (Chapter 1, Figure 4), 186 of the 506 metabolites detected in the cerebellum showed significant alteration in the FXTAS mice ($p < 0.05$) (Figure 6). From these 186 metabolites, we used manual curation to identify enzymes that are responsible for the synthesis/degradation of the metabolite, following selection criteria that is detailed in the Methods (Supplementary Figure S1), which yielded 28 candidate genes to test for genetic interaction with the CGG repeat (Supplementary Table S1). These 28 candidate genes account for 12.9% of the 186 metabolites (Supplementary Table S1).

Table 1 : Eight candidate genes that exhibit modulation of r(CGG)$_{90}$ toxicity in *Drosophila*

#	Mouse Gene		*Drosophila* Ortholog	BDSC stock	Effect on r(CGG)$_{90}$ toxicity
1	*Cda*	Cytidine Deaminase	*CG8353*	51915	Enhanced
2	*Cers5*	Ceramide Synthase 5	*Schlank*	29340	Enhanced
3	*Chat*	Choline O-Acetyltransferase	*ChAT*	60028	Enhanced
4	*Coasy*	Coenzyme A Synthase	*Ppat-Dpck*	57231	Enhanced
5	*Ggct*	Gamma-glutamylcyclotransferase	*CG4306*	65890	Suppressed
6	*Impdh1*	Inosine Monophosphate Dehydrogenase 1	*Ras*	31653	Enhanced
7	*Pcyt2*	Phosphate Cytidylyltransferase 2, Ethanolamine	*Pect*	63710	Enhanced
8	*Sphk1*	Sphingosine Kinase 1	*Sk2*	36741	Enhanced

Drosophila genetic screen identifies 8 genes that exhibit significant interaction with FXTAS CGG toxicity

Out of the 28 candidates selected from manual curation, the *Drosophila* screen identified 8 genes that exhibit enhancement or suppression of CGG associated toxicity in FXTAS *Drosophila* (Table 1, Chapter 2 Supplementary Table S1). Knockdown of 7 of the 8 genes resulted in enhancement of the rough eye phenotype: *CG8353, ChAT, Pect, Ppat-dpck, Ras, Schlank and Sk2* which are *Drosophila* orthologues for *Cytidine Deaminase (Cda), Choline O-Acetyltransferase (Chat), Phosphate Cytidylyltransferase 2, Ethanolamine (Pcyt2), Coenzyme A Synthase (Coasy), Inosine Monophosphate Dehydrogenase (Impdh1), Ceramide Synthase (Cers5) and Sphingosine Kinase (Sphk1)*, respectively (Table 1, Supplementary Figure S7, Table S2). Interestingly, knockdown of *CG4306*, the fly orthologue of *Gamma-glutamylcyclotransferase (Ggct)*, demonstrated significant suppression of CGG toxicity (Table 1, Supplementary Figure S2). Taken together, high-throughput metabolomics followed by the FXTAS *Drosophila* genetic screen led to

the identification of eight genetic modifiers of CGG toxicity in FXTAS. From the eight genetic modifiers of CGG toxicity in FXTAS, we focused on three enzymes based on the correlation between the *Drosophila* genetic data and the upstream and downstream metabolic alterations observed in the FXTAS mouse model.

Knockdown of *Ras (Impdh1)* results in enhancement of premutation CGG repeat mediated neurodegeneration

Based on the mouse metabolic profiling data, one of the candidate enzyme genes selected for the *Drosophila* genetic screen through manual curation was *Impdh1*, which encodes Inosine 5'Monophosphate Dehydrogenase (IMP). Impdh1 is a rate-limiting enzyme in guanine nucleotide biosynthesis, and the significant increased levels of its substrate IMP in the mouse metabolic profiling (Chapter 1, Figure 9), prompted us to hypothesize that *Imphd1* may play a role in FXTAS pathogenesis. When we performed the genetic screen in FXTAS Drosophila, upon knockdown of

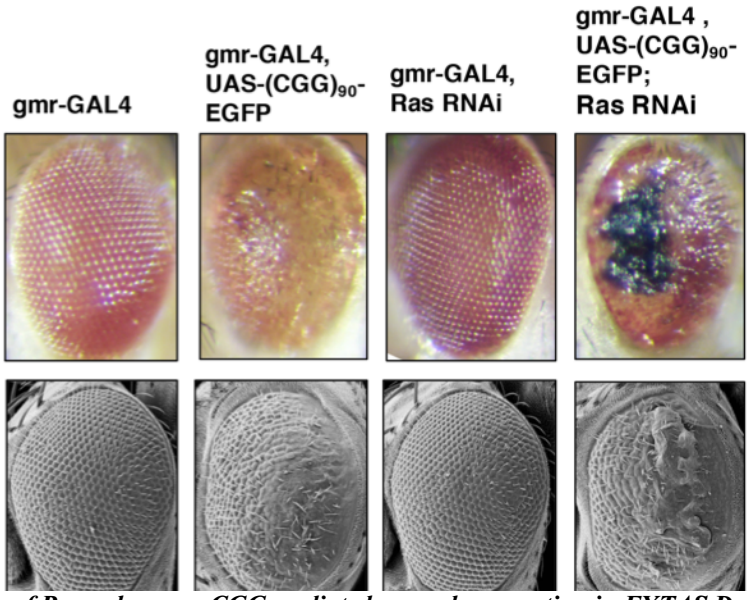

Figure 13: Knockdown of Ras enhances rCGG mediated neurodegeneration in FXTAS Drosophila
Knockdown of *Ras* (fly ortholog of *Impdh)* enhances r(CGG)$_{90}$ mediated neurodegeneration in FXTAS *Drosophila.* Top panel displays the light microscopy, from left to right: WT control (gmr-*GAL4*) (column 1), (CGG)$_{90}$ control (gmr-*GAL4,* UAS-(CGG)$_{90}$-EGFP) (column 2). WT fly expressing RNAi knockdown of *Ras* demonstrates no toxicity (column 3) while the (CGG)$_{90}$ fly expressing RNAi knockdown of *Ras* demonstrates enhancement of the CGG-associated neurotoxicity (column 4). Bottom panel shows the corresponding scanning electron microscopy images.

Ras, the fly orthologue of *Imdph1*, the fly progeny demonstrated significant enhancement of the r(CGG)$_{90}$ associated toxicity, while no toxicity was seen in the wildtype control (Figure 13).

Sphingolipid metabolism is perturbed in FXTAS: knockdown of *Schlank (Cers5)* and *Sk2 (Sphk1)* result in enhancement of premutation CGG repeat mediated neurodegeneration

In the mouse metabolic profiling, another set of genes that emerged as potential candidate genetic modifiers were *Cers5* and *Sphk1*, encoding the enzymes Ceramide Synthase and Sphingosine Kinase, respectively. Both Ceramide Synthase and Sphingosine Kinase are key players in Sphingolipid metabolism, and Ceramide Synthase especially is responsible for synthesizing Ceramide—the backbone of all sphingolipids.

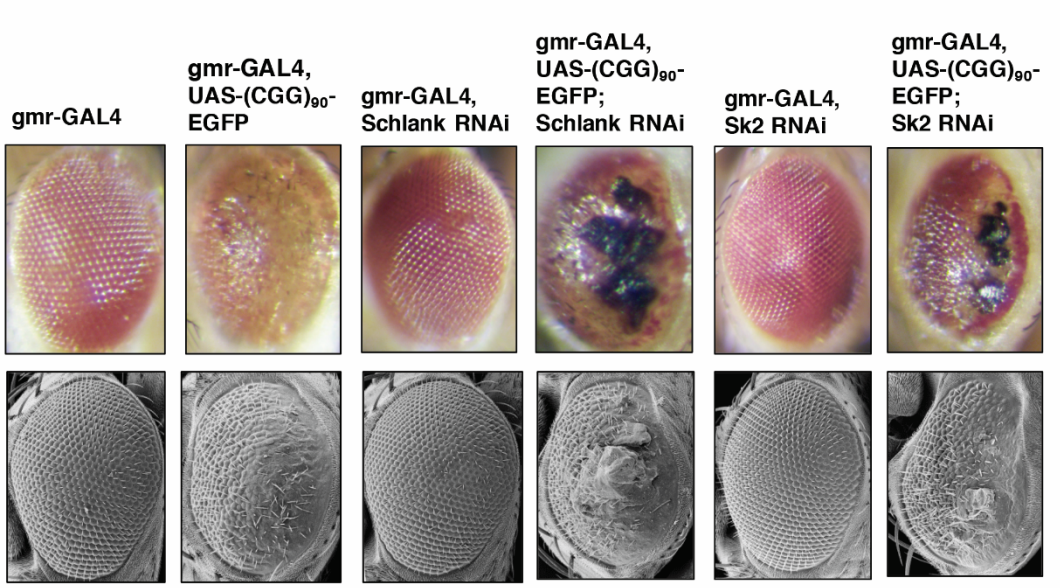

Figure 14: Knockdown of Schlank and Sk2 enhance r(CGG)$_{90}$ mediated neurodegeneration in FXTAS Drosophila Knockdown of *Schlank* and *Sk2* (fly orthologue of *Cers5* and *Sphk1*) enhance r(CGG)$_{90}$ mediated neurodegeneration in FXTAS *Drosophila.* Top panel displays the light microscopy images from *Drosophila* of the indicated genotypes crossed to gmr-GAL4 flies and gmr-GAL4, UAS-(CGG)$_{90}$ EGFP flies. From left to right: WT control (gmr-GAL4) (column 1), (CGG)$_{90}$ control (gmr-GAL4, UAS-(CGG)$_{90}$-EGFP) (column 2), WT fly expressing RNAi knockdown of *Schlank* (column 3) does not show any phenotype. The (CGG)$_{90}$ fly expressing RNAi knockdown of *Schlank* results in enhancement of the CGG-associated neurotoxicity (column 4). Column 5 and 6 show RNAi knockdown of *Sk2* in wildtype and (CGG)$_{90}$ flies, respectively, demonstrating that knockdown of *Sk2* in the (CGG)$_{90}$ fly results in enhancement of CGG-associated toxicity. Bottom panel shows the corresponding scanning electron microscopy images.

To probe for genetic interaction, we employed the *Drosophila* model of FXTAS which allows for facile genetic screening (Jin et al., 2003). Knockdown of *Schlank (Cers5)* and *Sk2 (Sphk1) r*esulted in significant enhancement of the CGG toxicity in the fly progeny, indicating that *Schlank* and *Sk2* interact with the CGG repeat of FXTAS and significantly enhance the CGG associated neurotoxicity (Figure 14). Importantly, knockdown of *Schlank* and *Sk2* in the wildtype fly did not result in change in eye phenotype (Figure 14).

Sphingolipid levels are significantly altered in postmortem cerebellar tissue from *FMR1* premutation carriers

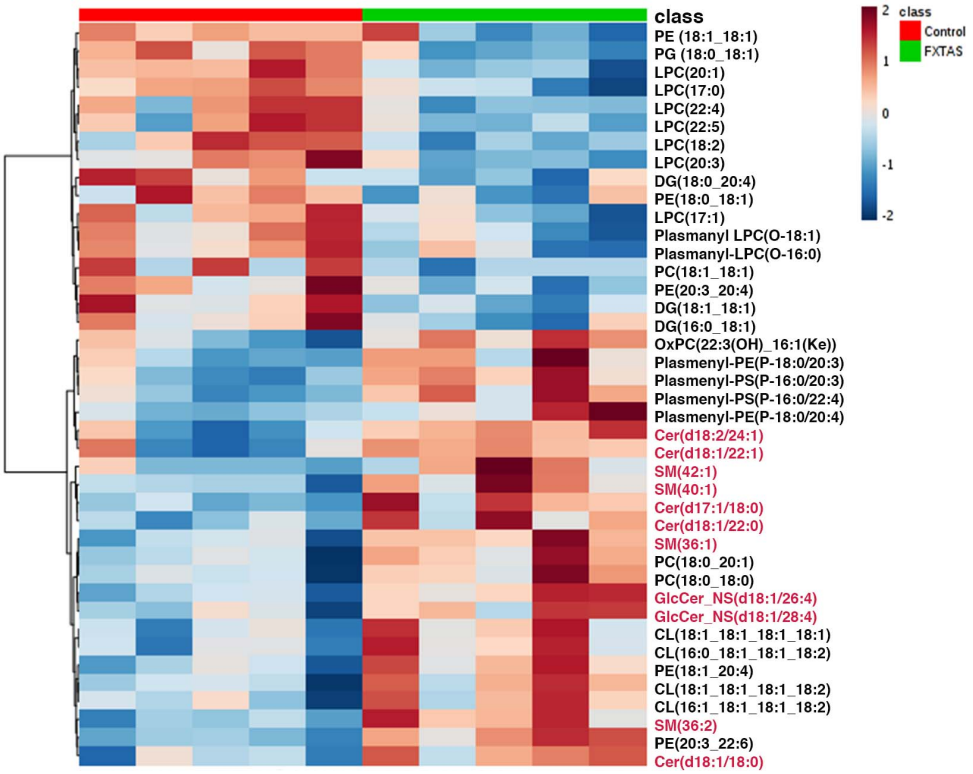

Figure 15: A heatmap depicting the 41 most significantly altered lipids (p<0.05) in FXTAS vs. control human postmortem cerebellar tissue.
Heatmap was generated using Euclidean distance measure, and Ward clustering algorithm using MetaboAnalyst 4.0 (Chong and Xia, 2018). *Red* indicates high and *blue* indicates low intensity of the metabolite relative to the median (*white).* Cer=Ceramide, CL=Cardiolipin, DG=Diradylglycerolipids, GlcCer=Glycosphingolipids, LPC=Lysophosphatidylcholine, OxPC=Oxidized Phosphatidylcholine, PC=Phosphatidylcholine, PE=Phosphatidylethanolamine, PG= Phosphatidylglycerol, SM=Sphingomyelin

Intrigued by our findings in the metabolomics of FXTAS mice cerebella as well as the subsequent *Drosophila* screen, we obtained postmortem cerebellum tissues from 5 aged human FXTAS premutation carriers and 5 controls (Table S3) and performed untargeted high-resolution lipid profiling. Significantly, we found that out of the top 41 most significantly altered lipids in the FXTAS cerebellum compared to control, 25% consisted of sphingolipids, predominantly ceramides and sphingomyelins ($p<0.05$) (Figure 15). As the representative boxplot demonstrates (Figure 16), the levels of sphingolipids are significantly elevated in the *FMR1* premutation carriers compared to controls.

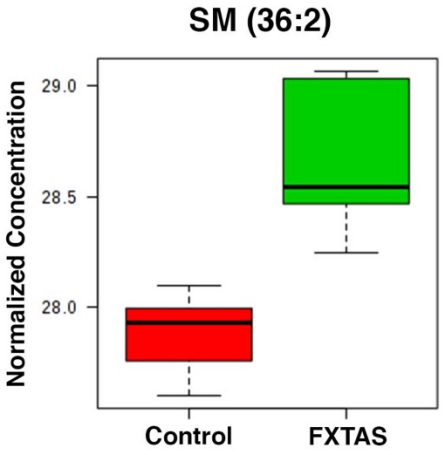

Figure 16: Box plot showing levels of Sphingomyelin (36:2) in FXTAS vs. control postmortem cerebellar tissue.

SM= Sphingomyelin

Additional genetic modifiers are identified in a comprehensive fly genetic screen for the Sphingolipid pathway

Our finding that the Sphingolipid pathway is significantly perturbed in FXTAS prompted us to perform a more comprehensive screen of potential genetic modifiers that are involved in the Sphingolipid pathway. We set out to test all the metabolic genes with fly orthologues in the

Sphingolipid pathway by knocking down the genes in FXTAS *Drosophila* (Table S4). In addition to *Schlank (CERS) and Sk2 (SPHK1)*, which were tested in the initial metabolomics screen, out of 18 additional genes tested in the Sphingolipid pathway, 4 genes resulted in significant enhancement of CGG-associated neurodegeneration in the FXTAS fly eye: *Gba1a (GBA1), Glct-1 (UGCG), Cerk (CERK) and Sply (SGPL1)* (Figure 17, Table S4).

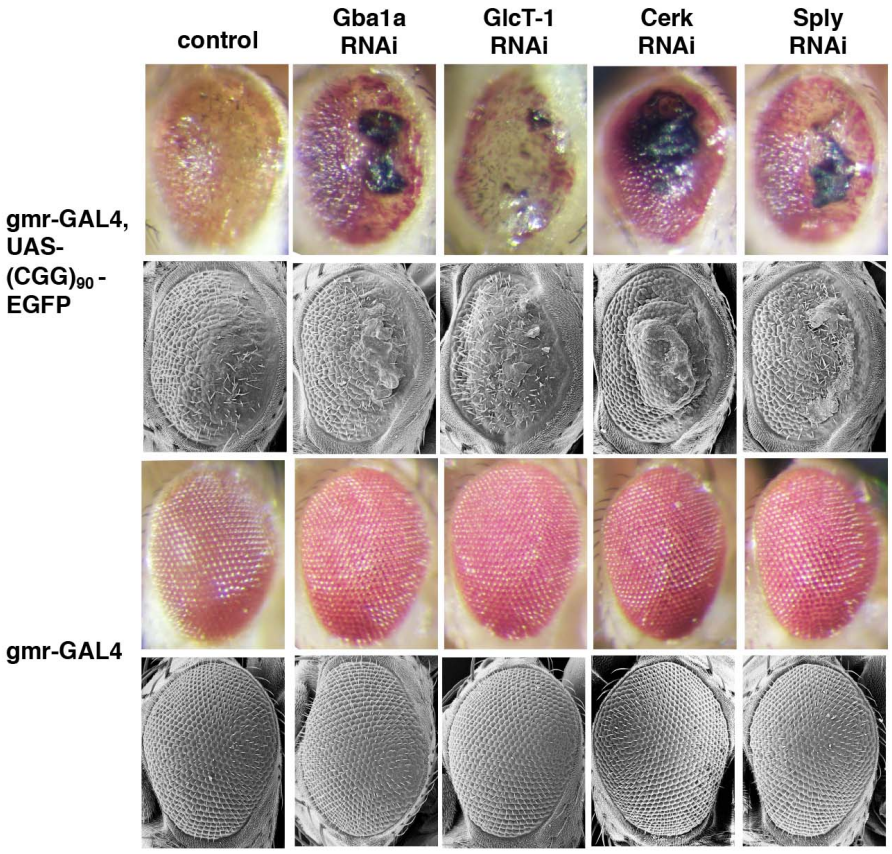

Figure 17: Knockdown of Sphingolipid genes enhances r(CGG)$_{90}$ mediated neurodegeneration in FXTAS Drosophila

Knockdown of *Gba1a* (*Gba*), *Glct-1 (Ugcg), Cerk (Cerk), Sply (Sgpl1)* enhance r(CGG)$_{90}$ mediated neurodegeneration in FXTAS *Drosophila.* Top panel, first row displays the light microscopy images from *Drosophila* of the indicated genotypes crossed to gmr-GAL4, UAS-(CGG)$_{90}$ EGFP flies. From left to right: (CGG)$_{90}$ control (gmr-GAL4, UAS-(CGG)$_{90}$-EGFP) (column 1), (CGG)$_{90}$ flies expressing RNAi knockdown of *Gba1a, Glct-1, Cerk* and *Sply* result in enhancement of the CGG-associated neurotoxicity (column 2-5). Second row shows the corresponding scanning electron microscopy (SEM) images. Bottom panel displays light microscopy and SEM images of the indicated genotypes crossed to gmr-GAL4 only.

DISCUSSION

In this study, we demonstrated successful use of *Drosophila* genetics for functional validation of the untargeted metabolic profiling data. As a result, we identified twelve genetic modifiers of CGG toxicity, which include the enzymes Ceramide Synthase and Sphingosine Kinase (Sphingolipid metabolism) and IMP Dehydrogenase (Purine metabolism). To the authors' knowledge, this constitutes the first report of metabolic profiling performed on the cerebella of a FXTAS mouse model, and the first identification of *Schlank (Cers5), Sk2 (Sphk1), Ras (Impdh1), CG8353 (Cda), CG4306 (Ggct), ChAT (ChAT), Pect (Pcyt2), Ppat-dpck (Coasy), Gba1a (GBA1) ,Glct-1 (UGCG), Cerk (CERK)and Sply (SGPL1)* as genetic modifiers of the expanded CGG premutation repeat mediated neurodegeneration in a FXTAS *Drosophila* model.

Six Ceramide Synthase variants exist in mammals, and among them, *Cers1* is expressed in the cerebellum (Purkinje cells), as well as the brain (neurons) and skeletal muscle (Tidhar and Futerman, 2013). *Schlank* is the *Drosophila* orthologue of Cers1-6. Through *Drosophila* genetics, we have demonstrated that *Schlank* modulates CGG neurotoxicity caused by the expanded premutation $(CGG)_{90}$ repeat. Previous literature has reported evidence linking CerS and cerebellum integrity, suggesting that the genetic interaction between the expanded CGG repeat and *Cers* may directly lead to disruptions in cerebellum integrity. In fact, Ginkel et al. generated CerS1-deficient mice that exhibited a foliation defect, progressive shrinkage and neuronal apoptosis in the cerebellum (Ginkel et al., 2012). In a separate study, Zhao et al. have reported that deficiency of CerS1 in mice results in progressive Purkinje cell loss and that loss of CerS1 significantly affects sphingolipid homeostasis as well as protein and organelle homeostasis (Zhao et al., 2011). Significantly, their work indicated that defects in Sphingolipid metabolism can directly result in Purkinje cell death (Zhao et al., 2011). In this study, we found that while shRNA

mediated knockdown of *Schlank* did not have any significant effect on the wildtype fly eye, *Schlank* interacted with the expanded CGG repeat, resulting in a strong enhancement of the FXTAS rough eye phenotype. Taken together, our data strongly supports the hypothesis that in the presence of the expanded CGG premutation in FXTAS, the biological function of CerS is altered, resulting in perturbation of associated metabolites in the sphingolipid pathway and neurotoxicity, especially in Purkinje cells.

Furthermore, it is worthwhile to note that Ceramide Synthase plays a pivotal role in the Sphingolipid pathway as a rate-limiting enzyme for the formation of the backbone of all sphingolipids—ceramide. Though warranting further study, the results of our *Drosophila* genetic screen raise the possibility that the genetic interaction between such critical "gateway" enzymes and the premutation CGG repeat may be the initiating factor in the global metabolic disruptions seen in FXTAS mice as well as human premutation carriers.

Sphingosine kinases can be stimulated by diverse stimuli—such as PDGF, VEGF, TNF-α to generate intracellular Sphingosine 1-phosphate (S1P) (Spiegel and Milstien, 2003). Once considered to be a mere intermediate, S1P is now known to be a critical signaling molecule for neural and vascular development (Mizugishi et al., 2005) and plays a prominent role in various cellular processes such as stress response, growth, differentiation, as well as calcium balance (Spiegel and Milstien, 2003). Intriguingly, S1P has been found to regulate cell growth (Olivera and Spiegel, 1993; Zhang et al., 1991) and to suppress programmed cell death (Cuvillier et al., 1996), whereas the precursors of S1P—Sphingosine and Ceramide—have been found to promote growth arrest and cell death (Hannun and Obeid, 2002; Kolesnick, 2002). This observation led

Spiegel et al. to propose that the relative levels of ceramide and S1P determine the cell fate, functioning as a "sphingolipid rheostat".

In this study, we observed that S1P is significantly increased in the aged FXTAS vs. aged WT comparison. In our *Drosophila* genetic screen, knockdown of *Sk2*, an orthologue of *SphK1* (and *SphK2* to a lesser extent), resulted in enhanced CGG-associated neurotoxicity while the wildtype flies were not affected by the knockdown (Figure 4). A potential explanation is that S1P may play a suppressive role against the neurotoxicity in FXTAS, and that in the presence of the premutation repeat, knockdown of *Sk2* prevents the increased production of S1P and results in enhancement of the neurotoxic phenotype. Indeed, in the wildtype fly, *Sk2* knockdown does not have an obvious effect, but in the presence of the CGG repeats, the flies demonstrate significant neurotoxicity. Furthermore, S1P's role in calcium balance may also be linked to the increased toxicity in FXTAS, as FXTAS has been recently shown to be associated with dysregulation of calcium homeostasis (Robin et al., 2017). In light of these findings, activating *SphK1* and/or increasing the intracellular concentration of S1P may be a potential path towards developing therapeutics for FXTAS.

In our comprehensive screen of metabolic genes in the Sphingolipid pathway, we identified additional genetic modifiers of CGG-associated neurodegeneration—*Gba1a (GBA1), Glct-1 (UGCG), Cerk (CERK)* and *Sply (SGPL1)*. Among these, *GBA1* encodes the lysosomal enzyme β-Glucosylceramidase (GlcCerase), which is responsible for hydrolyzing glucosylceramide into ceramide and glucose. Whereas individuals with a deficiency of this enzyme develop a rare, autosomal recessive disorder called Gaucher disease (Stirnemann et al., 2017), a multi-center analysis has demonstrated that heterozygous mutations in *GBA1* are associated with the

neurodegenerative disorder, Parkinson's disease (PD) (Sidransky et al., 2009). Interestingly, reduced GCase activity has also been observed in PD patients without mutations in *GBA1* (Murphy et al., 2014), suggesting that GCase dysfunction also plays a role in the pathogenesis of the more common idiopathic Parkinson's disease. Although not yet clearly understood, the role of *GBA1* pathogenesis is believed to have two potential mechanisms in PD. The gain of function mechanism suggests that misfolded mutant GCase in the endoplasmic reticulum (ER) may cause ER stress leading to the accumulation of α-synuclein and inhibition of protein trafficking from ER to Golgi (Stojkovska et al., 2018). On the other hand, the loss of function mechanism postulates that loss of GCase function may lead to the accumulation of lipids such as GluCer, which directly stabilizes α-synuclein aggregates and promotes accumulation of α-synuclein. Loss of function of GCase can also contribute to general lysosomal dysfunction, defective mitophagic and autophagic clearance pathways as well as Ca^{2+} dysfunction (Stojkovska et al., 2018). Given this background, the finding that *GBA1,* well known for its role in the pathogenesis of Parkinson's disease, is also a genetic modifier of CGG-associated neurodegeneration of FXTAS is intriguing and invites further research on the role of lysosomal dysfunction as well as sphingolipid regulation in FXTAS pathogenesis.

This study has used global unbiased metabolic profiling data from FXTAS mice to generate candidate genes to test using a well-established *Drosophila* model of FXTAS. Given the vast breadth and complexity of metabolomics, the interpretation of such data can often be limited to finding global trends or pathway alterations. However, as we demonstrate in this paper, the rapid, inexpensive and high-throughput nature of *Drosophila* genetic screening affords a facile method to validate the metabolomics findings by testing for genetic interactions. This method can be easily applied to other metabolomics analyses thanks to the availability of *Drosophila* models for a

variety of human diseases (McGurk et al., 2015; Prüßing et al., 2013; Sen and Cox, 2017; Wolf et al., 2006).

For future directions, it would be beneficial to further explore the enzyme gene candidates validated through *Drosophila* genetics in this paper, such as *CERS, SPHK1 and GBA1* as well as others, as potential treatment targets. This could open up another door to much-needed treatment opportunities for FXTAS patients (Kong et al., 2017). Furthermore, the 186 significantly altered metabolites presented in Chapter 1, as well as the 41 significantly altered lipids in the human postmortem cerebella of *FMR1* premutation carriers present a novel and useful resource in the search for biomarkers for FXTAS.

ACKNOWLEDGEMENTS

This work was supported by the National Institutes of Health [NS051630 to D.L.N, P.J., U54 HD083082 to D.L.N., 2T32GM007526 support for Y.G. and NS091859 to E.G.A, P.J.]. This study was supported in part by the Emory Integrated Lipidomics Core (EILC), which is subsidized by the Emory University School of Medicine and is one of the Emory Integrated Core Facilities. Additional support was provided by the Georgia Clinical & Translational Science Alliance of the National Institutes of Health under Award Number UL1TR002378. The content is solely the responsibility of the authors and does not necessarily reflect the official views of the National Institutes of Health.

SUPPLEMENTAL MATERIALS

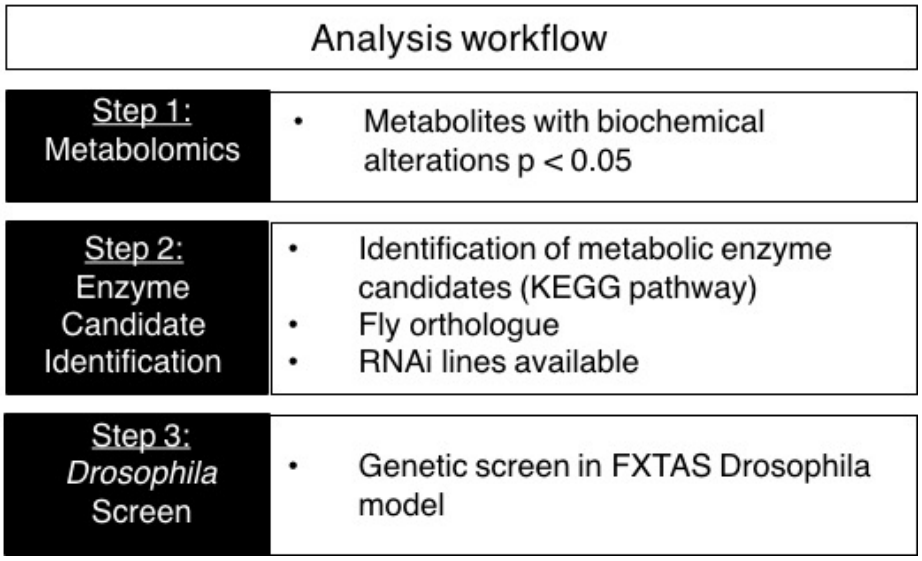

Figure S1. Analysis workflow for functional validation of metabolic profiling. A delineation of the workflow for functional validation after untargeted metabolic profiling of FXTAS and WT mice cerebellum. 186 altered metabolites ($p<0.05$) were manually curated for enzyme candidates that modulate the levels of that metabolite following a selection criteria. 28 gene candidates were then screened for genetic interaction with CGG toxicity using the FXTAS *Drosophila* model.

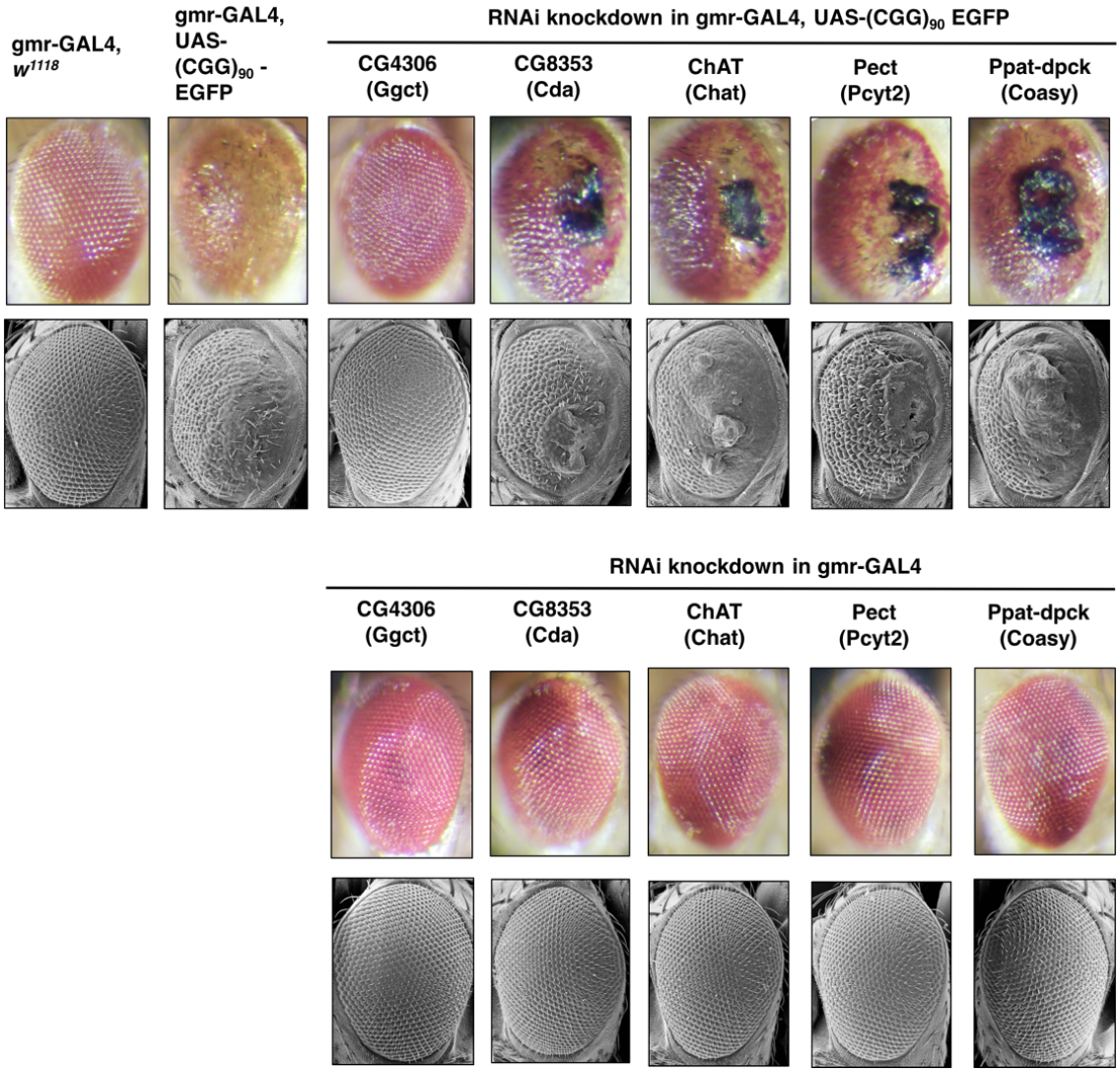

Figure S2. Eight candidate metabolic genes show genetic modulation of CGG toxicity in the fly eye in genetic screen. FXTAS r(CGG)$_{90}$ flies expressing GAL4 under the eye-specific gmr driver were crossed with flies harboring shRNA transgene against the target candidate gene, downstream from the UAS sequence (UAS-TRiP). Progeny that express the shRNA against target gene in the eye were collected, aged for 7 days and visualized using light microscopy and SEM. Results of the genetic screen revealed eight candidate genes that show significant modulation of the CGG-toxicity associated rough eye phenotype in FXTAS *Drosophila*. First panel, first row displays the light microscopy, from left to right: WT control (gmr-GAL4) (column1), (CGG)$_{90}$ control (gmr-

GAL4, UAS-$(CGG)_{90}$-EGFP) (column2), $(CGG)_{90}$ flies expressing RNAi knockdown of the *Drosophila* genes *CG4306(Ggct),* and *CG8353 (Cda) and Chat (ChAt), Pect (Pcyt2) and Ppat-dpck (Coasy).* Second row shows the corresponding scanning electron microscopy images. Images for *Schlank, Sk2 and Ras* are shown in Figure 13 and 14, respectively. Second panel displays light microscopy and SEM of the gmr-GAL4 only controls, demonstrating that no change occurs upon knockdown of the genes in a wildtype fly.

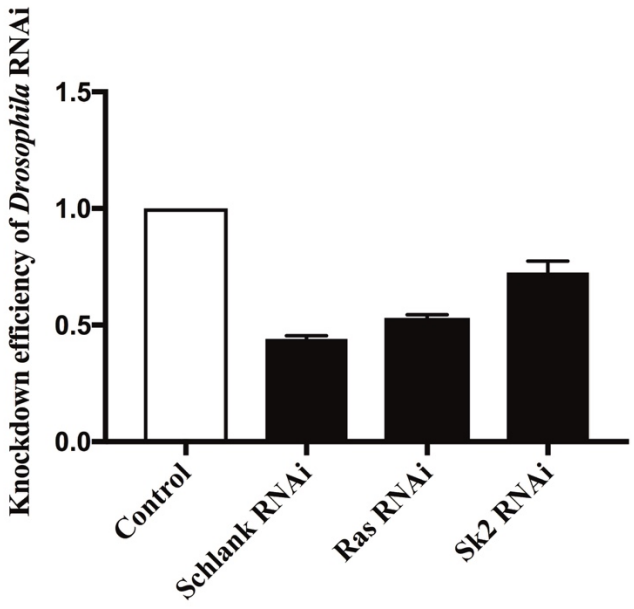

Figure S3. Knockdown efficiency of *Drosophila* RNAi. RT-PCR was performed to compare the expression of *Schlank, Ras*, and *Sk2* in the actin-GAL4 flies crossed to RNAi lines with control actin-GAL4 flies, normalized to housekeeping genes *Sdha and Cyp1,* respectively. Results revealed significant RNAi knockdown efficiency, especially for *Schlank* and *Ras*.

Table S1. Results of *Drosophila* screen (genes curated based on mouse global metabolic profiling) FXTAS r(CGG)$_{90}$ flies expressing GAL4 under the eye-specific gmr driver were crossed with flies harboring shRNA transgene against the target candidate gene, downstream from the UAS sequence (UAS-TRiP). Progeny that express the shRNA against target gene in the eye were collected, aged for 7 days and visualized using light microscopy and SEM. Results of the genetic screen revealed eight candidate genes that show significant modulation of the CGG-toxicity associated rough eye phenotype in FXTAS *Drosophila*.

#	Metabolite	Mouse Gene		*Drosophila* Ortholog	BDSC stock	Screen Phenotype
1	Inosine 5'-monophosphate	*Ampd2*	*Adenosine Monophosphate Deaminase 2*	*AMPdeam*	38953	No change
2	Urea	*Arg1*	Arginase 1	*arg*	56881	No change
3	Deoxycarnitine; Carnitine	*Bbox1*	Gamma-Butyrobetaine Hydroxylase	*CG5321*	57482	No change
4	2'-deoxycytidine	*Cda*	Cytidine Deaminase	*CG8353*	51915	Enhanced
5	Cytidine 5'-diphosphocholine; Cytidine-5'-diphosphoethanolamine	*Cept1*	Choline/Ethanolamine Phosphotransferase 1	*bbc*	50535	No change
6	Sphingosine; ceramide (d18:1/20:0, d16:1/22:0, d20:1/18:0)	*Cers5*	Ceramide Synthase 5	*schlank*	29340	Enhanced
7	Choline	*Chat*	Choline O-Acetyltransferase	*ChAT*	60028	Enhanced
8	Creatine phosphate	*Ckb*	Creatine Kinase B	*Argk*	35221	No change
9	Carnosine	*Cndp2*	Carnosine Dipeptidase 2	*CG17337*	62263	No change
10	Coenzyme A	*Coasy*	Coenzyme A Synthase	*Ppat-Dpck*	57231	Enhanced
11	Palmitoylcarnitine (C16); Carnitine	*Cpt1a*	Carnitine Palmitoyltransferase 1	*whd*	34066	No change
12	Palmitoylcarnitine (C16); Carnitine	*Cpt2*	Carnitine Palmitoyltransferase 2	*CPT2*	51900	No change
13	Hypotaurine	*Csad*	Cysteine Sulfinic Acid Decarboxylase	*b*	27511	No change
14	Hypotaurine	*Gad1*	Glutamate Decarboyxlase	*Gad1*	28079	No change

15	5-oxoproline	*Ggct*	Gamma-glutamylcyclotransferase	*CG4306*	65890	Suppressed
16	Glycerol 3-phosphate	*Gpat3*	Glycerol-3-Phosphate Acyltransferase 3	*CG3209*	42863	No change
17	3-hydroxyisobutyrate	*Hibch*	3-Hydroxyisobutyryl-CoA Hydrolase	*CG5044*	52917	No change
18	Inosine 5'-monophosphate; Xanthosine	*Impdh1*	Inosine Monophosphate Dehydrogenase 1	*Ras*	31653	Enhanced
19	Inosine 5'-monophosphate (IMP)	*Itpa*	Inosine Triphosphatase	*CG8891*	50598	No change
20	Coenzyme A	*Aasdhppt*	Holo-[actyl-carrier-protein] Synthase	*CG32099*	67784	No change
21	Pantothenate	*Pank1*	Pantothenate Kinase	*Fbl*	35259	No change
22	Cytidine 5'-diphosphocholine; Cytidine-5'-diphosphoethanolamine	*Pcyt1a*	Phosphate Cytidylyltransferase 1, Choline	*Cct1*	32854	No change
23	Cytidine 5'-diphosphocholine; Cytidine-5'-diphosphoethanolamine	*Pcyt2*	Phosphate Cytidylyltransferase 2, Ethanolamine	*Pect*	63710	Enhanced
24	Pyridoxal	*Pdxk*	Pyridoxal Kinase	*Pdxk*	57788	No change
25	Pyridoxal	*Phospho2*	Pyridoxal Phosphate Phosphatase	*CG12237*	38343	No change
26	Sphingosine; Sphingosine 1-phosphate	*Sphk1*	Sphingosine Kinase 1	*Sk2*	36741	Enhanced
27	N6,N6,N6-trimethyllysine	*Tmlhe*	Trimethyllysine Hydroxylase Epsilon	*CG4335*	57768	No change
28	Pantothenate	*Vnn1*	Pantetheinase	*Btnd*	60020	No change

Table S2. Primers for RT-PCR

Drosophila gene	Forward	Reverse
Schlank	TGCCAGTGAGTGACCAGTAG	ACAGCTTCATCTTTGGCGTG
Ras	TCTACCAGGTGTCCACGTAC	CGGTACTTCTTAAGGCGCAC
Sk2	ACGACGTGAGCGATACCTTCT	TGTTGCTCCTTAACAATGCTACC
Sdha	CATGCTGCTGTGTTCCGCGA	ACCATCCAGGGGCTTGCTGA
Cyp1	TCGGCAGCGGCATTTCAGAT	TGCACGCTGACGAAGCTAGG

Table S3. Sample information for postmortem cerebellar tissues

Sample	Age	Sex	CGG repeat size
FXTAS 1	69	M	58
FXTAS 2	89	F	30, 57
FXTAS 3	84	F	27, 59
FXTAS 4	81	M	67
FXTAS 5	70	M	75
Control 1	85	M	N/A
Control 2	70	F	N/A
Control 3	89	F	N/A
Control 4	70	F	N/A
Control 5	86	F	N/A

Table S4. Results of Drosophila screen (Sphingolipids).

FXTAS r(CGG)$_{90}$ flies expressing GAL4 under the eye-specific gmr driver were crossed with flies harboring shRNA transgene against the target candidate gene, downstream from the UAS sequence (UAS-TRiP). Progeny that express the shRNA against target gene in the eye were collected, aged for 7 days and visualized using light microscopy and SEM. Results of the genetic screen revealed four candidate genes that show significant modulation of the CGG-toxicity associated rough eye phenotype in FXTAS *Drosophila*.

#	Human Gene		*Drosophila* Ortholog	BDSC stock	Screen Phenotype
1	*ACER2*	Alkaline Ceramidase 2	*bwa*	29409	No change
2	*AGXT*	Alanine-Glyoxylate and Serine-Pyruvate Aminotrasnferase	*Spat*	51935	No change
3	*ASAH2*	N-Acylsphingosine Amidohydrolase 2	*CDase*	36764	No change
4	*CERK*	Ceramide Kinase	*Cerk*	35361	Enhanced
5	*DEGS2*	Delta 4-Desaturase, Sphingolipid 2	*ifc*	32514	No change
6	*GBA*	Glucosylceramidase Beta	*Gba1a*	38379	Enhanced
7	*GBA2*	Glucosylceramidase Beta 2	*CG33090*	36688	No change
8	*GLA*	Galactosidase Alpha	*CG7997*	63655	No change
9	*KDSR*	3-Ketodihydrosphingosine Reductase	*CG10425*	64494	No change
10	*PLPP1*	Phospholipid Phosphatase 1	*wun*	32429	No change
11	*SGPL1*	Sphingosine-1-Phosphate Lyase 1	*Sply*	43304	Enhanced
12	*SMPD1*	Sphingomyelin Phosphodiesterase 1	*CG3376*	36760	No change
13	*SMPD2*	Sphingomyelin Phosphodiesterase 2	*CG12034*	36759	No change
14	*SMPD4*	Sphingomyelin Phosphodiesterase 4	*CG6962*	51682	No change
15	*SPTLC1*	Serine Palmitoyltransferase Long Chain Base Subunit 1	*Spt-I*	55685	No change
16	*SPTLC2*	Serine Palmitoyltransferase Long Chain Base Subunit 2	*lace*	51475	No change
17	*UGCG*	UDP-Glucose Ceramide Glucosyltransferase	*GlcT-1*	67304	Enhanced
18	*UGT8*	UDP Glycosyltransferase 8	*CG30438*	51790	No change

CHAPTER 3: Identification of genetic modifiers of FXTAS by combining whole genome sequencing with fly genetics

ABSTRACT

Fragile X-associated tremor/ataxia syndrome (FXTAS) is an adult-onset neurodegenerative disorder caused by the premutation CGG repeat expansion (55-200 repeats) within the 5'UTR of *FMR1*. A significant proportion of male premutation carriers develop the FXTAS phenotype later in adulthood, which includes intention tremor, cerebellar ataxia, progressive neurodegeneration, parkinsonism and cognitive decline, while other male carriers do not exhibit disease at all. Importantly, a mechanistic understanding of FXTAS disease pathogenesis is yet to be completely elucidated, and as a result, we do not have an explanation for the significant variability in the onset and phenotypic presentation of FXTAS. In an effort to tackle this conundrum, we set out to identify genetic modifiers that modulate CGG toxicity and that may account for the variable phenotype and onset of disease. We performed whole genome sequencing on 110 male premutation carriers (CGG_{55-200}) and prioritized candidate variants to select candidate genetic modifiers. Out of the 104 genes tested, we found that 19 genes genetically modulate CGG associated neurotoxicity in the fly eye, such as *Prosbeta5 (PSMB5), pAbp (PABPC1L), e(y)1 (TAF9)* and *CG14231 (OSGEPL1).* Taken together, our analyses suggest the presence of multiple genetic modifiers that modulate the CGG-associated neurotoxicity in FXTAS. Furthermore, we show that combining whole genome sequencing with a *Drosophila* genetic screen could facilitate the identification of novel genetic modifiers of human diseases.

KEYWORDS

Neurodegeneration, FXTAS, FMR1 premutation, genetic modifier, WGS

INTRODUCTION

Fragile X-associated tremor/ataxia syndrome (FXTAS) is a late-onset neurodegenerative debilitating disorder characterized by cerebellar dysfunction, with the main clinical presentations of intention tremor and cerebellar ataxia (Hagerman and Hagerman, 2015; Jacquemont et al., 2003). Premutation carriers with 55-200 expanded CGG repeats in the 5'UTR of *FMR1* are predisposed to developing FXTAS. On average, individuals carry 5-54 CGG repeats, whereas CGG repeats greater than 200 leads to fragile X syndrome (FXS) due to DNA methylation-mediated silencing of *FMR1* transcription and translation (Colak et al., 2014; Hagerman and Hagerman, 2002; Kremer et al., 1991; Verkerk et al., 1991). Importantly, premutation carriers are not rare in the population, with an estimated prevalence of 1:259 women and 1:813 men (Dombrowski et al., 2002; Rousseau et al., 1995). A persisting conundrum is that not all premutation carriers develop FXTAS; approximately 40% of males and 16% of females develop FXTAS in late adulthood (Hagerman and Hagerman, 2015; Jacquemont et al., 2004). The incomplete penetrance of FXTAS has motivated the search for genetic modifiers that may serve as genetic biomarkers for prognosis, and more importantly, as potential therapeutic targets (Kong et al., 2017).

In the study of FXTAS, mouse and fly models have been developed to study the molecular and genetic basis of FXTAS. Our group has previously established a Drosophila model of FXTAS that expresses the premutation CGG repeat in the context of the human *FMR1* 5'UTR. Owing to its advantages of rapid reproduction and affordability as well as facile genetics, the FXTAS *Drosophila* model has been instrumental in showing that the premutation CGG repeats are sufficient to cause FXTAS pathology, as well as in the identification of hnRNP A2/B1 and Pur α

as RNA binding proteins sequestered by the CGG premutation expansion (Jin et al., 2003, 2007; Sofola et al., 2007). Expression of $r(CGG)_{90}$ under the eye-specific driver in *Drosophila*, gmr-GAL4, leads to a rough eye phenotype in the fly, characterized by cell death, loss of pigmentation and ommatidial disruption (Jin et al., 2003).

Here we demonstrate that using FXTAS *Drosophila* as a genetic screening tool can be powerful in the validation of candidate genes derived from WGS of FXTAS premutation carrier males. Out of the 104 genes tested, we have identified 19 genes as potential genetic modifiers of FXTAS, which indicates the presence of multiple genetic modifiers that modulate neurotoxicity in FXTAS, and these genes can be used as potential therapeutic targets.

METHODS

Study Population

The protocols and consent forms were approved by the Institutional Review Board at Emory University, and informed consent was obtained from all subjects. Subjects were identified from previous FX research projects at Emory, recruitment efforts at scientific conferences, and through collaborations with other research groups. Subjects were screened for eligibility based on premutation carrier status, presence or absence of symptoms of tremor and/or ataxia, age, and gender. Only one family member per pedigree was enrolled in the study. After a subject was determined to be eligible, either a blood or saliva sample was collected. In addition, a brief medical history was collected from the subject or a family member, and pertinent medical records were collected. If medical records did not provide sufficient information for determining eligibility, a video exam was conducted by study personnel and reviewed by a neurologist. “Case” subjects were defined as male or female premutation carriers with symptoms of tremor or ataxia before age

65, as reviewed by a neurologist. “Control” individuals were defined as male premutation carriers that reached age 69 without significant tremor or ataxia symptoms, as reviewed by a neurologist.

Sample preparation for WGS

DNA was extracted from biological samples using Qiagen Qiamp DNA Blood Mini Kit, Gentra Puregene extraction kit, or prepIT-L2P protocol from Oragene. FRAXA CGG repeat numbers were determined by a fluorescent sequencer method (Meadows et al., 1996). For males samples that did not amplify or females with only one allele, a second PCR protocol was used (Brown et al., 1993). The PCRs for FRAXA consisted of 1X PCR Buffer (Gibco/BRL), 10% dimethyl sulfoxide (DMSO), 370 μM deazaG, 500 μM d(ACT), 0.3 μM each primer, 15 ng T4 gene 32, and 1.05 U Roche Expand Long Taq. Primers for the *FMR1* gene were :

C:5’Cy5GCTCAGCTCCGTTTCGGTTTCACTTCCGGT3’

F:5’AGCCCCGCACTTCCACCAGCTCCTCCA3’ (Fu et al., 1991).

Samples were stored and sent in batches for WGS at Hudson Alpha.

WGS

For HiSeq X Ten sequencing, DNA samples were normalized to 1,000ng of DNA in 50ul of water, sheared to ~350-400bp fragments with a Covaris LE-220 instrument, and end-repaired and A-tailed using New England Biolabs End-Repair and A-Tailing kits, under the manufacturer’s recommended conditions. Following each step, the library was purified via Agencourt AMPure XP beads and eluted in water. Standard Illumina paired-end adaptors were ligated to the A-tailed DNA via New England BioLabs Rapid Ligation kit, purified using AMPure XP beads, and amplified with KAPA Biosystems HIFI PCR kit using 6 cycles of PCR. The primers were standard Illumina primers with a custom 7-base sample barcode in the i7 position. The final library was

quality controlled using size verification via PerkinElmer LabChip GX and real-time PCR using the KAPA SYBR FAST qPCR Master Mix, primers, and standards according to the manufacturer's directions. Libraries were normalized to 2.5 nM stocks for use in clustering and sequencing.

Samples were processed on the Illumina X10 with 150bp reads. Raw data from HudsonAlpha was transferred to the Human Genetics Computational Cluster (HGCC) at Emory University and mapped to the Human Genome Build GRCH38 (hg38) with a 95% stringency. All samples were mapped using PEMapper and called using PECaller (Johnston et al., 2017). Appropriate QC metrics were used to ensure that only high-quality samples were kept in the data set. These included read depth, mapping percentage, Ts/Tv ratio, Silent/Replacement ratio, theta, theta in exons, fraction of non-reference homozygote calls and number of novel variants called. With the exception of samples of African ancestry, samples were excluded from the final data set if they were more than three standard deviations from the mean for any metric. Samples were also excluded if they had >5% missing calls at sites. Variants were excluded if they were missing >10% of calls across all samples or for HWE violations with p values < .00001. The entire data set was annotated using Bystro (bystro.io) (Kotlar et al., 2018).

Drosophila **screen**

Transgenic flies expressing r$(CGG)_{90}$ were previously described. The gmr-GAL4 and UAS-TRiP lines were obtained from Bloomington Stock Centre (Bloomington, IN, USA). All *Drosophila* lines were maintained, and crosses were performed in standard medium at 25 °C. After performing the crosses, progeny was collected and aged to 7 days. The screen was performed by

scoring eye phenotype, which was visualized using light microscopy and confirmed with scanning electron microscopy.

Scanning Electron Microscopy

Following dehydration in increasing concentrations of ethanol (25%, 50%, 75%, 100%), whole flies were incubated for 1 hr with hexamethyldisilazane (Electron Microscopy Sciences). After removing the hexamethyldisilazane, the flies were dried overnight in a fume hood and subsequently analyzed using Topcon DS-130F and DS-150F Field Emission Scanning Electron Microscope.

RESULTS

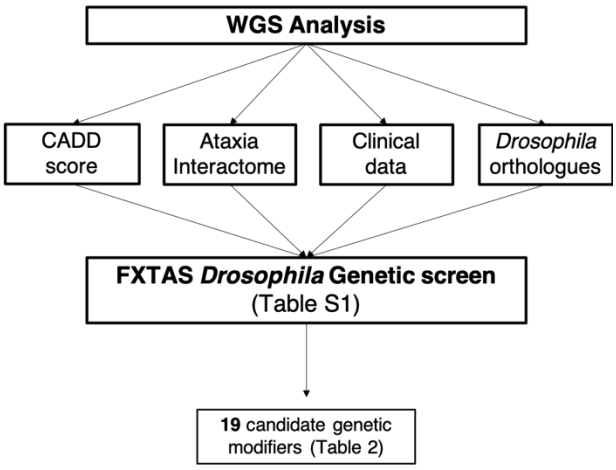

Figure 18: Schematic depicting the analysis workflow from WGS analysis to Drosophila screen.

Candidate genes were selected based on the variant CADD score, inclusion in the Ataxia interactome (Lim et al., 2006), clinical phenotype data of the variant carriers as well as the existence of *Drosophila* orthologues and availability of RNAi lines. 104 genes were selected to test for genetic modulation in FXTAS *Drosophila*. 19 genes demonstrated significant modulation of CGG-associated neurodegeneration in the FXTAS fly eye.

Whole genome sequencing and *Drosophila* screen identifies 19 genes as genetic modifiers of FXTAS

With the goal of identifying genetic modifiers of FXTAS, we recruited and collected whole blood samples from 110 *FMR1* premutation carriers for WGS. Despite being one of the largest recruitment cohorts of *FMR1* premutation carriers to date, we were not statistically powered to identify variants that may act as genetic modifiers predisposing or protecting against disease. Therefore, we employed a carefully curated criteria to select candidate genes based on the WGS data (Figure 18), prioritizing variants based on CADD score, as well as enrichment of the variants in early vs. delayed onset phenotypes of the premutation carriers and any reported interaction of the gene with known ataxia genes (Lim et al., 2006) (see Material and Methods).

	Chr:pos Variant	Human Gene	*Drosophila* Gene	
1	chr1:33036780	*AK2*	***Adk2***	High CADD score
2	chr6:35078619	*ANKS1A*	***CG4393***	
3	chr5:69174962	*CCNB1*	***CycB***	
4	chr4:110510288	*ENPEP*	***CG32473***	
5	chr2:127292669	*ERCC3*	***hay***	
6	chr2:120990472	*GLI2*	***ci***	
7	chr1:200992313	*KIF21B*	***Klp31E***	
8	chr3:97959130	*MINA*	***CG2982***	
9	chr2:189753972	*OSGEPL1*	***CG14231***	
10	chr20:44916864	*PABPC1L*	***pAbp***	
11	chr9:128720227	*PKN3*	***pkn***	
12	chr14:23034812	*PSMB5*	***prosbeta5***	
13	chr15:55234786	*RAB27A*	***Rab27***	
14	chr2:210002690	*RPE*	***CG30499***	
15	chr15:45101228	*DUOX2*	***Duox***	Indel/frameshift
16	chr12:7795090	*NANOG*	***Bsh***	
17	chr14:23565950	*AP1G2*	***Ap-1gamma***	Ataxia Interactome Genes
18	chr11:66625654	*RBM14*	***lark***	
19	chr5:69365721	*TAF9*	***e(y)1***	

Table 2: List of 19 human genes and corresponding Drosophila orthologues that demonstrated genetic modulation of CGG-associated neurodegeneration in the FXTAS Drosophila screen.

The table indicates the genomic location of the variant in the premutation carrier population. 14 genes had variants with high CADD scores, 2 had indel/frameshift variants, and 3 genes were part of the Ataxia Interactome (Lim et al.,2006).

As a result, we selected 104 genes to screen in the FXTAS *Drosophila* model by knocking down the candidate gene in the FXTAS fly eye using the UAS-GAL4 system, then screening for enhancement or suppression of the rough eye phenotype (Figure 18, Table S2). Out of the 104 candidate genes screened, 19 genes exhibited genetic modulation of CGG toxicity, such as *Prosbeta5 (PSMB5), pAbp (PABPC1L), e(y)1 (TAF9)* and *CG14231 (OSGEPL1).* (Figure 18-19, Table 2, Table S1).

14 of the 19 genetic modifier genes had variants with high CADD scores in *FMR1* premutation carriers, with CADD scores greater than 30. Two of the genetic modifier genes had variants that were indels or frameshift variants. The remaining three of the genetic modifier genes were among those reported to interact with known ataxia genes (Lim et al., 2006).

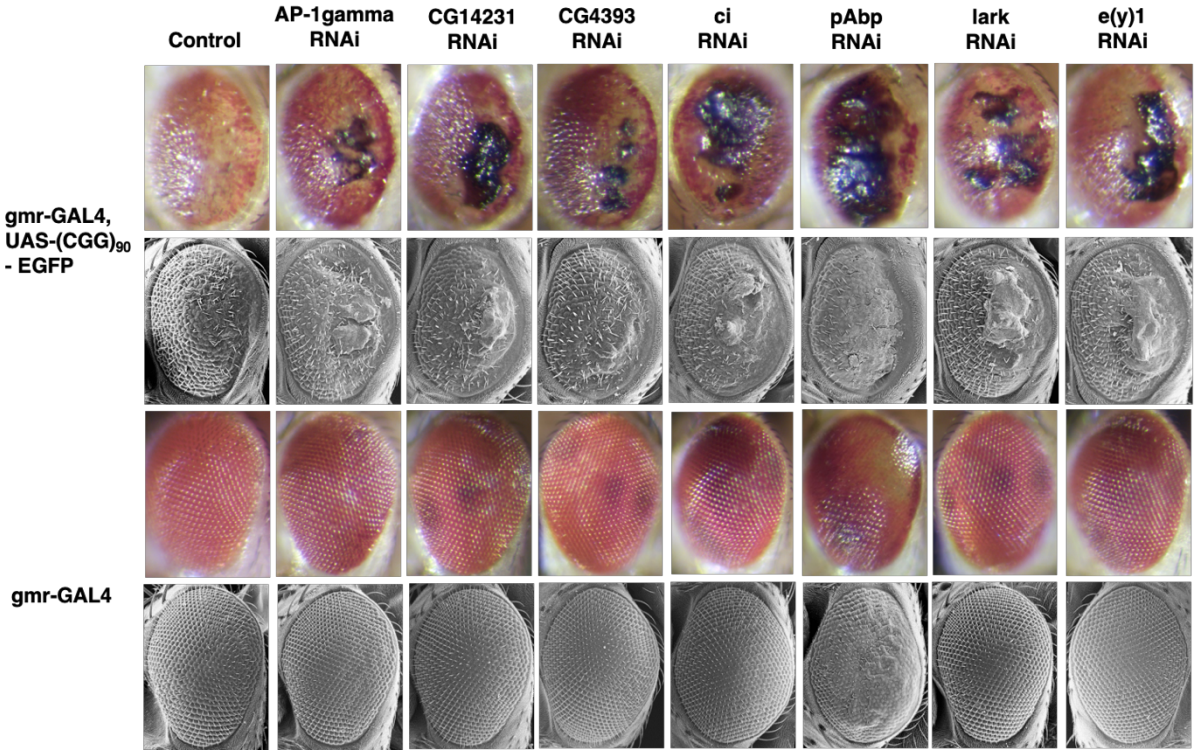

Figure 19: Drosophila screen identifies 19 genetic modifiers of CGG-associated neurotoxicity.

Top panel and bottom panel display the light microscopy (first row) and scanning electron microscopy (SEM) images (second row) from Drosophila of the indicated genotypes crossed to gmr-GAL4, UAS-$(CGG)_{90}$ EGFP and gmr-GAL4 flies as control, respectively. Figure shows RNAi knockdown of *Ap-1gamma, CG14231, CG4393, ci, pAbp, lark and e(y)1* result in enhancement of CGG-associated neurodegeneration while WT flies expressing RNAi knockdown of the respective genes do not show any phenotype.

Translating Ribosome Affinity Purification Sequencing (TRAP-Seq) on cerebella of FXTAS and control mice add additional insight to *Drosophila* screen results

Human Gene	TRAP seq log2 fold change (FXTAS mice vs. WT mice)	*Drosophila* Phenotype upon knockdown
AK2	-0.578	suppression
ANKS1A	Not detected	enhancement
AP1G2	Infinite (WT mRNA = 0)	enhancement
CCNB1	Not detected	suppression
DUOX2	**-0.378**	**enhancement**
ENPEP	Not detected	enhancement
ERCC3	-0.857	suppression
GLI2	**-1.22**	**enhancement**
KIF21B	**-0.272**	**enhancement**
MINA	Not detected	suppression
NANOG	0.00361	enhancement
OSGEPL1	**-1.87**	**enhancement**
PABPC1L	Not detected	enhancement
PKN3	Not detected	enhancement
PSMB5	**0.335**	**suppression**
RAB27A	**-3.41**	**enhancement**
RBM14	1.05	enhancement
RPE	Infinite (WT mRNA = 0)	enhancement
TAF9	2.12	enhancement

Table 3: Translating Ribosome Affinity Purification Sequencing shows differences in mRNA bound to ribosomes in FXTAS vs. WT.
Negative log fold change indicates decreased mRNA bound to ribosomes in FXTAS than in WT. Positive log fold indicates increased mRNA bound to ribosomes in FXTAS. Third column indicates the *Drosophila* phenotype upon knockdown of the gene. *Red* indicates genes that show a direct relationship between *Drosophila* and mouse data, in which knockdown of the gene results in enhancement in *Drosophila* and FXTAS mice display lower levels of the mRNA than WT. *Blue* indicates genes that show a direct relationship between *Drosophila* and mouse data, in which suppression of the gene results in enhancement in *Drosophila* and FXTAS mice display higher levels of the mRNA than WT.

In an effort to further validate these genetic modifiers, we took advantage of an unpublished dataset where we have assessed the differences in the translatomes of FXTAS vs. control by performing TRAP-Seq to compare the levels of mRNA bound to ribosomes in cerebellum tissue from FXTAS $(CGG)_{90}$ mice (Hashem et al., 2009) vs. control littermates. As Table 3 shows, in 6 of the 19 genes, the TRAP-seq data correlated directly with the results of the *Drosophila* screen. In 5 of the 6 genetic modifiers, the genes that displayed lower levels of mRNA in the FXTAS mice

also resulted in enhancement of CGG-associated neurotoxicity upon knockdown in FXTAS *Drosophila* expressing r(CGG)$_{90}$. However, for one genetic modifier, *Psmb5,* the mRNA levels were higher in FXTAS than wildtype, and upon knockdown of this gene in *Drosophila*, the FXTAS flies exhibited a suppression of CGG-associated neurodegeneration.

DISCUSSION

By combining whole genome sequencing of 110 human *FMR1* premutation carriers with *Drosophila* genetics, we have identified 14 candidate genes as strong enhancers of CGG-associated neurotoxicity in FXTAS and 5 candidate genes such as *PSMB5* as strong suppressors of CGG-associated neurodegeneration. These genes are promising candidates for biomarker discovery and therapeutic development and warrant further investigation. Herein we discuss some of the candidate genetic modifiers (Figure 1B).

AK2 encodes Adenylate Kinase, a ubiquitously expressed enzyme involved in cellular adenine and guanine nucleotide homeostasis. Three isozymes of Adenylate Kinase exist: AK1, AK2 and AK3, among which AK2 and AK3 are expressed in the mitochondria (Nobumoto et al., 1998). Given that Adenylate kinase plays a pivotal role in the phosphate utilization and AMP de novo biosynthesis pathways, the genetic interaction between *AK2* and r(CGG)$_{90}$ repeats provides another indication that metabolic perturbations are a critical component of FXTAS pathogenesis. Furthermore, since *AK2* encodes a mitochondrial enzyme, the identification of *AK2* as a genetic modifier may further corroborate the close relationship between mitochondrial function and FXTAS pathology.

RBM14 encodes RNA Binding Protein 14, an RNA-binding protein that plays a role in DNA repair, as well as transcription and RNA splicing (Kai et al., 2016; Simon et al., 2017). *RBM14* is a gene known to interact with known Ataxia proteins (Lim et al., 2006). Furthermore, RBM14 has been reported to be a component of Paraspeckles, a nuclear body consisting of nuclear RNA binding proteins such as RBM14, FUS and TAF15, that are induced in a stressful setting such as viral infection and proteasome inhibition (Clemson et al., 2009; Sasaki and Hirose, 2009). The function of these Paraspeckles remain to be studied. Most significantly, along with FUS, RBM14 has been shown to be recruited to sites of DNA damage. However, while FUS knockdown inhibits the formation of γH2AX in response to Double Strand Breaks (DSBs), knockdown of *RBM14* actually results in prolonged γH2AX foci (Wang et al., 2013; Yuan et al., 2014). The exact mechanisms of how FUS and RBM14 contribute to DNA repair has yet to be elucidated. Given our knowledge that γH2AX foci are present in FXTAS inclusions, it would be very interesting to further investigate the genetic interaction between *RBM14* and CGG-associated neurotoxicity.

ENPEP is a gene that encodes the enzyme Glutamyl Aminopeptidase, which plays a role in Peptide hormone metabolism as well as the Renin-Angiotensin System. Curiously, the variant found in *FMR1* premutation carriers, $ENPEP^{rs33966350\text{-}A}$, not only has a high predicted CADD score of 42 but is also an Expression Quantitative Trait Locus (eQTL) associated with decreased expression of *ENPEP* mRNA across a spectrum of tissues (Supplementary Figure S1, Genotype-Tissue Expression (GTEx) Project). In FXTAS *Drosophila*, knockdown of the *Drosophila* orthologue of *ENPEP* resulted in significant enhancement of CGG-associated neurodegeneration (Table S1). Although in our 110 *FMR1* premutation carriers we did not see a significant enrichment of $ENPEP^{rs33966350\text{-}A}$ in carriers with early onset of disease, based on the *Drosophila* screen, we hypothesize that the premutation carriers harboring $ENPEP^{rs33966350\text{-}A}$ may be at increased risk of

showing symptoms of CGG-associated toxicity. It would be of strong value to test this hypothesis in future experiments.

Finally, *TAF9* encodes TATA box binding protein (TBP)-associated factor 9, and is part of the Ataxia Interactome (Lim et al., 2006). In particular, TAF9 is a component of the TBP-free TAF-containing-SPT3-TAF9-GCN5-acetyltransferase transcription complex, and therefore has been associated with ATXN7 and Spinocerebellar Ataxia 7 (Nakamura et al., 2012). Intriguingly, the highest CADD variant in *TAF9* found in *FMR1* premutation carriers, $TAF9^{rs4252233\text{-}A}$, is an eQTL that is associated with increased expression of mRNAs of several genes across multiple tissues: *TAF9* as well as *SMN2* (Survival of Motor Neuron 2), the gene most well-known for its role in Spinal Muscular Atrophy (SMA). (Supplementary Figures S2-3). Since knockdown of the *TAF9* orthologue resulted in enhanced CGG-induced neurotoxicity in *Drosophila*, we hypothesize that the $TAF9^{rs4252233\text{-}A}$ may play a protective role in FXTAS progression or onset. However, in our current study population, we did not see an enrichment of $TAF9^{rs4252233\text{-}A}$ in asymptomatic *FMR1* premutation carriers. It may also be worthwhile to use *Drosophila* genetics to test whether *SMA* may be a genetic modifier of CGG-associated neurotoxicity, since $TAF9^{rs4252233\text{-}A}$ has been shown to modulate the expression of *SMA* as well.

ACKNOWLEDGEMENTS

This work was supported by the National Institutes of Health [NS051630 to D.L.N, P.J, NS091859 to P.J., S.S., S.T.W. and E.G.A.]

SUPPLEMENTAL MATERIALS

Table S1. Results of *Drosophila* screen

#	Human Gene	*Drosophila* Ortholog	UAS TRiP stock	Drosophila Phenotype
1	ACAD9	*Egm*	36739	Enhanced but n<10
2	ACO2	Acon	34028	No phenotype
		CG4706	51359	No phenotype
			58074	Slightly enhanced
3	ADPGK	CG6650	57528	No phenotype
4	AGBL3	NnaD	33549	No phenotype
			44036	No phenotype
			51430	Slightly enhanced
5	AHCY	Ahcy	51477	No phenotype
6	AK2	Adk2	55320	Suppressed
7	ALDH1L2	CG8665	62266	No phenotype
8	AMHR2	wit	25949	No phenotype
			41906	No phenotype
9	ANKHD1	mask	31574	No phenotype
			34571	No phenotype
10	ANKS1A	CG4393	58087	Enhanced
11	AP1G2	AP-1gamma	27533	Enhanced
12	AREL1	CG4238	36086	No phenotype
13	ARHGEF3	RhoGEF64C	31130	No phenotype
14	ATF6B	Atf6	26211	No phenotype
15	ATRIP	mus304	61355	No phenotype
16	ATRNL1	dsd	53318	No phenotype
17	ATXN2L	Atx2	36114	No phenotype
			44012	No phenotype
18	C1QBP	P32	34585	No phenotype
19	CCNB1	CycB	34544	No phenotype
			38957	No phenotype
			38979	Suppressed
20	CDH15	CadN	27503	No phenotype
			41982	No phenotype
21	CNOT2	Rga	35460	No phenotype
			57549	No phenotype
22	DHX35	CG3225	55365	No phenotype
23	DICER	Dcr-1	28598	No phenotype
			34826	Slightly Enhanced
			42901	No phenotype
24	DMRTB1	dsx	26716	No phenotype
			35645	No phenotype
			41864	No phenotype
25	DUOX2	Duox	32903	Enhanced
			33975	No phenotype
			38907	No phenotype
26	DVL2	dsh	31306	Slightly enhanced
			31307	No phenotype
27	ENDOU	CG2145	60036	No phenotype
			61997	No phenotype
28	ENPEP	CG32473	43972	No phenotype
			54013	Enhanced
			58177	No phenotype
29	EPB41L3	cora	35003	No phenotype
30	ERCC3	hay	53345	Suppressed
31	EXOC7	Exo70	28041	Slightly enhanced
			55234	No phenotype
32	FBLN1	CG31999	31587	No phenotype
			31697	No phenotype

33	FPGS	CG2543	62271	No phenotype
34	FUS	caz	34839	Slightly enhanced
			32990	Slightly enhanced
35	GCAT	CG10361	44517	No phenotype
36	GLI2	ci	31320	Slightly enhanced
			31321	Enhanced
37	GORASP1	Grasp65	34082	No phenotype
38	GPAM	mino	63587	No phenotype
39	HHAT	rasp	28921	No phenotype
40	HSPA4	Hsc70Cb	33742	Slightly suppressed
41	IGF2BP2	Imp	34977	No phenotype
			38219	No phenotype
			55645	No phenotype
42	IPCEF1	cnk	31759	Slightly enhanced
			33366	No phenotype
43	ITGA10	scb	27545	Slightly enhanced
			38959	No phenotype
44	ITGB4	mys	27735	Slightly enhanced
			33642	Slightly enhanced
45	KCNJ16	Irk2	25820	No phenotype
			41981	No phenotype
46	KHNYN	CG42360	60444	No phenotype
47	KIF21B	Klp31E	35473	No phenotype
			40943	Enhanced
48	LAMA4	LanA	28071	Slightly enhanced
49	LGALS3BP	Tango10	57165	No phenotype
50	LIPN	CG6753	62921	No phenotype
51	LZTS2	CG15365	36856	No phenotype
52	MADD	Rab3-GEF	28954	No phenotype
53	MAGI3	Magi	25792	No phenotype
			33411	No phenotype
			35279	No phenotype
54	ME2	men	38256	No phenotype
			41652	No phenotype
55	MEOX2	btn	42530	No phenotype
56	MINA	CG2982	33596	Suppressed
57	MYO1C	Myo61F	41689	No phenotype
58	NANOG	bsh	29336	No phenotype
			43994	Enhanced
59	NDE1	nudE	38954	No phenotype
			41860	No phenotype
60	NIF3L1	CG4278	60362	No phenotype
61	NIF3L1	CG4278	60362	No phenotype
62	OSGEPL1	CG14231	43269	No phenotype
			54799	Enhanced
63	PABPC1L	pAbp	28821	Enhanced
			36127	No phenotype
			53247	No phenotype
64	PCK2	CG10924	36915	No phenotype
65	PDE11A	Pde6	25828	Slightly enhanced
			35743	No phenotype
66	PDGFB	Pvf1	39038	Slightly enhanced
67	PDLIM5	Zasp52	31561	Slightly enhanced

68	PEX5	Pex5	58064	Slightly enhanced
			42854	No phenotype
			55322	No phenotype
69	PHTF1	phtf	43631	No phenotype
			57270	No phenotype
70	PIK3R3	Pi3K21B	36810	No phenotype
			38991	No phenotype
71	PKN3	pkn	28335	Enhanced
			42567	No phenotype
			55876	No phenotype
72	PLSCR1	CG9084	63599	No phenotype
73	PLXNB3	PlexB	28911	No phenotype
			57813	No phenotype
74	PMS2	Pms2	55614	No phenotype
75	PPFIBP1	Liprin-beta	41672	No phenotype
			64045	No phenotype
76	PRDM1	Blimp-1	36634	No phenotype
			57479	No phenotype
77	PSMB5	Prosbeta5	34810	Suppressed
78	PTH2R	Dh44-R1	28780	No phenotype
79	PTPRN	IA-2	33672	Slightly enhanced
			44099	No phenotype
80	PURG	Pur-alpha	36849	No phenotype
81	RAB27A	Rab27	31887	Slightly enhanced
			35774	No phenotype
			50537	Enhanced
82	RBM14	lark	27703	Enhanced
83	RGL3	Rgl	28938	No phenotype
			33389	No phenotype
84	RNF157	CG9941	43234	No phenotype
85	RPE	CG30499	42816	Enhanced
			62232	No phenotype
86	RYR3	RyR	28919	No phenotype
			29445	Slightly enhanced
			31540	No phenotype
87	SEPT10	Sep2	28004	No phenotype
			31216	No phenotype
88	SGSM1	CG32506	28776	No phenotype
89	SH3GL2	EndoA	27679	Slightly enhanced
90	SLC2A6	Tret1-1	42880	No phenotype
91	SLC3A1	Mal-A5	41851	No phenotype
			52910	No phenotype
		Mal-B2	62253	No phenotype
92	SLC7A1	CG7255	58532	No phenotype
93	SND1	Tudor-SN	34865	No phenotype
94	SPINT1	CG13748	41623	No phenotype
		CG6495	29452	No phenotype
95	STAT4	Stat92E	31318	No phenotype
			33637	No phenotype
96	STX5	Syx5	29397	Enhanced but n<10
97	TAF6L	mia	57790	No phenotype

98	TAF9	e(y)1	32345	Enhanced
99	TIE1	Tie	54005	No phenotype
100	TLR5	Toll-9	30535	No phenotype
			34853	No phenotype
101	TMC3	CG3280	50984	No phenotype
102	TNC	CG30280	53271	No phenotype
			53693	No phenotype
103	TRPM6	Trpm	31291	Slightly enhanced
			31672	No phenotype
			35581	No phenotype
104	VRK3	ball	31350	No phenotype
			55330	No phenotype
			35571	No phenotype

FXTAS r(CGG)$_{90}$ flies expressing GAL4 under the eye-specific gmr driver were crossed with flies harboring an shRNA transgene against the target candidate gene, downstream from the UAS sequence (UAS-TRiP). Progeny that express the shRNA against target gene in the eye were collected, aged for 7 days and visualized using light microscopy and SEM. Results of the genetic screen of 104 genes revealed 19 candidate genes that show significant modulation of the CGG-toxicity associated rough eye phenotype in FXTAS *Drosophila*.

Supplementary Figure S1: *ENPEP*$^{rs33966350\text{-}A}$ is an eQTL that correlates with decreased expression of *ENPEP* in a spectrum of tissues. Multi-tissue eQTL comparison (The Genotype-Tissue Expression Project) shows the single-tissue eQTL for 48 tissues. In 41 out of 48, the Normalized Effect Size (NES), computed as the effect of the alternative allele (ALT) relative to the reference allele (REF), is negative, demonstrating that the expression of the gene is diminished with the alternative allele.

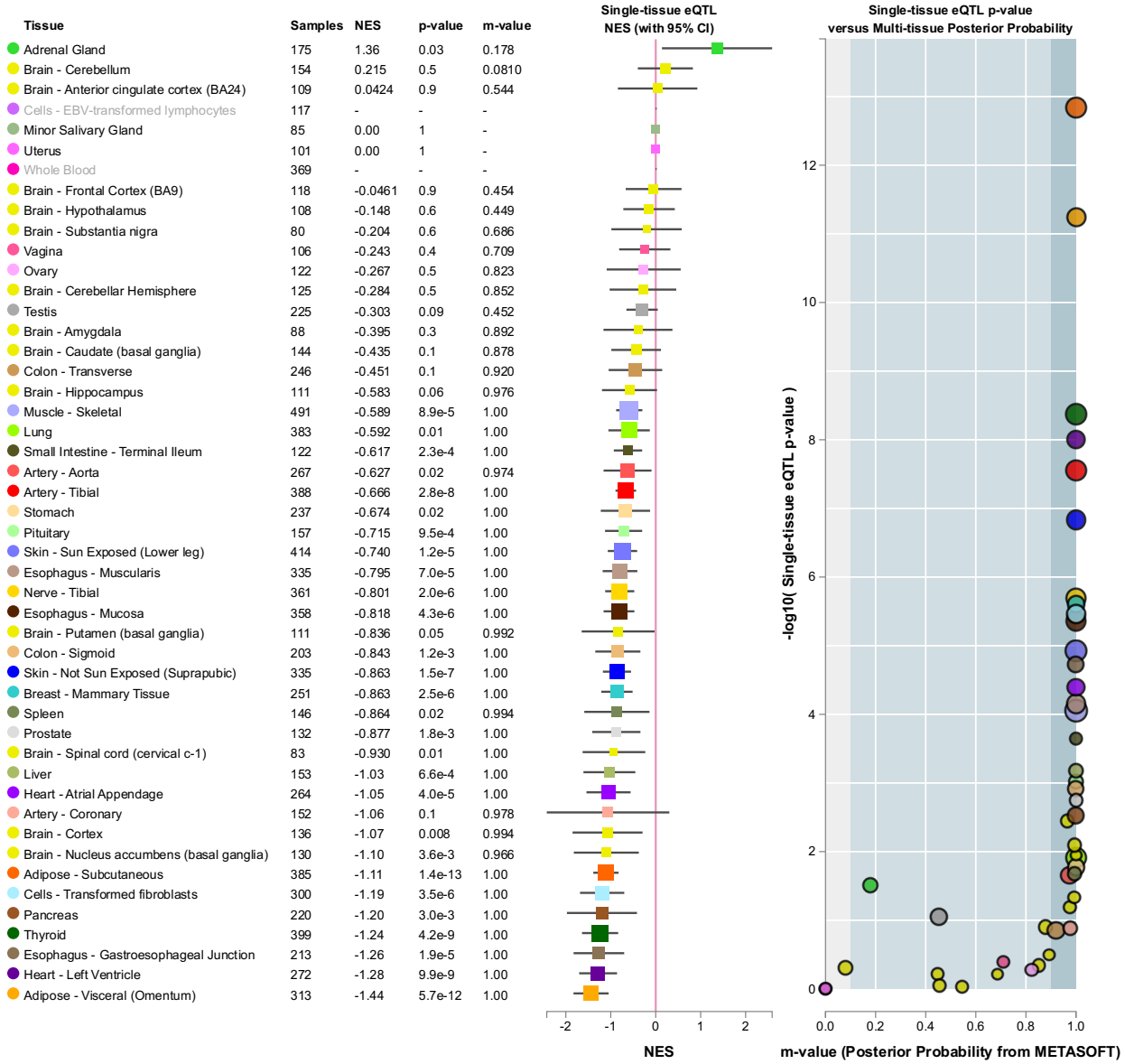

Tissue	Samples	NES	p-value	m-value
Adrenal Gland	175	1.36	0.03	0.178
Brain - Cerebellum	154	0.215	0.5	0.0810
Brain - Anterior cingulate cortex (BA24)	109	0.0424	0.9	0.544
Cells - EBV-transformed lymphocytes	117	-	-	-
Minor Salivary Gland	85	0.00	1	-
Uterus	101	0.00	1	-
Whole Blood	369	-	-	-
Brain - Frontal Cortex (BA9)	118	-0.0461	0.9	0.454
Brain - Hypothalamus	108	-0.148	0.6	0.449
Brain - Substantia nigra	80	-0.204	0.6	0.686
Vagina	106	-0.243	0.4	0.709
Ovary	122	-0.267	0.5	0.823
Brain - Cerebellar Hemisphere	125	-0.284	0.5	0.852
Testis	225	-0.303	0.09	0.452
Brain - Amygdala	88	-0.395	0.3	0.892
Brain - Caudate (basal ganglia)	144	-0.435	0.1	0.878
Colon - Transverse	246	-0.451	0.1	0.920
Brain - Hippocampus	111	-0.583	0.06	0.976
Muscle - Skeletal	491	-0.589	8.9e-5	1.00
Lung	383	-0.592	0.01	1.00
Small Intestine - Terminal Ileum	122	-0.617	2.3e-4	1.00
Artery - Aorta	267	-0.627	0.02	0.974
Artery - Tibial	388	-0.666	2.8e-8	1.00
Stomach	237	-0.674	0.02	1.00
Pituitary	157	-0.715	9.5e-4	1.00
Skin - Sun Exposed (Lower leg)	414	-0.740	1.2e-5	1.00
Esophagus - Muscularis	335	-0.795	7.0e-5	1.00
Nerve - Tibial	361	-0.801	2.0e-6	1.00
Esophagus - Mucosa	358	-0.818	4.3e-6	1.00
Brain - Putamen (basal ganglia)	111	-0.836	0.05	0.992
Colon - Sigmoid	203	-0.843	1.2e-3	1.00
Skin - Not Sun Exposed (Suprapubic)	335	-0.863	1.5e-7	1.00
Breast - Mammary Tissue	251	-0.863	2.5e-6	1.00
Spleen	146	-0.864	0.02	0.994
Prostate	132	-0.877	1.8e-3	1.00
Brain - Spinal cord (cervical c-1)	83	-0.930	0.01	1.00
Liver	153	-1.03	6.6e-4	1.00
Heart - Atrial Appendage	264	-1.05	4.0e-5	1.00
Artery - Coronary	152	-1.06	0.1	0.978
Brain - Cortex	136	-1.07	0.008	0.994
Brain - Nucleus accumbens (basal ganglia)	130	-1.10	3.6e-3	0.966
Adipose - Subcutaneous	385	-1.11	1.4e-13	1.00
Cells - Transformed fibroblasts	300	-1.19	3.5e-6	1.00
Pancreas	220	-1.20	3.0e-3	1.00
Thyroid	399	-1.24	4.2e-9	1.00
Esophagus - Gastroesophageal Junction	213	-1.26	1.9e-5	1.00
Heart - Left Ventricle	272	-1.28	9.9e-9	1.00
Adipose - Visceral (Omentum)	313	-1.44	5.7e-12	1.00

Supplementary Figure S2: *TAF9*$^{rs4252233\text{-}A}$ is an eQTL that correlates with increased expression of *TAF9* in a spectrum of tissues. Multi-tissue eQTL comparison (The Genotype-Tissue Expression Project) shows the single-tissue eQTL for 48 tissues. In 36 out of 48, the Normalized Effect Size (NES), computed as the effect of the alternative allele (ALT) relative to the reference allele (REF), is positive, demonstrating that the expression of the gene is increased with the alternative allele.

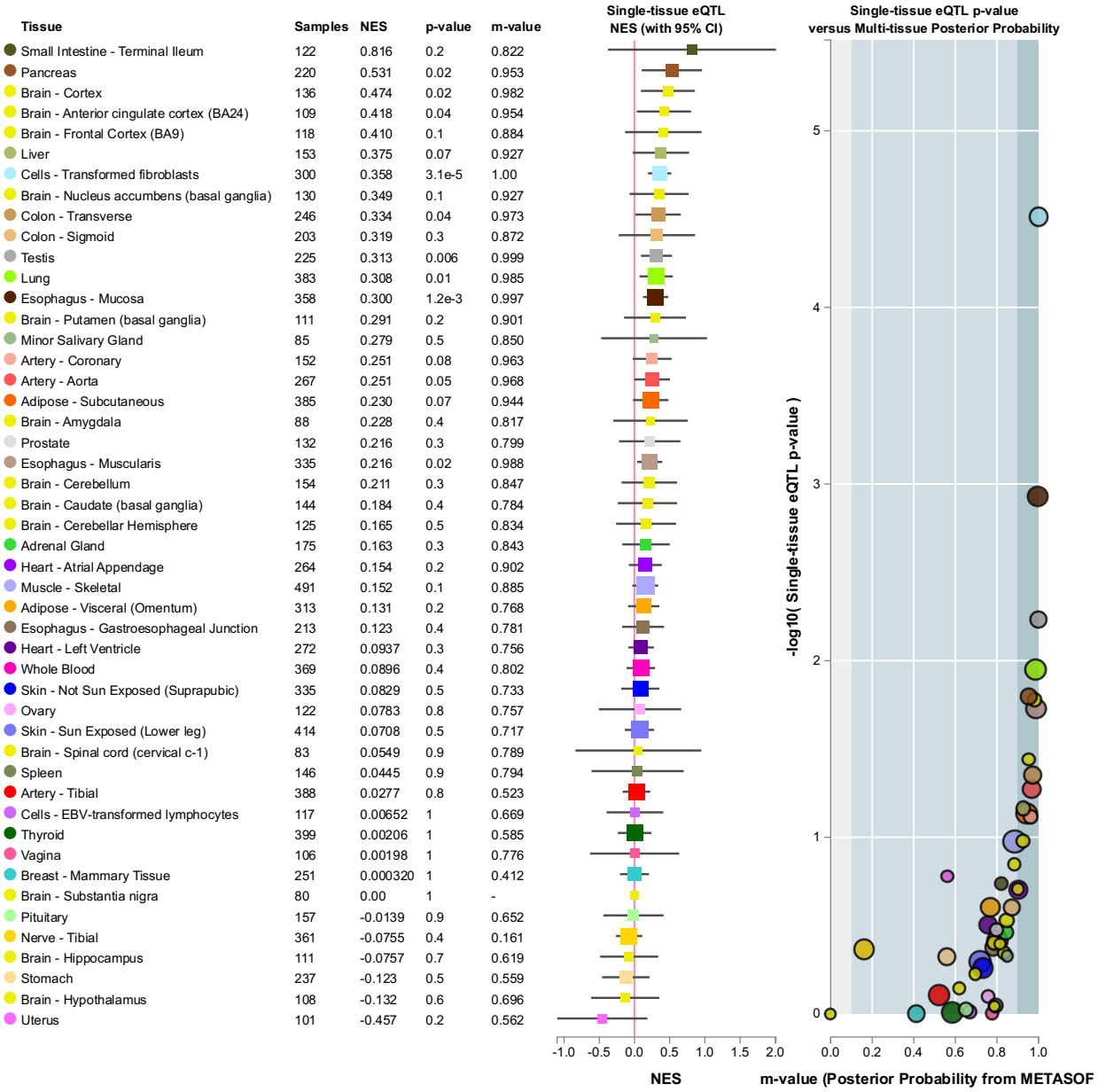

Tissue	Samples	NES	p-value	m-value
Small Intestine - Terminal Ileum	122	0.816	0.2	0.822
Pancreas	220	0.531	0.02	0.953
Brain - Cortex	136	0.474	0.02	0.982
Brain - Anterior cingulate cortex (BA24)	109	0.418	0.04	0.954
Brain - Frontal Cortex (BA9)	118	0.410	0.1	0.884
Liver	153	0.375	0.07	0.927
Cells - Transformed fibroblasts	300	0.358	3.1e-5	1.00
Brain - Nucleus accumbens (basal ganglia)	130	0.349	0.1	0.927
Colon - Transverse	246	0.334	0.04	0.973
Colon - Sigmoid	203	0.319	0.3	0.872
Testis	225	0.313	0.006	0.999
Lung	383	0.308	0.01	0.985
Esophagus - Mucosa	358	0.300	1.2e-3	0.997
Brain - Putamen (basal ganglia)	111	0.291	0.2	0.901
Minor Salivary Gland	85	0.279	0.5	0.850
Artery - Coronary	152	0.251	0.08	0.963
Artery - Aorta	267	0.251	0.05	0.968
Adipose - Subcutaneous	385	0.230	0.07	0.944
Brain - Amygdala	88	0.228	0.4	0.817
Prostate	132	0.216	0.3	0.799
Esophagus - Muscularis	335	0.216	0.02	0.988
Brain - Cerebellum	154	0.211	0.3	0.847
Brain - Caudate (basal ganglia)	144	0.184	0.4	0.784
Brain - Cerebellar Hemisphere	125	0.165	0.5	0.834
Adrenal Gland	175	0.163	0.3	0.843
Heart - Atrial Appendage	264	0.154	0.2	0.902
Muscle - Skeletal	491	0.152	0.1	0.885
Adipose - Visceral (Omentum)	313	0.131	0.2	0.768
Esophagus - Gastroesophageal Junction	213	0.123	0.4	0.781
Heart - Left Ventricle	272	0.0937	0.3	0.756
Whole Blood	369	0.0896	0.4	0.802
Skin - Not Sun Exposed (Suprapubic)	335	0.0829	0.5	0.733
Ovary	122	0.0783	0.8	0.757
Skin - Sun Exposed (Lower leg)	414	0.0708	0.5	0.717
Brain - Spinal cord (cervical c-1)	83	0.0549	0.9	0.789
Spleen	146	0.0445	0.9	0.794
Artery - Tibial	388	0.0277	0.8	0.523
Cells - EBV-transformed lymphocytes	117	0.00652	1	0.669
Thyroid	399	0.00206	1	0.585
Vagina	106	0.00198	1	0.776
Breast - Mammary Tissue	251	0.000320	1	0.412
Brain - Substantia nigra	80	0.00	1	-
Pituitary	157	-0.0139	0.9	0.652
Nerve - Tibial	361	-0.0755	0.4	0.161
Brain - Hippocampus	111	-0.0757	0.7	0.619
Stomach	237	-0.123	0.5	0.559
Brain - Hypothalamus	108	-0.132	0.6	0.696
Uterus	101	-0.457	0.2	0.562

Supplementary Figure S3: *TAF9*$^{rs4252233\text{-}A}$ is an eQTL that correlates with increased expression of *SMN2* in a spectrum of tissues. Multi-tissue eQTL comparison (The Genotype-Tissue Expression Project) shows the single-tissue eQTL for 48 tissues. In 46 out of 48, the Normalized Effect Size (NES), computed as the effect of the alternative allele (ALT) relative to the reference allele (REF), is positive, demonstrating that the expression of the gene is increased with the alternative allele.

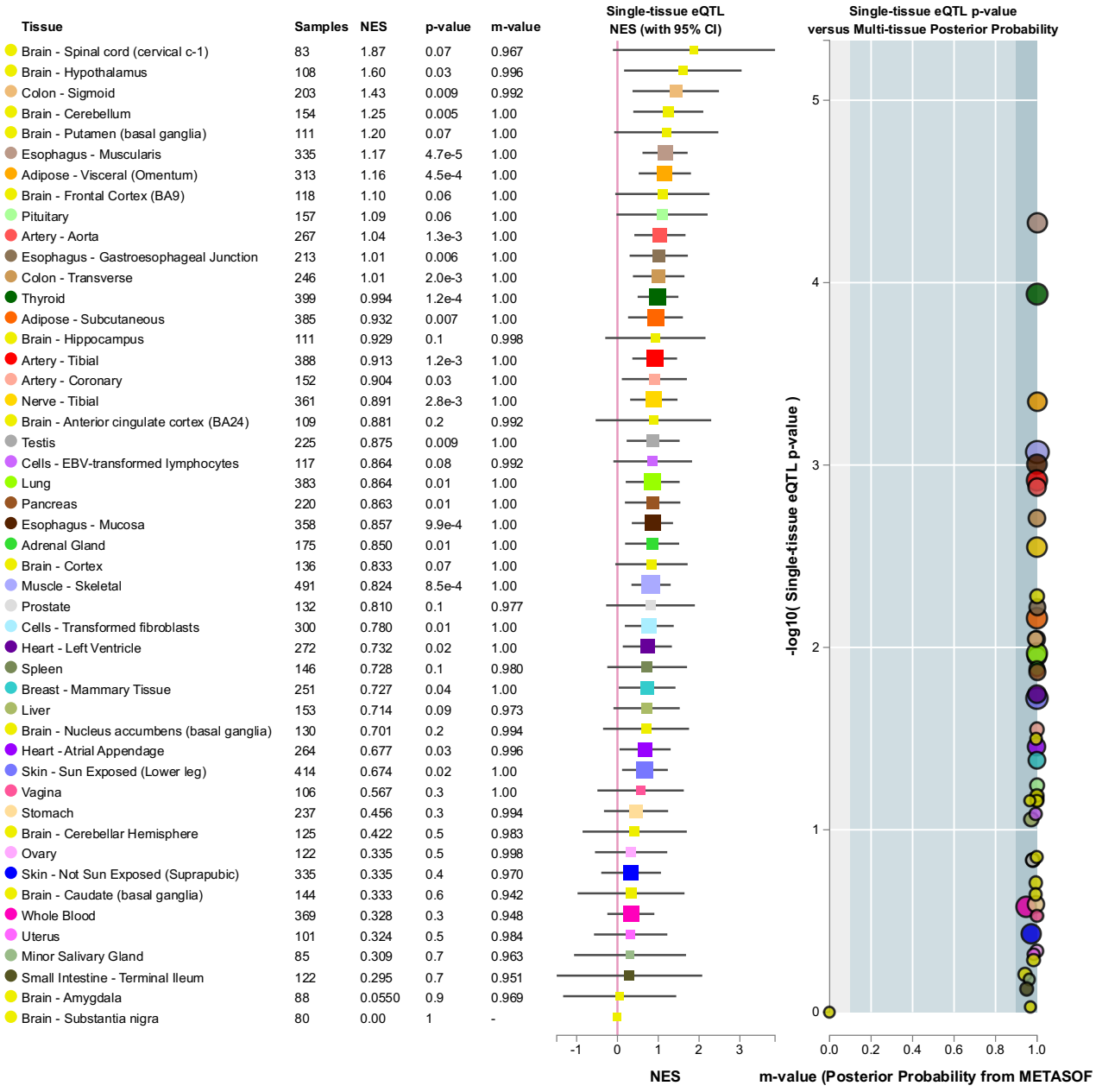

CHAPTER 4: Targeting *PSMB5* may ameliorate neuronal toxicity in Fragile X-Associated Tremor/Ataxia Syndrome

ABSTRACT

Expansion of 55-200 CGG repeats in the 5'UTR of *FMR1* predisposes carriers to Fragile X-associated tremor/ataxia syndrome (FXTAS), a late-onset debilitating neurodegenerative disorder. Importantly, FXTAS demonstrates incomplete penetrance, which strongly suggests the presence of genetic modifiers. As described in the preceding chapter, we performed whole genome sequencing (WGS) on 110 male premutation carriers ($CGG_{55\text{-}200}$) and prioritized candidate variants to screen for candidate genetic modifiers using a *Drosophila* model of FXTAS. We found that 19 genes genetically modulate CGG-associated neurotoxicity in the fly eye, such as *Prosbeta5 (PSMB5), pAbp (PABPC1L), e(y)1 (TAF9), CG14231 (OSGEPL1)*. Interestingly, knockdown of *Prosbeta5 (PSMB5)* in the FXTAS fly resulted in significant suppression of CGG-associated neurotoxicity. Moreover, TRAP-seq performed on FXTAS mice cerebella showed an increased level of *PSMB5* mRNA compared to wildtype. Here, we further investigated the role of *PSMB5* as a genetic modifier of FXTAS and its potential as a therapeutic target. Significantly, knockdown of *PSMB5* suppressed CGG associated neurodegeneration in the fly as well as in the mammalian N2A cell line, and an eQTL variant in *PSMB5, PSMB5*$^{rs11543947\text{-}A}$, was found to be associated with decreased expression of *PSMB5* and delayed onset of FXTAS in human *FMR1* premutation carriers. Finally, we demonstrate evidence that *PSMB5* knockdown results in suppression of CGG neurotoxicity via both the RAN translation and RNA-mediated toxicity mechanisms thereby presenting a novel potential therapeutic strategy for FXTAS.

KEYWORDS

Neurodegeneration, FXTAS, CGG repeat, Premutation, PSMB5, genetic modifier, RNA toxicity, RAN translation

INTRODUCTION

Our current understanding of the pathogenesis of FXTAS stands by two main proposed mechanisms: RNA toxicity and repeat-associated non-AUG (RAN) translation. The RNA toxicity mechanism of FXTAS pathogenesis results from sequestration of key RNA binding proteins to the CGG repeats, preventing them from performing their normal physiological function (Kong et al., 2017). The RNA-binding proteins that have been shown to be sequestered include the heterogeneous nuclear ribonucleoprotein (hnRNP A2/B1), which results in alteration of dendritic transport upon sequestration via the CGG repeats; Pur α, which plays a significant role in DNA replication, neuronal mRNA transport, and translation as well as Sam68, TDP43 and the DiGeorge syndrome critical region 8 protein, DGCR8 (Jin et al., 2007; Muslimov et al., 2011; Sellier et al., 2010, 2013; Sofola et al., 2007).

The second mechanism of FXTAS pathogenesis is via repeat-associated non-AUG (RAN) translation of the CGG repeats into polypeptides, the predominant species being FMRpolyG (Sellier et al., 2017; Todd et al., 2013). First discovered in the CAG repeat expansion in human spinocerebellar ataxia type 8 (SCA8) and myotonic dystrophy type 1 (DM1) (Zu et al., 2011), RAN translation has since been shown to play a potentially pathogenic role in ALS/FTD as well as FXTAS (Cleary and Ranum, 2014). Recently, Sellier et al. have shown that FMRpolyG interacts with the nuclear lamina protein LAP2β and that the mechanism of pathogenesis may act through the resulting perturbation of the lamina architecture (Sellier et al., 2017). Both *FMR1* mRNA and FMRpolyG peptide have been found in the human postmortem brain inclusions that are characteristic of FXTAS pathology, suggesting that both mechanisms may contribute to the disease (Tassone et al., 2004; Todd et al., 2013).

Here we show that knockdown of one of the 19 identified genetic modifiers (Table S1, Chapter 3), *Proteasome subunit beta-type 5 (PSMB5*), ameliorates CGG-associated neurotoxicity in flies as well as in mammalian cells. Through the *PSMB5* eQTL variant $PSMB5^{rs11543947\text{-}A}$, we demonstrate a correlation between decreased *PSMB5* mRNA expression and delayed-onset of FXTAS in human premutation carriers. Finally, we indicate that both mechanisms of FXTAS pathogenesis, RNA toxicity and RAN translation, may account for the suppression of CGG-associated toxicity in FXTAS upon lowering the expression of *PSMB5*.

METHODS

Drosophila screen

Transgenic flies expressing $r(CGG)_{90}$ were previously described. The gmr-GAL4 and UAS-TRiP lines were obtained from Bloomington Stock Centre (Bloomington, IN, USA). All *Drosophila* lines were maintained, and crosses were performed in standard medium at 25 °C. After performing the crosses, progeny was collected and aged to 7 days. The screen was performed by scoring eye phenotype, which was visualized using light microscopy and confirmed with scanning electron microscopy.

Scanning Electron Microscopy

Following dehydration in increasing concentrations of ethanol (25%, 50%, 75%, 100%), whole flies were incubated for 1 hr with hexamethyldisilazane (Electron Microscopy Sciences). After removing the hexamethyldisilazane, the flies were dried overnight in a fume hood and subsequently analyzed using Topcon DS-130F and DS-150F Field Emission Scanning Electron Microscope.

Cell culture, transfection, cell viability assays

For transfection of FLAG-DGCR8, HEK293T were plated in Dulbecco's Modified Eagle Medium. After 24 hours, cells were transfected with pFLAG/HA-DGCR8 (Addgene #10921) using Lipofectamine 3000 (Invitrogen) according to manufacturer instructions. Forty-eight hours later, cells were transfected again with 5'UTR CGG 99x FMR1-EGFP plasmid (Addgene #63091) or empty vector control (pCDNA 3.1+).

For the cell viability assay, Neuro2A were plated in EMEM (Eagle's Minimum Essential Medium (Corning, NY), 10-009-CV) with decreased FBS (2.5%). For *PSMB5* siRNA knockdown, 24h following plating of cells in a 96-well plate, cells were co-transfected with 3 pmol/well siRNA and 200 ng/well plasmid DNA using Lipofectamine 2000 (Invitrogen, CA). siRNAs used were *PSMB5* siRNA or control siGENOME Non-Targeting siRNA Control Pools (Dharmacon, CO, L-043960-01-0005 D-001206-14-05). Plasmid DNA consisted of 5'UTR CGG 99x FMR1-EGFP plasmid (Addgene #63091) or empty vector control (pCDNA 3.1+). Ninty-six hours after transfection, cell viability was measured using Cell Titer Blue (Promega, WI, #8081) according to the manufacturer's instructions. For testing the effect of Ixazomib citrate (Ark Pharm, IL, #AK54343) on cell viability, 24h after plating onto a 96-well plate, the cells were transfected first with 200 ng/well plasmid DNA using Lipofectamine 2000 (Invitrogen, CA). Plasmid DNA consisted of 5'UTR CGG 99x FMR1-EGFP plasmid (Addgene #63091) or empty vector control (pCDNA 3.1+). Twelve hours later after transfection, the EMEM was replaced with EMEM containing Ixazomib Citrate (Ark Pharm, AK545343) at 0.25 nM or DMSO control. 84 hours after addition of drug/DMSO, cell viability was measured using Cell Titer Blue (Promega, WI, #8081) according to the manufacturer's instructions.

Luciferase Assays and Western Blotting

HEK293 (CRL-1573, ATCC) cells were cultured and passaged at 37°C, 5% CO_2 in DMEM supplemented with 10% FBS without antibiotics. For luciferase assays, HEK293 cells were plated on 96-well plates at 2.0×10^4 cells/well in 100 µl media and reverse transfected with ON-TARGET siRNAs against human *PSMB5* (#1-4: J-004522-07-0002, J-004522-06-0002, J-004522-05-0002, J-004522-08-0002) or non-targeting controls (D-001810-10, Dharmacon) at 15 nM using Lipofectamine RNAiMAX (ThermoFisher Scientific). In brief, siRNA and RNAiMAX were diluted in Opti-MEM, combined, incubated for 10 mins at room temperature, then added to cells. For subsequent plasmid transfection, 48 hours after plating cells were transfected with 50 ng/well pcDNA3.1(+)/NL-3xF plasmid using Viafect (Promega). Luciferase assays were performed 24 hours after plasmid transfection, as described by Kearse et al. (2016) and Green et al. (2017).

For western blotting experiments, HEK293 cells were plated in 12-well plates at 2×10^5 cells/well in 1 ml media and reverse transfected, as described above, with siRNAs at 15 nM. Forty-eight hours after plating cells were transfected with 800 ng/well pcDNA3.1(+)/NL-3xF using jetPRIME (Polyplus, 114-15) according to manufacturer protocol. Twenty-four hours after plasmid transfection, cells were lysed on-plate in ice-cold RIPA buffer. The lysate was homogenized using a 28.5 G syringe (without centrifugation), mixed with 6x reducing Laemmli buffer, heated at 90°C for 10 mins, resolved by SDS-PAGE, and transferred to a PVDF membrane before incubation in primary antibody. FLAG M2: F1804, mouse [sigma] (1:1,000) in 5% milk in TBST. PSMB5: PSMB5 (D1H6B) Rabbit mAb [Cell Signaling] (1:1,000), Beta-Actin: A1978, Mouse [sigma] dilution (1:2000) same conditions.

Immunoprecipitation

The IP protocol for FLAG-DGCR8 was based on a described protocol with modifications (Macias et al., 2012). HEK293T cells transfected with pFLAG/HA DGCR8 (Addgene #10921) were grown in 60 mm plates. Forty-eight hours after transfection, cells were washed with ice-cold PBS, then scraped and centrifuged at 1000 rpm for 5 min at 4°C. For each immunoprecipitation 30 ul of protein G Dynabeads were used. The beads were first washed with 1 ml wash buffer (20 mM Hepes-KOH pH pH 7.9, 100 mM KCl, 0.2 mM EDTA, 0.5 mM DTT, 0.2mM PMSF, 5% glycerol) twice, then beads were resuspended in 300 ul of wash buffer and incubated with 5 ul of mAb-FLAG antibody (1mg/ml) (F1804, Sigma, MO) or IgG1 control (1mg/ml) (12-371, Sigma, MO), rotating at room temp for 45 minutes. The cell pellets were resuspended in 1 ml lysis buffer (wash buffer supplemented with RNAse OUT (ThermoFisher, MA, 10777019) and sonicated on ice using Misonix Sonicator 3000 Ultrasonic Cell Disruptor with Temperature Control (Misonix, NY) (3 times, 27 sec on, 27 sec off). Extracts were spun down at 7000 rpm for 5 minutes at 4°C. The supernatant was transferred to a new tube and spun down again at 14000 rpm, 10 min, 4°C. Protein concentration for cell lysates were quantified using a BCA assay. Before adding antibody-conjugated beads to extracts, the beads were washed with 1 ml of wash buffer 3 times, rotating to remove any unbound antibody. Equal amount of lysates based on protein concentrations were added to antibody-conjugated beads. Immediately after adding the lysates to beads, the mixture was flicked using a finger to mix, then incubated for 2 hours at 4°C, tumbling end over end. Beads were washed 3x with lysis buffer. After the final wash, 20 ul of FLAG peptide (10 ng/ul) (F3290, Sigma, MO) was added (final concentration 0.5 mg/ml) for 2 hours at 4°C, rotating, to elute the protein from the beads.

For RNA extraction, 200 ul of 1x RQ1-RNase-free DNAse buffer was added to each tube and the samples were treated with RQ1-RNase-free DNAse (Promega, WI, 6106) according to the

manufacturer's instructions. SDS was added to yield a final concentration of 1%, then the samples were treated with proteinase K for 30 minutes at 55°C, flicking the tube occasionally using a finger. Total RNA was extracted using Phenol:Chloroform:Isoamyl Alcohol 25:24:1 (P3803, Sigma, MO)

For Western blotting, samples were denatured in 2x Laemmli Sample Buffer (Bio-Rad, Hercules, CA) at 95°C, separated by SDS-polyacrylamide gel electrophoresis (PAGE) on Mini-PROTEAN TGX Precast Mini Gels (Bio-Rad), transferred onto 0.2 um PVDF membrane by Trans-Blot Turbo Blotting System and Mini Transfer Pack (Bio-Rad) and probed with primary antibodies against FLAG (1:4000, mouse pAb, F1804, Sigma, MO) at 4°C overnight. Primary antibodies were labeled by HRP-linked secondary anti-mouse antibody (1:4000, Cell Signaling Technology). The enhanced chemiluminescent signals were detected using HyGLO Quick Spray Chemiluminescent HRP Antibody Detection Reagent (Thomas Scientific, NJ) and were visualized by the ChemiDoc Touch Imaging System (Bio-Rad). cDNA was synthesized with SuperScript III reverse transcriptase (Invitrogen) using random hexamer primers. Real-Time PCR was performed with primers in Table S3.

RESULTS

The eQTL variant in *PSMB5*, *PSMB5*$^{rs11543947\text{-}A}$, is associated with decreased expression of *PSMB5* mRNA and correlates with delayed onset of ataxia and tremor in human *FMR1* premutation carriers.

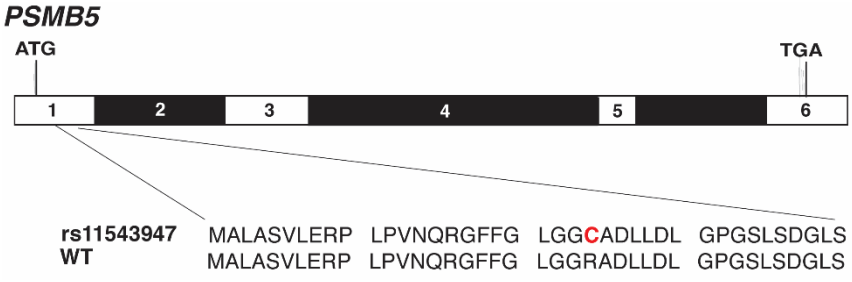

Figure 20: Schematic displaying the location of PSMB5$^{rs11543947\text{-}A}$ in PSMB5. *PSMB5$^{rs11543947\text{-}A}$ results in a G->A transition that results in the missense replacement of Cys for Arg24.*

One of the candidate genes of the *Drosophila* screen was *Proteasome Subunit Beta-5 (PSMB5)*, which was selected based on a variant that we found in our *FMR1* premutation carrier population, *PSMB5*$^{rs11543947\text{-}A}$. *PSMB5*$^{rs11543947\text{-}A}$ results in the replacement of cysteine for arginine in the 24th position of the protein, PSMB5 (Figure 20). *PSMB5*$^{rs11543947\text{-}A}$ has a high CADD score of 34, indicating that it is predicted to be among the top 0.1% deleterious variants in the genome (Table 2, Chapter 3, Kircher et al., 2014). Intriguingly, as data from the Genotype-Tissue Expression Project (GTEX) indicates, *PSMB5*$^{rs11543947\text{-}A}$ is also an expression quantitative trait locus (eQTL) associated with decreased expression of *PSMB5* mRNA (Figure 21). Therefore, with each additional variant allele of *PSMB5*$^{rs11543947\text{-}A}$, an individual is expected to have decreased

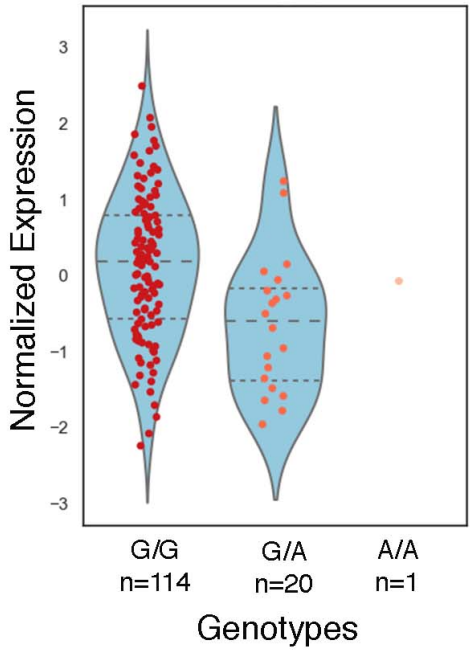

Figure 21: PSMB5$^{rs11543947\text{-}A}$ is an eQTL resulting in decreased expression of PSMB5 mRNA. Violin plot depicts the diminished expression level of PSMB5 mRNA in brain (cortex) tissue of human samples from G/G genotype (left) to G/A (middle) (GTEX Project).

baseline expression of *PSMB5* across a vast spectrum of tissues (Figure 21, Supplementary Figure S1). We were interested to find that in the comparison of premutation carriers exhibiting delayed onset of both tremor and ataxia with premutation carriers with early onset, *PSMB5*$^{rs11543947\text{-}A}$ was enriched in premutation carriers with delayed onset of both core phenotypes of FXTAS: tremor and ataxia (Table 4). Early onset was defined as onset of both tremor and ataxia before age 65 and delayed onset was defined as the absence of both tremor and ataxia above age 69, as assessed by a neurologist's evaluation. Based on this finding, we hypothesized that premutation carriers with a lower baseline expression of *PSMB5* may be protected against the CGG-associated neurodegeneration associated with the premutation expansion in *FMR1*.

	Allele frequency in study population	**Allele frequency in general population**	**Odds ratio**
No Ataxia and Tremor	0.115	0.0607	2.02
Early Ataxia and Tremor	0.048	0.0607	0.688

Table 4: PSMB5$^{rs11543947\text{-}A}$ is enriched in delayed onset premutation carriers compared to premutation carriers with early onset of ataxia and tremor.

Table shows the frequency of *PSMB5*$^{rs11543947\text{-}A}$ variant allele in premutation carriers with no onset of FXTAS symptoms (ataxia and tremor), and the frequency in premutation carriers with early onset of both FXTAS symptoms, as well as the general population frequency (Lek et al., 2016).

Knockdown of *Proteasome subunit beta-5 (PSMB5)* suppresses CGG-associated neurodegeneration in the fly eye and mammalian cell line.

We set out to test out this hypothesis by taking advantage of the UAS-GAL4 system to knockdown expression of the fly orthologue of *PSMB5 (Prosbeta5)* in the FXTAS *Drosophila* eye and observed strong suppression of CGG-associated neurodegeneration upon *Prosbeta5* knockdown (Figure 22). Conversely, overexpression of *Prosbeta5* resulted in inversion of the effect, such that the fly eyes exhibited enhancement of the rough eye phenotype (Figure 22).

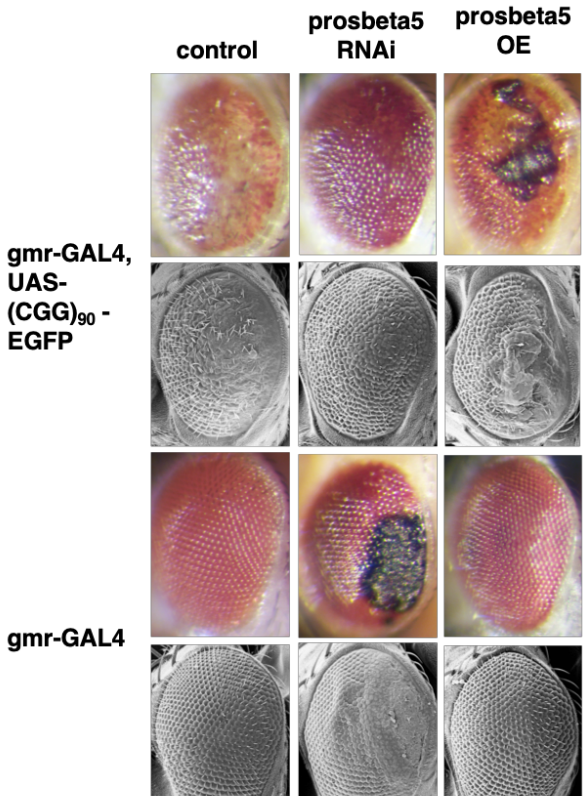

Figure 22: Knockdown of Prosbeta5 in gmr-GAL4, UAS-(CGG)$_{90}$ EGFP flies suppresses of CGG-associated neurotoxicity.

Knockdown of *Prosbeta5* in gmr-GAL4, UAS-(CGG)$_{90}$ EGFP flies suppresses of CGG-associated neurotoxicity while *Prosbeta5* knockdown in WT gmr-GAL4 flies resulted in enhancement. Demonstrating epistasis, overexpression of *Prosbeta5* in contrast results in enhancement of neurotoxicity in the flies. Top panel and bottom panel display the light microscopy (first row) and scanning electron microscopy (SEM) images (second row) from *Drosophila* of the indicated genotypes crossed to gmr-GAL4, UAS-(CGG)$_{90}$ EGFP and gmr-GAL4 flies as control, respectively.

Knockdown of *Prosbeta5* in the WT fly eye resulted in enhancement of the rough eye phenotype as well, suggesting that significant knockdown of *Prosbeta5* is inherently toxic in the absence of CGG repeats but in the background of CGG-associated neurotoxicity, knockdown of *Prosbeta5* suppresses the toxicity (Figure 22). All in all, the genetic evidence in the fly and human premutation carriers suggests that knockdown of *PSMB5* may ameliorate CGG-induced neurodegeneration.

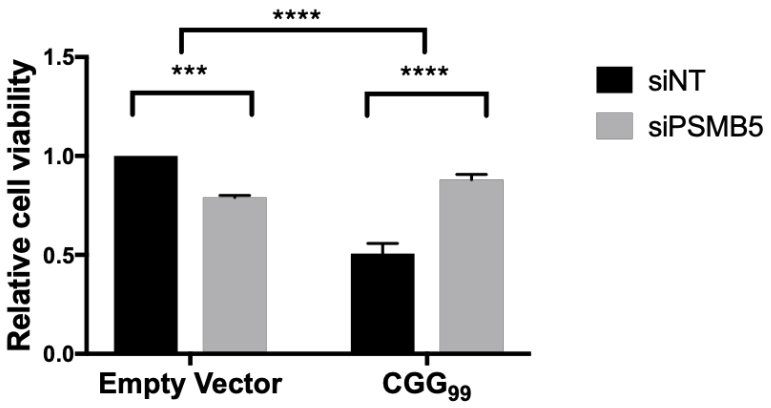

Figure 23: siRNA knockdown of Psmb5 results in suppression of CGG associated neurotoxicity in Neuro2A cells (Two-way ANOVA model, Sidak's multiple comparison test). * indicates $p < 0.05$, **** indicates $p < 0.0001$

To further test this hypothesis in a mammalian model system, we transfected mouse Neuro2A cells with the 5'UTR CGG 99x FMR1-EGFP plasmid expressing 99 CGG repeats in the context of the human 5'UTR *FMR1*, in frame with EGFP, as well as an empty vector control. Notably, upon siRNA knockdown of *Psmb5*, we observed a significant amelioration of CGG associated toxicity in N2A cells after 96 h (Figure 23, Supplementary Figure S2). In line with the finding in the flies, knocking down *Psmb5* in Neuro2A cells transfected with empty vector control resulted in decreased cell viability (Figure 23).

Amelioration of CGG toxicity is specific to *PSMB5*

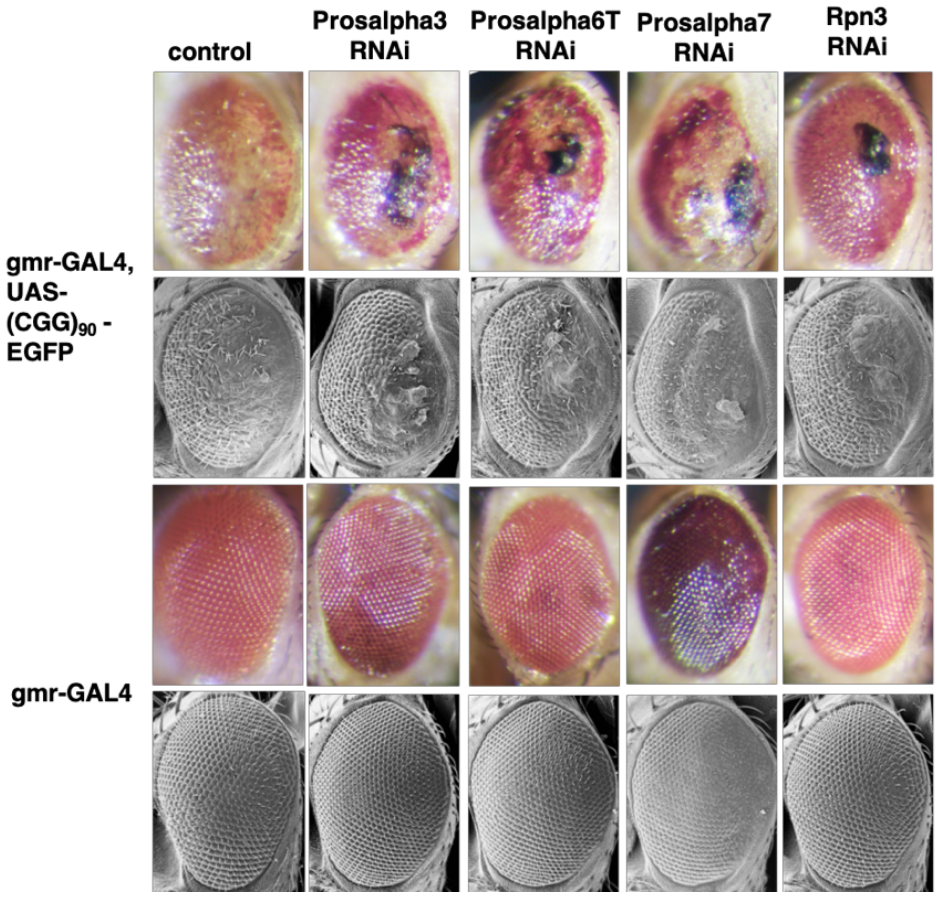

Figure 24: Screen of Drosophila orthologues of proteasome subunits demonstrates enhancement of four genes, such as Prosalpha3 (PSMA4), Prosalpha6T (PSMA1), Prosalpha7 (PSMA3), Rpn3 (PSMD3) upon RNAi knockdown.
RNAi lines of *Drosophila* proteasome subunits were crossed with gmr-GAL4, UAS-$(CGG)_{90}$ EGFP flies and resulted in significant enhancement of CGG-associated neurotoxicity for four genes (Table S1). Top panel and bottom panel display the light microscopy (first row) and scanning electron microscopy (SEM) images (second row) from *Drosophila* of the indicated genotypes crossed to gmr-GAL4, UAS-$(CGG)_{90}$ EGFP and gmr-GAL4 flies as control, respectively.

Intrigued by these findings, we wanted to verify whether the amelioration of CGG-associated neurotoxicity is specific to *PSMB5* knockdown, or whether it also involves other subunits of the proteasome complex. The 26S proteasome consists of the 20S core particle and the 19S regulatory particle (Livneh et al., 2016). Therefore, we tested all genes related to the 20S core particle subunits and the 19S regulatory particle that have *Drosophila* orthologs as well as

Drosophila TRiP lines available for screening (Table S1). Out of 41 human genes that encode components of the 26S complex, 35 orthologous genes in the fly were screened as six genes did not have fly orthologs or TRiP lines available. Of the 35, fly orthologues of four genes demonstrated enhancement of CGG-associated neurodegeneration upon knockdown, such as *Prosalpha3 (PSMA4), Prosalpha6T (PSMA1), Prosalpha7 (PSMA3)* and *Rpn3 (PSMD3)* (Figure 24). Over 88% of the genes tested showed no genetic modulation of the CGG-associated neurotoxicity upon knockdown, and significantly, none of the screened genes showed suppression of CGG associated toxicity upon knockdown. All in all, our results clearly suggest that the alleviation of CGG toxicity is specific to the beta-5 subunit of the proteasome, and knockdown of other subunits of the *Drosophila* proteasome complex did not recapitulate the suppression of CGG toxicity seen in *Prosbeta5* knockdown.

Inhibition of Psmb5 alleviates CGG-associated toxicity in Neuro2A cells

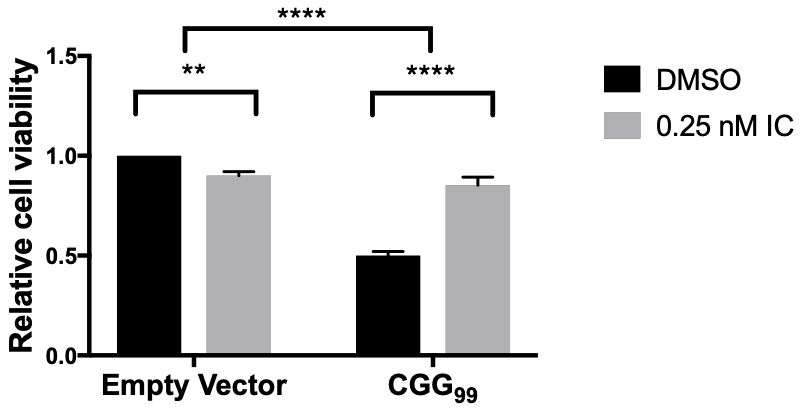

Figure 25: Pharmacologic inhibition of Psmb5 with 0.25 nM Ixazomib Citrate results in suppression of CGG associated neurotoxicity in Neuro2A cells
(Two-way ANOVA model, Sidak's multiple comparison test). ** indicates $p < 0.01$, **** indicates $p < 0.0001$

We wanted to further validate whether this amelioration of CGG-associated toxicity is specific to the *PSMB5* by taking advantage of the fact that several potent FDA-approved selective

inhibitors of PSMB5 are already available on the market, such as Ixazomib Citrate (Raedler, 2016). We tested the effects of Ixazomib Citrate on mammalian cells by administering 0.25 nM of Ixazomib Citrate to Neuro2A cells following transfection of a plasmid expressing CGG repeats in the context of the human *FMR1* 5'UTR. We observed that in Neuro2A cells treated with DMSO after expression of the rCGG repeats, only approximately 50% of control cells survived after 84 h (n=3) (Figure 25). However, upon administration of Ixazomib citrate for 84 h, we observed a significant alleviation of CGG-associated toxicity such that 85% of cells survived (Figure 25). In contrast, for Neuro2A cells transfected with empty vector, treatment with Ixazomib Citrate resulted in decreased cell viability (Figure 25).

Knockdown of *Psmb5* significantly diminishes RAN translation in a frame-independent manner

Impressed that our genetic findings of CGG toxicity alleviation upon *Psmb5* knockdown was recapitulated in the *Drosophila* as well as in Neuro2A cells through various methods, we sought to identify the mechanism behind the amelioration of toxicity. We began by addressing the two main established modes of CGG toxicity: RAN translation and RNA toxicity.

First, we assessed whether knockdown of *PSMB5* alters RAN translation. To do so, we utilized a set of transfectable, plasmid-based nanoluciferase (NL) reporters (Kearse et al., 2016) for canonical and RAN translation. The reporter for canonical translation, AUG-NL-3xF, comprises a short, unstructured 5' untranslated region (UTR), an AUG-initiated NL open reading

frame (ORF), and a C-terminal 3xFLAG (3xF) tag to enable detection by Western blotting. The reporter for RAN translation of *FMR1* in the +1 frame comprises the 5' UTR of human *FMR1*

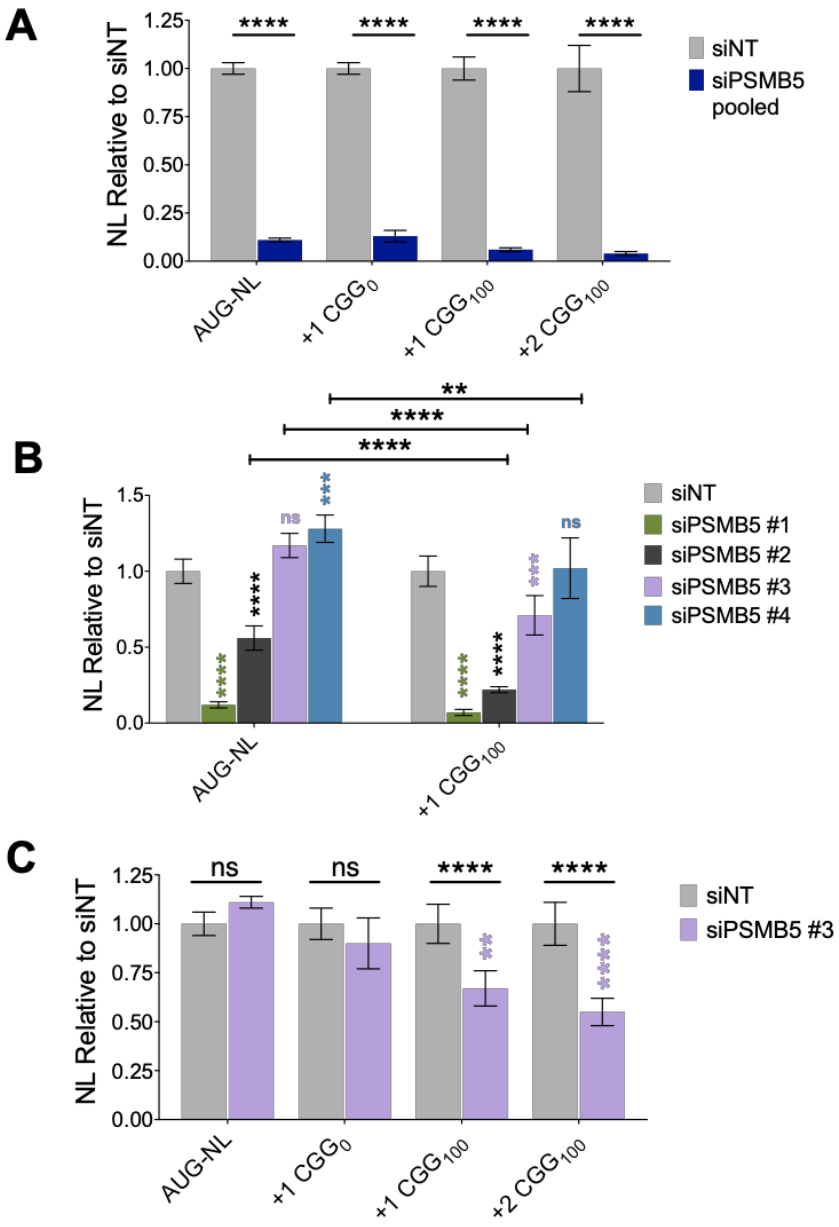

Figure 26: PSMB5 Knockdown significantly diminishes RAN translation of FMR1 5'UTR CGG repeats.

A. Plasmid-transfected nanoluciferase (NL)-based reporters for canonical and RAN translation were expressed in HEK293 cells, following transfection of pooled siRNAs against PSMB5 or non-targeting siRNAs (siNT). All graphs depict pooled data gathered across 2 replicates. Both canonical and RAN translation are diminished upon knockdown via pooled *PSMB5* siRNA. **B-C.** Expression of canonical- and RAN-translation reporters, following transfection of individual siRNAs against PSMB5 or siNT (two-way ANOVA with Sidak's multiple comparisons test; n=6/condition; * P≤0.05, ** P≤0.01, *** P≤0.001, **** P≤0.0001). *PSMB5* siRNA #2 and #3 result in stronger suppression of RAN translation compared to normal translation, and the difference is most significant with *PSMB5* siRNA #3.

bearing 100 CGG repeats, a GGG- "initiated" NL open reading frame (which abrogates initiation at this site; Kearse et al., 2016; Green et al., 2017), and the same 3xF tag. Translation of this *FMR1* reporter initiates within the *FMR1* 5'UTR (Kearse et al., 2016). When *PSMB5* was knocked down by pooled siRNAs against *PSMB5*, we saw a steep decline in RAN translation, but also witnessed a substantial decline in canonical translation (Figure 26A). Therefore, we evaluated different species of siRNAs against *PSMB5* separately. Interestingly, we observed that two species of *PSMB5* siRNA exhibit differential effects on canonical and repeat-associated non-AUG initiated (RAN) translation, substantially diminishing RAN translation while having little or no effect on canonical translation (Figure 26B). Furthermore, we verified that the decline in RAN translation is frame-independent; knockdown of *PSMB5* resulted in significant decline of RAN translation in both the +1 and +2 frames (Figure 26C).

Knockdown of *PSMB5* may ameliorate CGG-associated toxicity by alleviating the effects of DGCR8 sequestration to the expanded *FMR1* premutation CGG repeat.

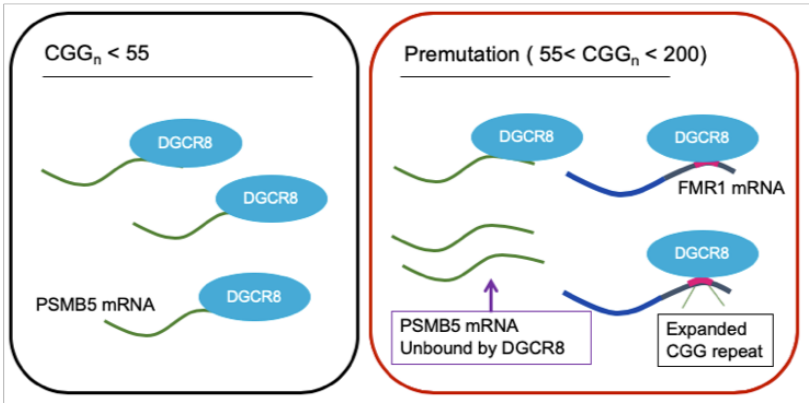

Figure 27: Schematic illustrates a proposed model depicting a potential mechanism of CGG-associated toxicity in FXTAS.

Schematic shows normally, DGCR8 binds *PSMB5* mRNA (left). In the presence of the expanded premutation FMR1 CGG repeat (right), DGCR8 is sequestered to the expanded CGG repeat, potentially leading to an increase of *PSMB5* mRNA unbound by DGCR8.

Encouraged by the finding that knockdown of *PSMB5* diminishes RAN translation, we also wondered whether the alleviating effects of *PSMB5* knockdown may be associated with the sequestration of RNA binding proteins (RBPs) to the expanded CGG repeat. We were motivated by our previous finding that endogenous levels of *Psmb5* mRNA bound to ribosomes is elevated in FXTAS mice compared to wildtype littermates (Table 3, Chapter 3). Furthermore, based on a database of high-throughput data such as CLIP-seq, Ribo-seq and RNA-seq (POSTAR2), we found that *PSMB5* mRNA has been shown to be bound by DGCR8, an RNA binding protein already reported to be sequestered by the *FMR1* premutation repeats (Sellier et al., 2013; Zhu et al., 2019).

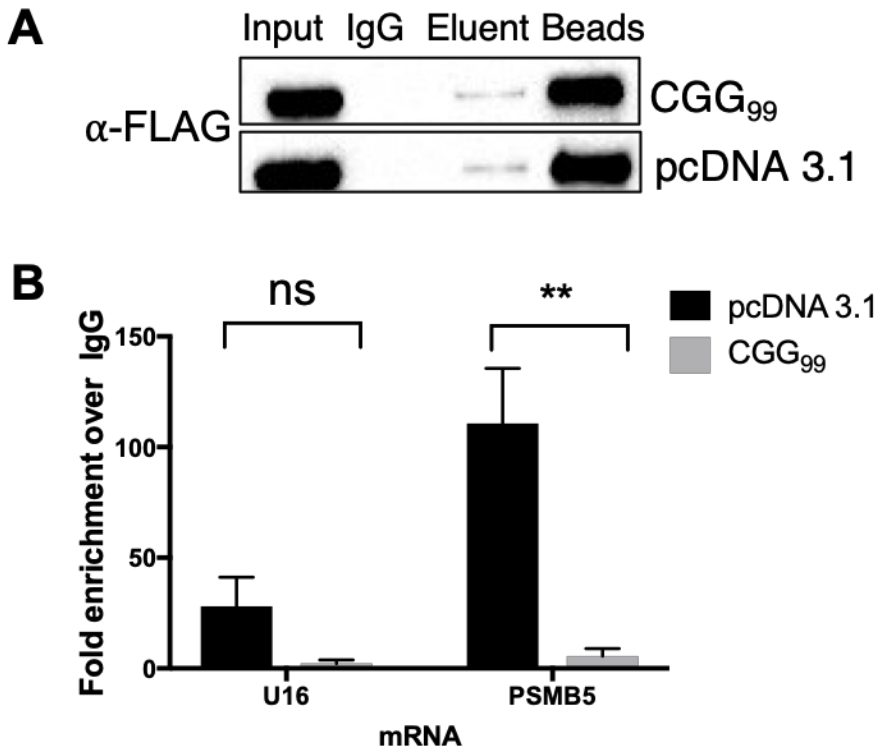

Figure 28: Immunoprecipitation of FLAG-DGCR8 shows less PSMB5 mRNA binds to DGCR8 in the presence of CGG repeats. **A.** FLAG-DGCR8 was overexpressed in HEK293T cells for 24 hours, then cells were subsequently transfected again with either 5'UTR CGG 99x FMR1-EGFP plasmid or pcDNA 3.1. Western blot shows upon immunoprecipitation with anti-FLAG antibody, equal amounts of FLAG-DGCR8 was pulled down and eluted. **B.** *PSMB5* mRNA bound to FLAG-DGCR8 diminishes significantly in the presence of the expanded CGG repeat. Following immunoprecipitation, the eluent was subject to RNA extraction. Using RT-qPCR, mRNA bound to FLAG-DGCR8 was quantified. Significantly less *PSMB5* mRNA was bound to FLAG-DGCR8 in the presence of the CGG repeat (Two-way ANOVA, Sidak's multiple comparison test). Differences in the levels of U16 snoRNA (also known to be bound by DGCR8) were not statistically significant. ** indicates $p < 0.005$

We hypothesized that if DGCR8 normally binds *PSMB5* mRNA, then upon sequestration of DGCR8 to the expanded CGG repeats, we may be able to observe a significant decline of *PSMB5* mRNA bound to DGCR8 (Figure 27). To test this, we transfected HEK 293T cells with a plasmid expressing FLAG-tagged human DGCR8. Forty-eight hours later, we subsequently transfected the cells with either a plasmid expressing $rCGG_{99}$ in the context of the human *FMR1* 5'UTR or an empty vector control. After 24 h, we performed immunoprecipitation for DGCR8 using anti-FLAG antibody and found that upon expression of the *FMR1* premutation CGG repeats, the level of *PSMB5* mRNA bound to DGCR8 dropped significantly (Figure 28). As a control, we also tested the levels of the snoRNA U16, another RNA known to be bound by DGCR8. We found a non-significant decrease of U16 snoRNA bound to DGCR8 in the presence of the premutation CGG repeat (Figure 28). Overall, these findings, along with the increased *PSMB5* mRNAs found in TRAP-seq of FXTAS mice lend support to the possibility that DGCR8 plays a role in *PSMB5* mRNA processing that is perturbed upon sequestration of DGCR8 to the CGG repeats (Figure 27).

DISCUSSION

The pathogenesis of neurodegenerative diseases is commonly linked to defects in the degradation of misfolded proteins. Three mechanisms promote effective removal of misfolded proteins, namely the ubiquitin (Ub)-proteasome system (UPS), chaperone mediated autophagy (CMA) and macroautophagy (Ciechanover, 2013). In many neurodegenerative diseases such as Huntington's Disease (HD), Parkinson's Disease (PD), Alzheimer's Disease (AD), and Amyotrophic Lateral Sclerosis (ALS), the pathology stems from misfolded aggregates that are resistant to degradation via these mechanisms, and their accumulation particularly affects post-

mitotic neurons (Ciechanover and Kwon, 2015). Capitalizing on this pathologic mechanism, therapeutic strategies on many neurodegenerative diseases have been designed to augment the degradation of protein aggregates by further activating the mechanisms of protein clearance (Caccamo et al., 2010; Sarkar et al., 2008; Spilman et al., 2010).

In FXTAS, activation of proteolytic mechanisms has yet to be implemented as a therapeutic approach. However, previous studies have indicated the potential of UPS as a therapeutic target for FXTAS. In *Drosophila*, impairment of β2 and β6 subunits of the proteasome were shown to enhance CGG-associated ommatidial degeneration in *Drosophila* (Oh et al., 2015) whereas overexpression of Hsp70, a molecular chaperone that assists in refolding, was shown to suppress the neurotoxicity even in the absence of misfolded proteins (Jin et al., 2003).

In addition to the UPS, activating autophagy via rapamycin has been shown to rescue neurodegenerative phenotypes (Berger et al., 2006; Pandey et al., 2007). However, contrary to other neurodegenerative disorders, previous reports clearly demonstrate that in FXTAS, activating autophagy via rapamycin actually enhances the CGG-associated neurodegeneration in *Drosophila* (Lin et al., 2013; Oh et al., 2015) . Instead, activating the mTOR pathway, rather than inhibiting mTOR via rapamycin, ameliorated CGG associated neurotoxicity in *Drosophila.* These findings were the first indication that although FXTAS is a neurodegenerative disease with a protein accumulation problem, the pathogenic mechanism may differ significantly from the other neurodegenerative pathologies, which are alleviated via rapamycin.

We uniquely report that while knockdown of most components of the 26S proteasome resulted in enhancement or no change in CGG-associated neurodegeneration, knockdown of

PSMB5, one of the core catalytic subunits of the 26S proteasome complex, significantly ameliorates CGG-induced neurodegeneration in various models— as demonstrated in *Drosophila*, mammalian cells, as well as a correlation of delayed onset FXTAS phenotypes in human premutation carriers.

Furthermore, this study has investigated both potential mechanisms of FXTAS toxicity to explain this finding. We have shown in mammalian cells that RAN translation is significantly diminished by knockdown of *PSMB5*, although excessive knockdown of *PSMB5* will even affect global translation. It remains to be determined whether this protective effect is unique to FXTAS or can be seen in other repeat-associated diseases.

We have also shown that at the mRNA level, the level of *PSMB5* mRNA bound to DGCR8 is significantly diminished in the presence of the premutation CGG repeats, suggesting that upon sequestration of DGCR8 to the CGG repeats, the role of DGCR8 in the regulation of *PSMB5* mRNA may be perturbed (Sellier et al., 2013).

Our finding has significant value for the development of future therapeutics as well as potential biomarkers for disease prognosis. Although not a curative strategy, our data in *Drosophila* and mammalian cells suggests that modestly diminishing *PSMB5* expression may be a promising therapeutic approach to delay the onset of a debilitating neurodegenerative disorder. Several FDA approved proteasome inhibitors are readily available, such as bortezomib (Velcade) and carfilzomib (Kyprolis) and Ixazomib Citrate (Ninlaro), the first oral proteasome inhibitor approved by the FDA (de la Puente and Azab, 2013; Muz et al., 2016). According to the evidence presented in this study, low-dose inhibition of PSMB5 at the protein level, via Ixazomib citrate,

may be a potential therapeutic strategy for the treatment of FXTAS. It remains to be seen whether manipulating the RNA expression or protein level of PSMB5 may also ameliorate neurotoxicity in other neurodegenerative diseases, or whether this is a unique mechanism in FXTAS.

Our finding that *PSMB5*$^{rs11543947\text{-}A}$, a variant in *PSMB5*, is enriched in delayed onset premutation carriers was limited in statistical significance due to the small sample size. Attaining adequate statistical power to identify such non-Mendelian variants that are not independently causative but may predispose or protect against a disease remains a challenge in the study of rare diseases. In light of these limitations, we believe that the identification of a potential genetic biomarker for prognosis is a significant leap forward. We hope that future studies will be able to further validate the potential of *PSMB5*$^{rs11543947\text{-}A}$ as a biomarker for disease prognosis in FXTAS.

In conclusion, we have demonstrated that knockdown of *PSMB5* suppresses CGG-associated neurodegeneration in *Drosophila* as well as in a mammalian *in vitro* model. Inhibiting the β5 subunit at the protein level by the proteasome inhibitor Ixazomib citrate also suppresses the CGG-generated toxicity *in vitro*. Through whole genome sequencing, we have identified *PSMB5*$^{rs11543947\text{-}A}$ as a variant that has high potential as a biomarker for delayed onset of disease. The association between *PSMB5*$^{rs11543947\text{-}A}$ and delayed onset of FXTAS aligns well with the molecular findings presented in various model systems due to its role as an eQTL that correlates with decreased expression of *PSMB5*. All in all, we are confident that PSMB5 offers a promising therapeutic target for alleviating the CGG-associated neurodegeneration in FXTAS.

ACKNOWLEDGEMENTS

This work was supported by the National Institutes of Health [NS051630 to D.L.N, P.J, NS091859 to P.J., S.S., S.T.W. and E.G.A.] The Genotype-Tissue Expression (GTEx) Project was supported by the Common Fund of the Office of the Director of the National Institutes of Health, and by NCI, NHGRI, NHLBI, NIDA, NIMH, and NINDS. The data used for the analyses described in this manuscript were obtained from the GTEx Portal on 03/19/19.

SUPPLEMENTAL MATERIALS

Supplementary Figure S1: *PSMB5*$^{rs11543947\text{-}A}$ is an eQTL that correlates with decreased expression of *PSMB5* in a spectrum of tissues. Multi-tissue eQTL comparison (The Genotype-Tissue Expression Project) shows the single-tissue eQTL for 48 tissues. In 46 out of 48, the Normalized Effect Size (NES), computed as the effect of the alternative allele (ALT) relative to the reference allele (REF), is negative, demonstrating that the expression of the gene is diminished with the alternative allele.

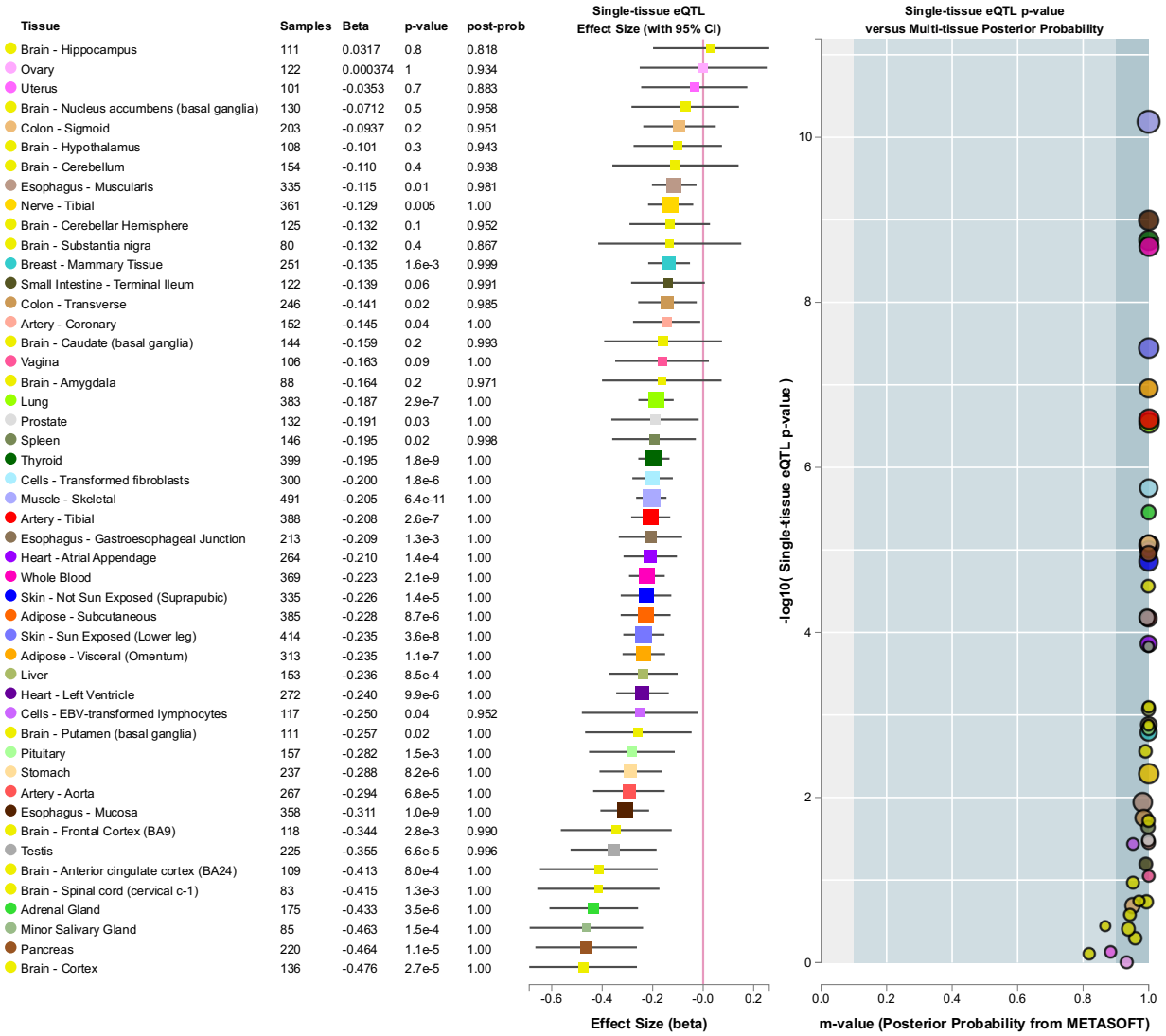

Supplementary Figure S2: siRNA knockdown of *Psmb5* in Neuro2A cells.

RT-PCR was performed to assess the level of *Psmb5* mRNA in Neuro2A cells transfected with *Psmb5* siRNA and control siRNA, along with 5'UTR CGG 99x FMR1-EGFP and pcDNA 3.1+, normalized to housekeeping genes Rpl and Tbp (Two-way ANOVA model, Tukey's multiple comparison test). **** indicates $p < 0.0001$.

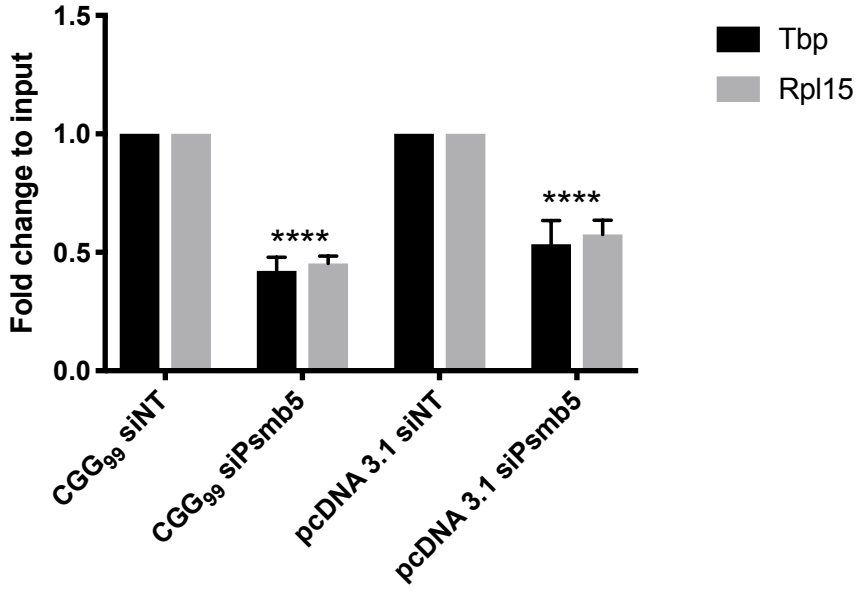

Table S1. *Drosophila* screen of subunits of the Proteasome complex

#	Human Gene	*Drosophila* Ortholog	UAS TRiP stock	Gmr-GAL4, UAS-$(CGG)_{90}$-EGFP *Drosophila* phenotype	Gmr-GAL4 only phenotype
1	*PSMA1*	*Prosalpha6T*	55243	Enhanced	No phenotype
		Prosalpha6	34811	No phenotype	No phenotype
			53974	Few Progeny	No phenotype
2	*PSMA2*	*Prosalpha2*	36898	No phenotype	No phenotype
			44560	No phenotype	No phenotype
3	*PSMA3*	*Prosalpha7*	33660	Enhanced	No phenotype
4	*PSMA4*	*Prosalpha3*	55217	Enhanced	No phenotype
			77145	Slightly enhanced	No phenotype
5	*PSMA5*	*Prosalpha5*	34786	No Progeny	Cell death
6	*PSMA6*	*CG30382*	27557	Slightly enhanced	No phenotype
7	*PSMA7*	*Prosalpha4*	36063	No Pheotype	No phenotype
			65161	No Progeny	No phenotype
		Prosalpha4T1	61980	No Pheotype	No phenotype
8	*PSMB1*	*Prosbeta6*	34801	No Progeny	Cell death
9	*PSMB2*	*Prosbeta4*	32390	No Progeny	No phenotype
		Prosbeta4R2	67790	No Pheotype	No phenotype
10	*PSMB3*	*Prosbeta3*	34868	No Progeny	Cell death
11	*PSMB4*	*Prosbeta7*	34812	No Progeny	No phenotype
12	*PSMB6/9*	*Prosbeta1*	34824	Few Progeny	No phenotype
13	*PSMB7/10*	*Prosbeta2*	67363	No Phenotype	No phenotype
14	*PSMB5/PSMB8*	*Prosbeta5R1*	77351	No Phenotype	No phenotype
15	*PSMC1*	*Rpt2*	34795	No Progeny	Cell death
16	*PSMC2*	*Rpt1*	33930	Enhanced	Cell death
17	*PSMC3*	*Rpt5*	32422	No Phenotype	No phenotype
18	*PSMC4*	*Rpt3*	34917	No Phenotype	No phenotype
19	*PSMC5*	*Rpt6*	34712	No Phenotype	No phenotype
20	*PSMC6*	*Rpt4*	32874	No Phenotype	No phenotype
21	*PSMD1*	*Rpn2*	34961	Slightly enhanced	No phenotype
22	*PSMD2*	*Rpn1*	34348	No Progeny	No phenotype
23	*PSMD3*	*Rpn3*	30503	Few Progeny	Cell death
			34561	Enhanced	No phenotype
24	*PSMD4*	*Rpn10*	34566	Slightly enhanced	No phenotype
25	*PSMD6*	*Rpn7*	34787	No Progeny	No phenotype
26	*PSMD7*	*Rpn8*	31567	No Progeny	No phenotype
27	*PSMD8*	*Rpn12*	34560	Few Progeny	No phenotype
28	*PSMD9*	*CG9588*	28527	No Phenotype	No phenotype
29	*PSMD11*	*Rpn6*	29385	No Progeny	No phenotype
30	*PSMD12*	*Rpn5*	34532	Slightly enhanced	No phenotype
31	*PSMD13*	*Rpn9*	34034	No Progeny	No phenotype
32	*PSMD14*	*Rpn11*	33662	No Progeny	No phenotype
33	*PSME3*	*REG*	55248	No phenotype	No phenotype
34	*ADRM1*	*Rpn13*	42785	Slightly enhanced	No phenotype
35	*UCHL5*	*Uch-L5*	35433	No phenotype	No phenotype
			64681	No phenotype	No phenotype

FXTAS r(CGG)$_{90}$ flies expressing GAL4 under the eye-specific gmr driver were crossed with flies harboring shRNA transgene against the target candidate gene, downstream from the UAS sequence (UAS-TRiP). Progeny that express the shRNA against target gene in the eye were collected, aged for 7 days and visualized using light microscopy and SEM. Results of the genetic screen of 35 genes revealed 4 proteasome subunits that show significant modulation of the CGG-toxicity associated rough eye phenotype in FXTAS Drosophila. These 4 genes did not alter the eye phenotype upon knockdown in wildtype GMR-GAL4 flies, but significantly enhanced the CGG-associated rough eye phenotype in Gmr-GAL4, UAS-(CGG)$_{90}$-EGFP *Drosophila*.

Table S2. FXTAS phenotype in premutation carriers.

Clinical phenotypes of 110 *FMR1* premutation carriers. 13 carriers were defined as delayed onset, displaying no symptoms of tremor and no symptoms of ataxia past age 69, as assessed by a neurologist. 31 carriers were defined as early onset, with onset of both tremor and ataxia before age 65, according to evaluation by a neurologist.

Phenotype	Number of samples
Asymptomatic > age 69	13
Late onset 1 phenotype (ataxia or tremor) > age 65	40
Mixed onset both phenotypes	10
Early onset 1 phenotype < age 65	16
Early onset both ataxia and tremor < age 65	31
Total	110

Table S3. Primers for RT-PCR

Gene	Forward	Reverse
Psmb5 (mouse)	CTTCGCAATAAGGAACGCATC	TTATCCCAGCCACAGATCATG
Tbp (mouse-housekeeping)	AAGAAGGGAGAATCATGGACC	GAGTAAGTCCTGTGCCGTAAG
Rpl15 (mouse-housekeeping)	TAAACGCCCAGTTCCTAAGG	ACTCTCAAAGCCCCACAATG
PSMB5 (human)	ACAGTCACCCCAAGAAACAC	CATCTACCAAGCCACCTACAG
U16 (human)	TGCCTGCTGTCAGTAAGCTG	TGCTCAGTAAGAATTTTCGTCAA

CHAPTER 5: CONCLUSIONS AND FUTURE DIRECTIONS

CONCLUSIONS

My dissertation focuses on the identification of genetic modifiers of FXTAS. In the search for genetic modifiers, both Chapters 1 & 2 and Chapters 3 & 4 employ a similar stepwise pipeline, albeit with distinct differences: 1) Candidate gene generation 2) Candidate gene selection 3) FXTAS *Drosophila* screen 4) Follow-up validation. In Chapter 1 & 2, we used metabolomics on the cerebella of a mouse model of FXTAS to generate potential metabolic gene candidates and employed candidate gene selection criteria to select 28 candidate genes to test in FXTAS Drosophila. As a result, we identified 8 genetic modifiers of CGG-associated neurotoxicity in FXTAS, including *Schlank* (Ceramide Synthase) and *Sk2* (Sphingosine Kinase)—enzymes of the Sphingolipid metabolic pathway. In order to validate these observations, we performed lipidomics on postmortem cerebellar tissue from human *FMR1* premutation carriers with FXTAS, and found that indeed, sphingolipids are altered in FXTAS vs. control. Furthermore, we performed a comprehensive screen of the genes in sphingolipid metabolism and found 4 additional genetic modifiers in the sphingolipid pathway.

In Chapter 3 & 4, candidate genes were generated via WGS of *FMR1* premutation carriers. Candidate genes were selected by taking into consideration the clinical phenotypes of the carriers of the variant, variant CADD scores, availability of fly orthologues and RNAi lines as well as genes of the ataxia interactome. The subsequent genetic screen in FXTAS *Drosophila* yielded 19 novel genetic modifiers of CGG-associated neurodegeneration in FXTAS, which included *PSMB5*. As a follow-up, various experiments were performed in *Drosophila* as well as Neuro2A cells to show that knockdown of *PSMB5* ameliorates CGG-associated neurotoxicity. This finding was especially exciting as FDA-approved inhibitors already exist for PSMB5, and the first oral PSMB5 inhibitor, Ixazomib Citrate, demonstrated suppression of CGG-associated neurotoxicity

in Neuro2A cells. Furthermore, the variant in *PSMB5, PSMB5*$^{rs11543947\text{-}A}$ was demonstrated to have high potential as a biomarker, as it is enriched in premutation carriers who do not display symptoms of FXTAS and is an eQTL correlating with diminished expression of *PSMB5* mRNA.

In summary, this dissertation has laid out a stepwise, succinct and successful methodology for identifying genetic modifiers of FXTAS, taking advantage of various model systems. In total, we have identified 31 novel genetic modifiers of FXTAS and have shown strong molecular evidence supporting the therapeutic potential of targeting PSMB5 for amelioration of FXTAS neurotoxicity, as well as the potential of using *PSMB5*$^{rs11543947\text{-}A}$ as a biomarker of delayed onset of disease.

FUTURE DIRECTIONS

Over the past decade, there has been considerable progress in our understanding of FXTAS and its pathogenesis. Two potential mechanistic models to explain the molecular pathogenesis of FXTAS have taken root and begun to solidify; namely, the RNA toxicity and the RAN protein toxicity mechanisms. In addition, we are beginning to develop a much more holistic understanding of other players in FXTAS pathogenesis, such as *ASFMR1,* mitochondrial dysfunction, and the implications of the 5hmC epigenetic mark (Ladd et al., 2007; Hukema et al., 2014; Napoli et al., 2011; Kaplan et al., 2012; Dioguardi et al., 2016). However, much of our understanding of FXTAS pathogenesis is incomplete, and many questions remain unanswered.

Understanding disease pathogenesis through metabolic profiling

This dissertation presents the first metabolic profiling of FXTAS mice that demonstrates significant perturbations in metabolic homeostasis upon expression of the expanded premutation repeat in Purkinje cells. From lipids to nucleotides, it is clear that although not many changes occur early on in the disease, the progression of disease through aging results in clear metabolic disruptions in the cerebellum. Through the *Drosophila* screen, we have identified a number of genetic modifiers that may provide more insight into the pathogenic mechanisms of disease. It is unclear whether the genetic interaction results from the gene products of these candidate genes physically being sequestered by the CGG repeats, or through indirect effects from the sequestration of other proteins that act upstream to these metabolic genes. It should also be noted that while it is possible that these metabolic changes may be attributed to processes of neurodegeneration, the fact that specific metabolic genetic modifiers have been identified suggests that genetic mechanisms may trigger certain metabolic changes that may initiate or enhance the expected metabolic alterations due to neurodegeneration. One way to test this would be to compare metabolic profiling of FXTAS mice with a mouse model of another neurodegenerative disease such as Huntington's in order to distinguish the metabolic changes that are shared in processes of neurodegeneration vs. CGG-repeat associated neurotoxicity.

Metabolic alterations as a more specific diagnostic tool for FXTAS

Based on the mouse metabolomics and the human postmortem brain lipidomics data, it is reasonable to predict that *FMR1* premutation carriers may have characteristic metabolic signatures. Indeed, Giulivi et. al. has reported three biomarkers, phenylethylamine normalized by aconitate or isocitrate, an oleamide normalized by isocitrate as useful methods to monitor brain pathophysiology in *FMR1* premutation carriers (Giulivi et al., 2016b). Additional studies are

warranted to further validate the usefulness of these three biomarkers as well as those potential biomarkers identified in this dissertation (such as ceramide, sphingosine, sphingosine 1-phosphate, IMP and xanthosine). Once these biomarkers are validated in animal models as well as in human samples (distinguishing the metabolic profiles of *FMR1* premutation carriers with/without phenotype), this could potentially open the door for the use of techniques such as spectroscopic magnetic resonance imaging (sMRI) for FXTAS diagnosis. sMRI allows for 3-dimnsional (3D) whole-brain assessment of metabolite levels *in vivo* without the use of contrast agents or radioactive tracers and has been more widely used for the diagnosis and management of brain tumors (Law, 2004). Given the phenotypic variability of FXTAS patients, the current diagnostic criteria uses various combinations of radiological and clinical findings to diagnose FXTAS as "definite", "probable" or "possible" (Jacquemont et al., 2003). If the metabolic landscape of FXTAS premutation carrier brains can be easily distinguished from age-matched controls based on several biomarkers, sMRI could offer an objective, consistent criterion to better delineate the degree of pathology for the purposes of diagnosis, management and prognosis (Apartis et al., 2012).

Sphingolipids – potential therapeutics

This dissertation also offered insight into Sphingolipids as a pathway that is perturbed in FXTAS, and specifically identified several genes in this pathway as potential genetic modifiers. For future studies, we can further investigate some of the Sphingolipid candidate genetic modifiers, such as *GBA*, that is already known to play a role in Parkinson's disease. It would be beneficial to determine whether *GBA* plays a significant role in altering neurotoxicity in FXTAS, and whether *GBA* can also be used as a potential treatment target.

Expanding our understanding of FXTAS through genetic modifiers

Although we have identified numerous players in FXTAS pathogenesis, we still lack enough mechanistic and chronological understanding to identify the best targets for treatment. Indeed, in terms of chronology, studies in mice have shown that premutation expanded CGG repeats in the mouse *Fmr1* gene perturb embryonic neocortical development (Cunningham et al., 2011). Also, in another study, cultured hippocampal neurons from mice expressing premutation CGG repeats exhibited shorter dendritic lengths and fewer branches between 7-21 days *in vitro* compared to wild-type littermates (Chen et al., 2010). These studies and others have raised the possibility that the onset of FXTAS may be the result of a lifelong pathologic process (Garcia-Arocena et al., 2010). If it is true that premutation carriers are predisposed to this lifelong pathologic process beginning in infancy, one of our next tasks would be to determine the factors that distinguish the premutation carriers who go on to develop FXTAS in late adulthood from those who are somehow protected. In addition, we would need to identify the earliest period for potential therapeutic intervention.

Variability in FXTAS is not limited to the onset of disease; there is also a broad spectrum of phenotypes (Garcia-Arocena et al., 2010). Although the main clinical manifestations remain locomotor in nature, FXTAS can also manifest as significant non-motor neurodegenerative phenotypes, such as cognitive decline/dementia and neuropsychiatric disturbances (Bourgeois et al., 2009; Garcia-Arocena et al., 2010). Adding to the phenotypic variability, in the low proportion of FXTAS patients who are female carriers, it is more common to see clinical features such as autoimmune-type dysfunction, hypothyroidism, and muscle pain than in men (Coffey et al., 2008; Garcia-Arocena et al., 2010). Thus, in addition to further decoding the molecular basis of FXTAS,

subsequent efforts should be directed toward the identification of genetic modifiers that account for the variability in onset and phenotype seen with FXTAS.

This work has laid down the blueprint for a productive pipeline for the generation and validation of candidate genetic modifiers. This pipeline can be used for the generation of additional candidate genetic modifiers, and further studies should be undertaken to examine and validate the other 30 genetic modifiers already identified in this study, in addition to *PSMB5*, some of which were discussed in Chapter 3.

Although we have presented high-throughput methods for the generation and validation of candidate genetic modifiers, unfortunately, high-throughput methods do not exist for the molecular validation of mechanisms for these candidate genetic modifiers. Therefore, taking advantage of large published datasets such as Cross-linking Immunoprecipitation (CLIP)-Seq data, as well as previous literature findings on these candidate genetic modifiers may prove to be valuable for carefully designing experiments to delineate the mechanistic roles of these genes in modifying CGG-associated neurotoxicity.

Apart from dissecting the mechanism for these genetic modifiers, simply validating them individually in a mammalian *in vitro* or *in vivo* model can also be very valuable. In this dissertation, we have shown that use of Neuro2A cells, a mouse neuroblastoma cell line available from ATCC, can be a very useful system to test the role of the genetic modifier in modulating CGG-associated neurotoxicity. Although not in the scope of this dissertation, *in vivo* experiments can also be performed using a murine model of FXTAS. For example, in future experiments, this could involve generation of a *Psmb5* conditional knockout mouse line (since one is not currently available) and

crossing these mice with the FXTAS mice to assess the effects of reducing *Psmb5* expression in Purkinje cells on suppression of CGG-mediated neurodegeneration.

Investigating the role of *PSMB5* knockdown on neurodegeneration

This dissertation has uncovered an intriguing relationship between lowering P*SMB5* expression and amelioration of CGG-associated neurotoxicity. Interestingly, we have also shown that inhibition of the protein product PSMB5 leads to suppression of CGG-associated neurodegeneration. In future studies, it would be important to further distinguish whether the suppression of neurodegeneration is caused by decreased *PSMB5* mRNA expression, or by the inhibition of the proteasome subunit PSMB5 or both. Furthermore, it would be important to investigate why the PSMB5 subunit is distinctive in showing this relationship, and whether it plays an independent role by itself or within the proteasome complex that warrants this unique interaction with the CGG-associated neurodegeneration.

In addition, since the efficiency in clearance of protein aggregates is linked to many neurodegenerative diseases, especially repeat-associated, it would be interesting to test whether *PSMB5* knockdown ameliorates neurotoxicity in other repeat diseases, such as ALS and Huntington's. We could also investigate whether knocking down *PSMB5* suppresses RAN translation in these disease models. Depending on the mechanism, the suppression of neurotoxicity via *PSMB5* knockdown could be unique to the interaction with CGG repeats, or it could also have a comparable effect on other repeat diseases as well.

Investigating *PSMB5*$^{rs11543947\text{-}A}$ as a prognostic biomarker for FXTAS

In this dissertation, I have proposed that *PSMB5*$^{rs11543947\text{-}A}$ could be potentially used as a prognostic biomarker for FXTAS, given that this variant is enriched in *FMR1* premutation carriers without any symptoms of FXTAS. Furthermore, the molecular evidence is also strongly supportive, as *PSMB5*$^{rs11543947\text{-}A}$ is an eQTL associated with decreased expression of the gene, and knockdown of *PSMB5* orthologues in fly and mouse suppresses CGG-associated neurotoxicity.

A potential future direction would be to perform targeted resequencing on *PSMB5* in a larger number of premutation carriers to determine whether *PSMB5*$^{rs11543947\text{-}A}$ modulates age-at-onset of FXTAS, and to identify additional variants in *PSMB5* that may also modulate age-at-onset of FXTAS. If we were to re-sequence 500 premutation carriers, for common variants such as *PSMB5*$^{rs11543947\text{-}A}$, which has a minor allele frequency of 5.5%, we will have 80% power to detect this variant if the relative risk is above 1.4. For rare variants with a minor allele frequency less than 1%, we will have 32% power to detect it if the relative risk is above 1.5. By performing targeted resequencing, we will be able to further identify and validate the potential role of variants in *PSMB5* as biomarkers for FXTAS.

REFERENCES

Apartis, E., Blancher, A., Meissner, W.G., Guyant-Maréchal, L., Maltête, D., Broucker, T. De, Legrand, A.-P., Bouzenada, H., Thanh, H.T., Sallansonnet-Froment, M., et al. (2012). FXTAS. Neurology *79*, 1898–1907.

Ariza, J., Rogers, H., Monterrubio, A., Reyes-Miranda, A., Hagerman, P.J., and Martínez-Cerdeño, V. (2016). A Majority of FXTAS Cases Present with Intranuclear Inclusions Within Purkinje Cells. The Cerebellum *15*, 546–551.

Van Assche, R., Temmerman, L., Dias, D.A., Boughton, B., Boonen, K., Braeckman, B.P., Schoofs, L., and Roessner, U. (2015). Metabolic profiling of a transgenic Caenorhabditis elegans Alzheimer model. Metabolomics *11*, 477–486.

Babicki, S., Arndt, D., Marcu, A., Liang, Y., Grant, J.R., Maciejewski, A., and Wishart, D.S. (2016). Heatmapper: web-enabled heat mapping for all. Nucleic Acids Res. *44*, W147–W153.

Berger, Z., Ravikumar, B., Menzies, F.M., Oroz, L.G., Underwood, B.R., Pangalos, M.N., Schmitt, I., Wullner, U., Evert, B.O., O'Kane, C.J., et al. (2006). Rapamycin alleviates toxicity of different aggregate-prone proteins. Hum. Mol. Genet. *15*, 433–442.

Bontekoe, C.J.M. (2001). Instability of a (CGG)98 repeat in the Fmr1 promoter. Hum.

Mol. Genet. *10*, 1693–1699.

Brand, A.H., and Perrimon, N. (1993). Targeted gene expression as a means of altering cell fates and generating dominant phenotypes. Development *118*, 401–415.

Bridgewater BR, E.A., BR, B., Q, L., MW, M., RJ, R., H, D., SJ, S., CD, D., and LAD, M. (2014). High Resolution Mass Spectrometry Improves Data Quantity and Quality as Compared to Unit Mass Resolution Mass Spectrometry in High-Throughput Profiling Metabolomics. J. Postgenomics Drug Biomark. Dev. *04*, 1–3.

Brown, W.T., Houck, G.E., Jeziorowska, A., Levinson, F.N., Ding, X., Dobkin, C., Zhong, N., Henderson, J., Brooks, S.S., and Jenkins, E.C. (1993). Rapid fragile X carrier screening and prenatal diagnosis using a nonradioactive PCR test. JAMA *270*, 1569–1575.

Burté, F., Houghton, D., Lowes, H., Pyle, A., Nesbitt, S., Yarnall, A., Yu-Wai-Man, P., Burn, D.J., Santibanez-Koref, M., and Hudson, G. (2017). metabolic profiling of Parkinson's disease and mild cognitive impairment. Mov. Disord. *32*, 927–932.

Caccamo, A., Majumder, S., Richardson, A., Strong, R., and Oddo, S. (2010). Molecular Interplay between Mammalian Target of Rapamycin (mTOR), Amyloid-β, and Tau. J. Biol. Chem. *285*, 13107–13120.

Chong, J., and Xia, J. (2018). MetaboAnalystR: an R package for flexible and reproducible analysis of metabolomics data. Bioinformatics *34*, 4313–4314.

Chong, J., Soufan, O., Li, C., Caraus, I., Li, S., Bourque, G., Wishart, D.S., and Xia, J. (2018). MetaboAnalyst 4.0: towards more transparent and integrative metabolomics analysis. Nucleic Acids Res. *46*, W486–W494.

Ciechanover, A. (2013). Intracellular protein degradation: From a vague idea through the lysosome and the ubiquitin–proteasome system and onto human diseases and drug targeting. Bioorg. Med. Chem. *21*, 3400–3410.

Ciechanover, A., and Kwon, Y.T. (2015). Degradation of misfolded proteins in neurodegenerative diseases: therapeutic targets and strategies. Exp. Mol. Med. *47*, e147–e147.

Cleary, J.D., and Ranum, L.P. (2014). Repeat associated non-ATG (RAN) translation: new starts in microsatellite expansion disorders. Curr. Opin. Genet. Dev. *26*, 6–15.

Clemson, C.M., Hutchinson, J.N., Sara, S.A., Ensminger, A.W., Fox, A.H., Chess, A., and Lawrence, J.B. (2009). An architectural role for a nuclear noncoding RNA: NEAT1 RNA is essential for the structure of paraspeckles. Mol. Cell *33*, 717–726.

Colak, D., Zaninovic, N., Cohen, M.S., Rosenwaks, Z., Yang, W.-Y., Gerhardt, J., Disney, M.D., and Jaffrey, S.R. (2014). Promoter-Bound Trinucleotide Repeat mRNA Drives Epigenetic Silencing in Fragile X Syndrome. Science (80-.). *343*, 1002–1005.

Conway, J.R., Lex, A., Gehlenborg, N., and Hancock, J. (2017). UpSetR: an R package for the visualization of intersecting sets and their properties. Bioinformatics *33*, 2938–2940.

Cutler, R.G., Kelly, J., Storie, K., Pedersen, W.A., Tammara, A., Hatanpaa, K., Troncoso, J.C., and Mattson, M.P. (2004). Involvement of oxidative stress-induced abnormalities in ceramide and cholesterol metabolism in brain aging and Alzheimer's disease. Proc. Natl. Acad. Sci. U. S. A. *101*, 2070–2075.

Cuvillier, O., Pirianov, G., Kleuser, B., Vanek, P.G., Coso, O.A., Gutkind, J.S., and Spiegel, S. (1996). Suppression of ceramide-mediated programmed cell death by sphingosine-1-phosphate. Nature *381*, 800–803.

DeHaven, C.D., Evans, A.M., Dai, H., and Lawton, K.A. (2010). Organization of GC/MS and LC/MS metabolomics data into chemical libraries. J. Cheminform. *2*, 9.

Dietzl, G., Chen, D., Schnorrer, F., Su, K.-C., Barinova, Y., Fellner, M., Gasser, B., Kinsey, K., Oppel, S., Scheiblauer, S., et al. (2007). A genome-wide transgenic RNAi library for conditional gene inactivation in Drosophila. Nature *448*, 151–156.

Dombrowski, C., Lévesque, S., Morel, M.L., Rouillard, P., Morgan, K., and Rousseau, F. (2002). Premutation and intermediate-size FMR1 alleles in 10 572 males from the general population: loss of an AGG interruption is a late event in the generation of fragile X syndrome alleles. Hum. Mol. Genet. *11*, 371–378.

Entezam, A., Biacsi, R., Orrison, B., Saha, T., Hoffman, G.E., Grabczyk, E., Nussbaum, R.L., and Usdin, K. (2007). Regional FMRP deficits and large repeat expansions into the full mutation range in a new Fragile X premutation mouse model. Gene *395*, 125–134.

Fu, Y.H., Kuhl, D.P., Pizzuti, A., Pieretti, M., Sutcliffe, J.S., Richards, S., Verkerk, A.J., Holden, J.J., Fenwick, R.G., and Warren, S.T. (1991). Variation of the CGG repeat at the fragile X site results in genetic instability: resolution of the Sherman paradox. Cell *67*, 1047–1058.

Ginkel, C., Hartmann, D., vom Dorp, K., Zlomuzica, A., Farwanah, H., Eckhardt, M., Sandhoff, R., Degen, J., Rabionet, M., Dere, E., et al. (2012). Ablation of neuronal ceramide synthase 1 in mice decreases ganglioside levels and expression of myelin-associated glycoprotein in oligodendrocytes. J. Biol. Chem. *287*, 41888–41902.

Giulivi, C., Napoli, E., Tassone, F., Halmai, J., and Hagerman, R. (2016a). Plasma metabolic profile delineates roles for neurodegeneration, pro-inflammatory damage and mitochondrial dysfunction in the FMR1 premutation. Biochem. J. *473*, 3871–3888.

Giulivi, C., Napoli, E., Tassone, F., Halmai, J., and Hagerman, R. (2016b). Plasma Biomarkers for Monitoring Brain Pathophysiology in FMR1 Premutation Carriers. Front. Mol. Neurosci. *9*, 71.

Greco, C.M., Hagerman, R.J., Tassone, F., Chudley, A.E., Del Bigio, M.R., Jacquemont, S., Leehey, M., and Hagerman, P.J. (2002). Neuronal intranuclear inclusions in a new cerebellar tremor/ataxia syndrome among fragile X carriers. Brain *125*, 1760–1771.

Greco, C.M., Berman, R.F., Martin, R.M., Tassone, F., Schwartz, P.H., Chang, A., Trapp, B.D., Iwahashi, C., Brunberg, J., Grigsby, J., et al. (2006). Neuropathology of fragile X-associated tremor/ataxia syndrome (FXTAS). Brain *129*, 243–255.

Hagerman, P.J., and Hagerman, R.J. (2015). Fragile X-associated tremor/ataxia syndrome. Ann. N. Y. Acad. Sci. *1338*, 58–70.

Hagerman, R.J., and Hagerman, P.J. (2002). The fragile X premutation: into the phenotypic fold. Curr. Opin. Genet. Dev. *12*, 278–283.

Hagerman, R.J., Leehey, M., Heinrichs, W., Tassone, F., Wilson, R., Hills, J., Grigsby, J., Gage, B., and Hagerman, P.J. (2001). Intention tremor, parkinsonism, and generalized brain atrophy in male carriers of fragile X. Neurology *57*, 127–130.

Hannun, Y.A., and Obeid, L.M. (2002). The Ceramide-centric universe of lipid-mediated cell regulation: stress encounters of the lipid kind. J. Biol. Chem. *277*, 25847–25850.

Hashem, V., Galloway, J.N., Mori, M., Willemsen, R., Oostra, B.A., Paylor, R., and Nelson, D.L. (2009). Ectopic expression of CGG containing mRNA is neurotoxic in mammals. Hum. Mol. Genet. *18*, 2443–2451.

Havelund, J.F., Heegaard, N.H.H., Færgeman, N.J.K., and Gramsbergen, J.B. (2017). Biomarker Research in Parkinson's Disease Using Metabolite Profiling. Metabolites *7*.

Jacquemont, S., Hagerman, R.J., Leehey, M., Grigsby, J., Zhang, L., Brunberg, J.A., Greco, C., Des Portes, V., Jardini, T., Levine, R., et al. (2003). Fragile X premutation tremor/ataxia syndrome: molecular, clinical, and neuroimaging correlates. Am. J. Hum. Genet. *72*, 869–878.

Jacquemont, S., Hagerman, R.J., Leehey, M.A., Hall, D.A., Levine, R.A., Brunberg, J.A., Zhang, L., Jardini, T., Gane, L.W., Harris, S.W., et al. (2004). Penetrance of the Fragile X–Associated Tremor/Ataxia Syndrome in a Premutation Carrier Population. JAMA *291*, 460.

Jin, P., Zarnescu, D.C., Zhang, F., Pearson, C.E., Lucchesi, J.C., Moses, K., and Warren,

S.T. (2003). RNA-Mediated Neurodegeneration Caused by the Fragile X Premutation rCGG Repeats in Drosophila. Neuron *39*, 739–747.

Jin, P., Duan, R., Qurashi, A., Qin, Y., Tian, D., Rosser, T.C., Liu, H., Feng, Y., Warren, S.T., Hoogeveen, A.T., et al. (2007). Pur alpha binds to rCGG repeats and modulates repeat-mediated neurodegeneration in a Drosophila model of fragile X tremor/ataxia syndrome. Neuron *55*, 556–564.

Johansen, K.K., Wang, L., Aasly, J.O., White, L.R., Matson, W.R., Henchcliffe, C., Beal, M.F., and Bogdanov, M. (2009). Metabolomic profiling in LRRK2-related Parkinson's disease. PLoS One *4*, e7551.

Johnston, H.R., Chopra, P., Wingo, T.S., Patel, V., Epstein, M.P., Mulle, J.G., Warren, S.T., Zwick, M.E., Cutler, D.J., and Cutler, D.J. (2017). PEMapper and PECaller provide a simplified approach to whole-genome sequencing. Proc. Natl. Acad. Sci. *114*, E1923–E1932.

Kai, M., Kai, and Mihoko (2016). Roles of RNA-Binding Proteins in DNA Damage Response. Int. J. Mol. Sci. *17*, 310.

Kircher, M., Witten, D.M., Jain, P., O'Roak, B.J., Cooper, G.M., and Shendure, J. (2014). A general framework for estimating the relative pathogenicity of human genetic variants. Nat. Genet. *46*, 310–315.

Koelmel, J.P., Kroeger, N.M., Ulmer, C.Z., Bowden, J.A., Patterson, R.E., Cochran, J.A., Beecher, C.W.W., Garrett, T.J., and Yost, R.A. (2017). LipidMatch: an automated workflow for rule-based lipid identification using untargeted high-resolution tandem mass spectrometry data. BMC Bioinformatics *18*, 331.

Kolesnick, R. (2002). The therapeutic potential of modulating the ceramide/sphingomyelin pathway. J. Clin. Invest. *110*, 3–8.

Kong, H.E., Zhao, J., Xu, S., Jin, P., and Jin, Y. (2017). Fragile X-Associated Tremor/Ataxia Syndrome: From Molecular Pathogenesis to Development of Therapeutics. Front. Cell. Neurosci. *11*, 128.

Kotlar, A. V, Trevino, C.E., Zwick, M.E., Cutler, D.J., and Wingo, T.S. (2018). Bystro: rapid online variant annotation and natural-language filtering at whole-genome scale. Genome Biol. *19*, 14.

Kremer, E., Pritchard, M., Lynch, M., Yu, S., Holman, K., Baker, E., Warren, S., Schlessinger, D., Sutherland, G., and Richards, R. (1991). Mapping of DNA instability at the fragile X to a trinucleotide repeat sequence p(CCG)n. Science (80-.). *252*, 1711–1714.

de la Puente, P., and Azab, A.K. (2013). Contemporary drug therapies for multiple myeloma. Drugs of Today *49*, 563.

Law, M. (2004). MR spectroscopy of brain tumors. Top. Magn. Reson. Imaging *15*, 291–313.

Lek, M., Karczewski, K.J., Minikel, E. V., Samocha, K.E., Banks, E., Fennell, T., O'Donnell-Luria, A.H., Ware, J.S., Hill, A.J., Cummings, B.B., et al. (2016). Analysis of protein-coding genetic variation in 60,706 humans. Nature *536*, 285–291.

Lim, J., Hao, T., Shaw, C., Patel, A.J., Szabó, G., Rual, J.-F., Fisk, C.J., Li, N., Smolyar, A., Hill, D.E., et al. (2006). A Protein–Protein Interaction Network for Human Inherited Ataxias and Disorders of Purkinje Cell Degeneration.

Lin, Y., Tang, C., He, H., and Duan, R. (2013). Activation of mTOR Ameliorates Fragile X Premutation rCGG Repeat-Mediated Neurodegeneration. PLoS One *8*, e62572.

Livneh, I., Cohen-Kaplan, V., Cohen-Rosenzweig, C., Avni, N., and Ciechanover, A. (2016). The life cycle of the 26S proteasome: from birth, through regulation and function and onto its death. Cell Res. *26*, 869–885.

Macias, S., Plass, M., Stajuda, A., Michlewski, G., Eyras, E., and Cáceres, J.F. (2012).

DGCR8 HITS-CLIP reveals novel functions for the Microprocessor. Nat. Struct. Mol. Biol. *19*, 760–766.

Mastrokolias, A., Pool, R., Mina, E., Hettne, K.M., van Duijn, E., van der Mast, R.C., van Ommen, G., 't Hoen, P.A.C., Prehn, C., Adamski, J., et al. (2016). Integration of targeted metabolomics and transcriptomics identifies deregulation of phosphatidylcholine metabolism in Huntington's disease peripheral blood samples. Metabolomics *12*, 137.

McGurk, L., Berson, A., and Bonini, N.M. (2015). Drosophila as an In Vivo Model for Human Neurodegenerative Disease. Genetics *201*, 377–402.

Meadows, K.L., Pettay, D., Newman, J., Hersey, J., Ashley, A.E., and Sherman, S.L. (1996). Survey of the fragile X syndrome and the fragile X E syndrome in a special education needs population. Am. J. Med. Genet. *64*, 428–433.

Mielke, M.M., and Lyketsos, C.G. (2010). Alterations of the Sphingolipid Pathway in Alzheimer's Disease: New Biomarkers and Treatment Targets? NeuroMolecular Med. *12*, 331–340.

Mizugishi, K., Yamashita, T., Olivera, A., Miller, G.F., Spiegel, S., and Proia, R.L. (2005). Essential Role for Sphingosine Kinases in Neural and Vascular Development. Mol. Cell. Biol. *25*, 11113–11121.

Murphy, K.E., Gysbers, A.M., Abbott, S.K., Tayebi, N., Kim, W.S., Sidransky, E., Cooper, A., Garner, B., and Halliday, G.M. (2014). Reduced glucocerebrosidase is associated with increased α-synuclein in sporadic Parkinson's disease. Brain *137*, 834–848.

Muslimov, I.A., Patel, M. V., Rose, A., and Tiedge, H. (2011). Spatial code recognition in neuronal RNA targeting: Role of RNA–hnRNP A2 interactions. J. Cell Biol. *194*, 441–457.

Muz, B., Ghazarian, R.N., Ou, M., Luderer, M.J., Kusdono, H.D., and Azab, A.K. (2016). Spotlight on ixazomib: potential in the treatment of multiple myeloma. Drug Des. Devel. Ther. *10*, 217–226.

Nakamura, Y., Tagawa, K., Oka, T., Sasabe, T., Ito, H., Shiwaku, H., La Spada, A.R., and Okazawa, H. (2012). Ataxin-7 associates with microtubules and stabilizes the cytoskeletal network. Hum. Mol. Genet. *21*, 1099–1110.

Nobumoto, M., Yamada, M., Song, S., Inouye, S., and Nakazawa, A. (1998). Mechanism of mitochondrial import of adenylate kinase isozymes. J. Biochem. *123*, 128–135.

Oh, S.Y., He, F., Krans, A., Frazer, M., Taylor, J.P., Paulson, H.L., and Todd, P.K. (2015). RAN translation at CGG repeats induces ubiquitin proteasome system impairment in models of fragile X-associated tremor ataxia syndrome. Hum. Mol. Genet. *24*, 4317–4326.

Olivera, A., and Spiegel, S. (1993). Sphingosine-1-phosphate as second messenger in cell proliferation induced by PDGF and FCS mitogens. Nature *365*, 557–560.

Pandey, U.B., Nie, Z., Batlevi, Y., McCray, B.A., Ritson, G.P., Nedelsky, N.B., Schwartz, S.L., DiProspero, N.A., Knight, M.A., Schuldiner, O., et al. (2007). HDAC6 rescues neurodegeneration and provides an essential link between autophagy and the UPS. Nature *447*, 860–864.

Park, J.-W., Park, W.-J., and Futerman, A.H. (2014). Ceramide synthases as potential targets for therapeutic intervention in human diseases. Biochim. Biophys. Acta *1841*, 671–681.

Patti, G.J., Yanes, O., and Siuzdak, G. (2012). Innovation: Metabolomics: the apogee of the omics trilogy. Nat. Rev. Mol. Cell Biol. *13*, 263–269.

Peng, B., Li, H., and Peng, X.-X. (2015). Functional metabolomics: from biomarker discovery to metabolome reprogramming. Protein Cell *6*, 628–637.

Piccinini, M., Scandroglio, F., Prioni, S., Buccinnà, B., Loberto, N., Aureli, M., Chigorno, V., Lupino, E., DeMarco, G., Lomartire, A., et al. (2010). Deregulated Sphingolipid Metabolism and Membrane Organization in Neurodegenerative Disorders. Mol. Neurobiol. *41*,

314–340.

Prüßing, K., Voigt, A., and Schulz, J.B. (2013). Drosophila melanogaster as a model organism for Alzheimer's disease. Mol. Neurodegener. *8*, 35.

Raedler, L.A. (2016). Ninlaro (Ixazomib): First Oral Proteasome Inhibitor Approved for the Treatment of Patients with Relapsed or Refractory Multiple Myeloma. Am. Heal. Drug Benefits *9*, 102–105.

Robin, G., López, J.R., Espinal, G.M., Hulsizer, S., Hagerman, P.J., and Pessah, I.N. (2017). Calcium dysregulation and Cdk5-ATM pathway involved in a mouse model of fragile X-associated tremor/ataxia syndrome. Hum. Mol. Genet. *26*, 2649–2666.

Roessner, U., and Bowne, J. (2009). What is metabolomics all about? Biotechniques *46*, 363–365.

Rousseau, F., Rouillard, P., Morel, M.L., Khandjian, E.W., and Morgan, K. (1995). Prevalence of carriers of premutation-size alleles of the FMRI gene--and implications for the population genetics of the fragile X syndrome. Am. J. Hum. Genet. *57*, 1006–1018.

Sarkar, S., Krishna, G., Imarisio, S., Saiki, S., O'Kane, C.J., and Rubinsztein, D.C. (2008). A rational mechanism for combination treatment of Huntington's disease using lithium and rapamycin. Hum. Mol. Genet. *17*, 170–178.

Sasaki, Y.T., and Hirose, T. (2009). How to build a paraspeckle. Genome Biol. *10*, 227.

Sellier, C., Rau, F., Liu, Y., Tassone, F., Hukema, R.K., Gattoni, R., Schneider, A., Richard, S., Willemsen, R., Elliott, D.J., et al. (2010). Sam68 sequestration and partial loss of function are associated with splicing alterations in FXTAS patients. EMBO J. *29*, 1248–1261.

Sellier, C., Freyermuth, F., Tabet, R., Tran, T., He, F., Ruffenach, F., Alunni, V., Moine, H., Thibault, C., Page, A., et al. (2013). Sequestration of DROSHA and DGCR8 by expanded CGG RNA repeats alters microRNA processing in fragile X-associated tremor/ataxia syndrome. Cell Rep. *3*, 869–880.

Sellier, C., Buijsen, R.A.M., He, F., Natla, S., Jung, L., Tropel, P., Gaucherot, A., Jacobs, H., Meziane, H., Vincent, A., et al. (2017). Translation of Expanded CGG Repeats into FMRpolyG Is Pathogenic and May Contribute to Fragile X Tremor Ataxia Syndrome. Neuron *93*, 331–347.

Sen, A., and Cox, R.T. (2017). Fly Models of Human Diseases. In Current Topics in Developmental Biology, pp. 1–27.

Sidransky, E., Nalls, M.A., Aasly, J.O., Aharon-Peretz, J., Annesi, G., Barbosa, E.R., Bar-Shira, A., Berg, D., Bras, J., Brice, A., et al. (2009). Multicenter Analysis of Glucocerebrosidase Mutations in Parkinson's Disease. N. Engl. J. Med. *361*, 1651–1661.

Simon, N.E., Yuan, M., and Kai, M. (2017). RNA-binding protein RBM14 regulates dissociation and association of non-homologous end joining proteins. Cell Cycle *16*, 1175–1180.

Sofola, O.A., Jin, P., Qin, Y., Duan, R., Liu, H., de Haro, M., Nelson, D.L., and Botas, J. (2007). RNA-Binding Proteins hnRNP A2/B1 and CUGBP1 Suppress Fragile X CGG Premutation Repeat-Induced Neurodegeneration in a Drosophila Model of FXTAS. Neuron *55*, 565–571.

Spiegel, S., and Milstien, S. (2003). Sphingosine-1-phosphate: an enigmatic signalling lipid. Nat. Rev. Mol. Cell Biol. *4*, 397–407.

Spilman, P., Podlutskaya, N., Hart, M.J., Debnath, J., Gorostiza, O., Bredesen, D., Richardson, A., Strong, R., and Galvan, V. (2010). Inhibition of mTOR by Rapamycin Abolishes Cognitive Deficits and Reduces Amyloid-β Levels in a Mouse Model of Alzheimer's Disease. PLoS One *5*, e9979.

Stirnemann, J., Belmatoug, N., Camou, F., Serratrice, C., Froissart, R., Caillaud, C., Levade, T., Astudillo, L., Serratrice, J., Brassier, A., et al. (2017). A Review of Gaucher Disease

Pathophysiology, Clinical Presentation and Treatments. Int. J. Mol. Sci. *18*, 441.

Stojkovska, I., Krainc, D., and Mazzulli, J.R. (2018). Molecular mechanisms of α-synuclein and GBA1 in Parkinson's disease. Cell Tissue Res. *373*, 51–60.

Tassone, F., Iwahashi, C., and Hagerman, P.J. (2004). FMR1 RNA within the intranuclear inclusions of fragile X-associated tremor/ataxia syndrome (FXTAS). RNA Biol. *1*, 103–105.

Tidhar, R., and Futerman, A.H. (2013). The complexity of sphingolipid biosynthesis in the endoplasmic reticulum. Biochim. Biophys. Acta - Mol. Cell Res. *1833*, 2511–2518.

Todd, P.K., Oh, S.Y., Krans, A., He, F., Sellier, C., Frazer, M., Renoux, A.J., Chen, K.-C., Scaglione, K.M., Basrur, V., et al. (2013). CGG Repeat-Associated Translation Mediates Neurodegeneration in Fragile X Tremor Ataxia Syndrome.

Trushina, E., Dutta, T., Persson, X.-M.T., Mielke, M.M., and Petersen, R.C. (2013). Identification of altered metabolic pathways in plasma and CSF in mild cognitive impairment and Alzheimer's disease using metabolomics. PLoS One *8*, e63644.

Verkerk, A.J.M.H., Pieretti, M., Sutcliffe, J.S., Fu, Y.-H., Kuhl, D.P.A., Pizzuti, A., Reiner, O., Richards, S., Victoria, M.F., Zhang, F., et al. (1991). Identification of a gene (FMR-1) containing a CGG repeat coincident with a breakpoint cluster region exhibiting length variation in fragile X syndrome. Cell *65*, 905–914.

Wang, G., Silva, J., Dasgupta, S., and Bieberich, E. (2008). Long-chain ceramide is elevated in presenilin 1 (PS1M146V) mouse brain and induces apoptosis in PS1 astrocytes. Glia *56*, 449–456.

Wang, W.-Y., Pan, L., Su, S.C., Quinn, E.J., Sasaki, M., Jimenez, J.C., Mackenzie, I.R.A., Huang, E.J., and Tsai, L.-H. (2013). Interaction of FUS and HDAC1 regulates DNA damage response and repair in neurons. Nat. Neurosci. *16*, 1383–1391.

Wolf, M.J., Amrein, H., Izatt, J.A., Choma, M.A., Reedy, M.C., and Rockman, H.A. (2006). From The Cover: Drosophila as a model for the identification of genes causing adult human heart disease. Proc. Natl. Acad. Sci. *103*, 1394–1399.

Yuan, M., Eberhart, C.G., and Kai, M. (2014). RNA binding protein RBM14 promotes radio-resistance in glioblastoma by regulating DNA repair and cell differentiation. Oncotarget *5*, 2820–2826.

Zhang, H., Desai, N.N., Olivera, A., Seki, T., Brooker, G., and Spiegel, S. (1991). Sphingosine-1-phosphate, a novel lipid, involved in cellular proliferation. J. Cell Biol. *114*, 155–167.

Zhao, L., Spassieva, S.D., Jucius, T.J., Shultz, L.D., Shick, H.E., Macklin, W.B., Hannun, Y.A., Obeid, L.M., and Ackerman, S.L. (2011). A Deficiency of Ceramide Biosynthesis Causes Cerebellar Purkinje Cell Neurodegeneration and Lipofuscin Accumulation. PLoS Genet. *7*, e1002063.

Zhu, Y., Xu, G., Yang, Y.T., Xu, Z., Chen, X., Shi, B., Xie, D., Lu, Z.J., and Wang, P. (2019). POSTAR2: deciphering the post-transcriptional regulatory logics. Nucleic Acids Res. *47*, D203–D211.

Zu, T., Gibbens, B., Doty, N.S., Gomes-Pereira, M., Huguet, A., Stone, M.D., Margolis, J., Peterson, M., Markowski, T.W., Ingram, M.A.C., et al. (2011). Non-ATG-initiated translation directed by microsatellite expansions. Proc. Natl. Acad. Sci. U. S. A. *108*, 260–265.